TECHNISCHE UNIVERSITÄT DRESDEN

Embedding of QDs into Ionic Crystals: Methods, Characterization and Applications

Dissertation

zur Erlangung des akademischen Grades

Doctor rerum naturalium (Dr. rer. nat.)

vorgelegt

der Fakultät Mathematik und Naturwissenschaften der Technischen Universität Dresden

von

M. Sc. Marcus Adam, geb. Müller
geboren am 20.01.1988 in Zeitz

eingereicht am 12.10.2015

Die Dissertation wurden in der Zeit von November 2012 bis Oktober 2015 an der Professur für Physikalische Chemie angefertigt.

There is a single light of science, and to brighten it anywhere is to brighten it everywhere.
Isaac Asimov (1919-1992)

Abstract

Colloidal semiconductor quantum dots (QDs) have gained substantial interest as adjustable, bright and spectrally tunable fluorophores in the past decades. Besides their in-depth analyses in the scientific community, first industrial applications as color conversion and color enrichment materials were implemented. However, stability and processability are essential for their successful use in these and further applications. Methods to embed QDs into oxides or polymers can only partially solve this challenge. Recently, our group introduced the embedding of QDs into ionic salts, which holds several advantages in comparison to polymer- or oxide-based counterparts. Both gas permeability and environmental-related degradation processes are negligible, making these composites an almost perfect choice of material. To evaluate this new class of QD-salt mixed crystals, a thorough understanding of the formation procedure and the final composites is needed. The present work is focused on embedding both aqueous-based and oil-based metal-chalcogenide QDs into several ionic salts and the investigations of their optical and chemical properties upon incorporation into the mixed crystals.

QDs with well-known, reproducible and high-quality synthetic protocols are chosen as emissive species. CdTe QDs were incorporated into NaCl as host matrix by using the straightforward "classical" method. The resulting mixed crystals of various shapes and beautiful colors preserve the strong luminescence of the incorporated QDs. Besides NaCl, also borax and other salts are used as host matrices.

Mercaptopropionic acid stabilized CdTe QDs can easily be co-crystallized with NaCl, while thioglycolic acid as stabilizing agent results in only weakly emitting powder-like mixed crystals.

This challenge was overcome by adjusting the pH, the amount of free stabilizer and the type of salt used, demonstrating the reproducible incorporation of highest-quality CdTe QDs capped with thioglycolic acid into NaCl and KCl salt crystals.

A disadvantage of the "classical" mixed crystallization procedure was its long duration which prevents a straightforward transfer of the protocol to less stable QD colloids, e.g., initially oil-based, ligand exchanged QDs. To address this challenge, the "Liquid-liquid-diffusion-assisted-crystallization" (LLDC) method is introduced. By applying the LLDC, a substantially accelerated ionic crystallization of the QDs is shown, reducing the crystallization time needed by one order of magnitude. This fast process opens the field of incorporating ligand-exchanged Cd-free QDs into NaCl matrices. To overcome the need for a ligand exchange, the LLDC can also be extended towards a two-step approach. In this modified version, the seed-mediated LLDC provides for the first time the ability to incorporate oil-based QDs directly into ionic matrices without a prior phase transfer.

The ionic salts appear to be very tight matrices, ensuring the protection of the QDs from the environment. As one of the main results, these matrices provide extraordinary high photo- and chemical stability. It is further demonstrated with absolute measurements of photoluminescence quantum yields (PL-QYs), that the PL-QYs of aqueous CdTe QDs can be considerably increased upon incorporation into a salt matrix by applying the "classical" crystallization procedure. The achievable PL enhancement factors depend strongly on the PL-QYs of the parent QDs and can be described by the change of the dielectric surrounding as well as the passivation of the QD surface. Studies on CdSe/ZnS in NaCl and CdTe in borax showed a crystal-induced PL-QY increase below the values expected for the respective change of the refractive index, supporting the derived hypothesis of surface defect curing by a $CdCl_x$ formation as one main factor for PL-QY enhancement.

The mixed crystals developed in this work show a high suitability as color conversion materials regarding both their stability and spectral tunability. First proof-of-concept devices provide promising results. However, a combination of the highest figures of merit at the same time is intended. This ambitious goal is reached by implementing a model-experimental feedback

approach which ensures the desired high optical performance of the used emitters throughout all intermediate steps. Based on the approach, a white LED combining an incandescent-like warm white with an exceptional high color rendering index and a luminous efficacy of radiation is prepared. It is the first time that a combination of this highly related figures of merit could be reached using QD-based color converters.

Furthermore, the idea of embedding QDs into ionic matrices gained considerable interest in the scientific community, resulting in various publications of other research groups based on the results presented here.

In summary, the present work provides a profound understanding how this new class of QD-salt mixed crystal composites can be efficiently prepared. Applying the different crystallization methods and by changing the matrix material, mixed crystals emitting from blue to the near infrared region of the electromagnetic spectrum can be fabricated using both Cd-containing and Cd-free QDs. The resulting composites show extraordinary optical properties, combining the QDs spectral tunability with the rigid and tight ionic matrix of the salt. Finally, their utilization as a color conversion material resulted in a high-quality white LED that, for the first time, combines an incandescent-like hue with outstanding optical efficacy and color rendering properties. Besides that, the mixed crystals offer huge potential in other high-quality applications which apply photonic and optoelectronic components.

Contents

Abbreviations

CCT	Correlated color temperature
C-dots	Carbon dots
CIE	Commision Internationale de l'Eclairage
CQS	Color quality scale
CRI	Color rendering index
DDT	1-Dodecanethiol
EDA	Ethylenediamine
EU	European Union
FWHM	Full-width-at-half-maximum
GSH	Glutathione
HID	High intensity discharge
IR	Infrared
LE	Luminous efficacy
LED	Light emitting diode
LER	Luminous efficacy of radiation
LLDC	Liquid-Liquid-Diffusion-Assisted-Crystallization
MPA	Mercaptopropionic acid
MSA	Mercaptosuccinic acid
MUA	Mercaptoundecanoic acid
NIR	Near infrared
NP	Nanoparticle
OA	Oleic acid
OAm	Oleylamine
OD	Optical density
PA	Palmitic acid
PLE	Photoluminescence excitation
PL-LT	Photoluminescence lifetime
PL-QY	Photoluminescence quantum yield
PMMA	(Poly)methylmethacrylate
PS	(Poly)styrene

PT	Phase transfer
QD	Quantum dot
RoHS	Restriction of Hazardous Substances
SILAR	Successive ionic layer adsorbtion and reaction
SSL	Solid state lighting
TEM	Transmission electron microscopy
TGA	Thioglycolic acid
TOP(O)	Trioctylphosphine(oxide)
UNESCO	United Nations Educational, Scientific and Cultural Organization
UV	Ultraviolet
Vis	Visible
w-LED	White light emitting diode

1. Introduction

In 2015, the UNESCO's "International Year of Light and Light-based Technologies" draws worldwide attention on one of the key factors influencing humanities evolution. [1] Starting already more than 100,000 years ago with the purposeful use of log fires, every evolutionary step in lighting technologies marked a remarkable increase in the general standard of living and education. The last and probably also largest step was the electrification of light, thus enabling the access to bright daylight conditions even at night in an easy and safe way. Nevertheless, general lighting is also one of the largest energy consumers, with a share in end-point electricity usage of nearly one fifth. [2] To reduce lighting's energy consumption or keep it at least constant in the future, several measures where implemented including the recent ban of incandescent bulbs within the European Union (EU). [3] Light emitting diodes (LEDs) are seen as one of the most promising candidates to fill this gap. Generating white light using LEDs can be done using either a combination of three or four differently colored LEDs or by placing down-converting phosphors on top of a blue or ultra-violet (UV)-LED. [4] State-of-the-art commercial white LEDs (w-LEDs) are mainly produced using the second approach and a rare-earth based phosphor. This setup provides only a cold, bluish shade of white, due to its lack of a sufficient amount of emitted photons in the red spectral region.
Semiconducting materials in the nanometer size regime, so-called quantum dots (QDs) appeared on the screen, recently. [5] In comparison to their bulk counterparts, QDs display different physical and chemical properties. Quantum confinement, as one of these, causes the QD band gap to scale with its size, thus enabling to tune the absorption and emission properties of the QDs by changing their size. Since their first description in the early 1980's, [6,7] a lot of research has been done enabling the reproducible synthesis of highly efficient, narrow-band emitting QDs covering the electromagnetic spectrum from UV to infrared (IR) with barely more than a handful of materials needed. [8–10] Therefore, QDs have successfully been applied as color conversion materials in scientific research and industrial applications. [11,12] Regarding the latter point, both QD Vision and Samsung shall be mentioned as pioneers. However, the QDs still suffer from the rigid conditions during the hybridization process onto the LED

as well as the diffusion of oxygen trough the encapsulating materials. For these reasons, the present work focuses on the incorporation of different QDs emitting in the visible (Vis) and IR region into several ionic matrices, forming so-called QD-salt mixed crystals. Aqueous dispersions of QDs are added to saturated salt solutions and stored, till oversaturation causes the mixed crystal formation. In a subsequent step, those are grinded to a fine powder and blended onto a blue LED as color conversion layer. By adjusting the amount of differently emitting mixed crystals, the hue of the final device can be tuned, providing a large range of accessible colors. Concerning the parental QD solutions, the first part of Chapter 2 provides the synthetic approaches for different QDs. The second part of this chapter deals with the production of the mixed crystals themselves, presenting the different measures to optimize the crystallization procedure. Regarding aqueous-based QDs, the addition of extra stabilizer as well as the reproducible incorporation of QDs into several matrices is discussed. In comparison, QDs with an organic-based synthetic approach are examined regarding their ligand exchange and phase transfer procedure into aqueous media and a short outlook on Cd-free materials is provided. Furthermore, the production of mixed crystals emitting in the IR-regime is shown. Finally, different crystallization methods are reviewed regarding the potential for different QDs and their applicability in terms of color conversion devices. Chapter 3 deals extensively with the optical and structural investigations of the parental QDs and their associated mixed crystals. Since the optical efficiency is one crucial factor for lighting applications, a main section of this chapter discusses the development of photoluminescence lifetime (PL-LT) and photoluminescence quantum yield (PL-QY) upon incorporation. Within this part, structural reasons for the observed behavior shall be derived and, if possible, applied to increase the overall efficiency of the materials. Secondly, transmission electron microscopy (TEM) investigations and the problems arising from insulating samples under electron beam irradiation are examined. Producing a high quality LED requires a basic understanding on the human vision and how this influences luminaire manufacturing, being the first part of Chapter 4. Subsequently, a model-experimental feedback approach to produce and optimize high quality warm w-LEDs using mixed crystals is presented. Within this approach, each step from QD synthesis via mixed crystals preparation to hybridization onto the blue LED is reviewed in respect of ensuring the applicability as color conversion materials for w-LEDs. Finally, Chapter 5 overviews recent achievements of other groups to provide a thorough insight into the young field of QD-salt mixed crystals.

References

[1] UNESCO; The International Year of Light, **2014**.

[2] International Energy Agency; Energy efficiency: Lighting, **2014**.

[3] VERORDNUNG (EG) Nr. 244/2009, **2009**.

[4] J.Y. Tsao, *IEEE Circuits and Devices Magazine*, **2004**, *20*(3), 28.

[5] QDVision; TCL 55 Quantum Dot TV with Color IQ Optics Debuts at CES 2015, **2015**.

[6] L. E. Brus, *The Journal of Chemical Physics*, **1984**, *80*(9), 4403.

[7] H. Weller, U. Koch, M. Gutiérrez, and A. Henglein, *Berichte der Bunsengesellschaft für Physikalische Chemie*, **1984**, *88*(7), 649.

[8] L. Bakueva, S. Musikhin, M. A. Hines, T.-W. F. Chang, M. Tzolov, G. D. Scholes, and E. H. Sargent, *Applied Physics Letters*, **2003**, *82*(17), 2895.

[9] P. O. Anikeeva, J. E. Halpert, M. G. Bawendi, and V. Bulović, *Nano Letters*, **2009**, *9*(7), 2532.

[10] N. Gaponik, S. G. Hickey, D. Dorfs, A. L. Rogach, and A. Eychmüller, *Small*, **2010**, *6*(13), 1364.

[11] E. Jang, S. Jun, H. Jang, J. Lim, B. Kim, and Y. Kim, *Advanced Materials*, **2010**, *22*(28), 3076.

[12] S. Kim, T. Kim, M. Kang, S. K. Kwak, T. W. Yoo, L. S. Park, I. Yang, S. Hwang, J. E. Lee, S. K. Kim, and S.-W. Kim, *Journal of the American Chemical Society*, **2012**, *134*(8), 3804.

2. Synthesis of Quantum Dots and Preparation of Mixed Crystals

2.1. Quantum Dots: Synthetic Approaches

During the last three decades, many different protocols for synthesizing semiconducting QDs have been established, including approaches in organic and aqueous media, methods involving microwaves, etc. [1–5] Nearly all of them have one thing in common: Their final products are inorganic QDs covered with a shell of organic molecules, mainly referred to as stabilizing agents or ligands. Depending on the nature of the synthetic protocol and the resulting QDs, suitable stabilizing agents include bi-functional short-chain thiols and amines, polymers as well as long-chain aliphatic carboxylic acids, amines, phosphines, thiols and many more. These molecules play a major role in preventing aggregation of single QDs to bulk assemblies. Secondly, they protect the inner core from environmental chemical reactions and saturate dangling bonds on the inorganic surface. Furthermore, their chemical structure defines the solubility and stability of the QDs within different solvents, a key parameter in this work. To ensure a sufficient stability of QD colloids within saturated salt solutions, several factors need to be taken into account.

Water-based QDs are inherently miscible with saturated aqueous solutions of inorganic salts making them the first candidates for the production of QD-salt mixed crystals. Nevertheless, their ligand shell needs to be strong and thick enough to withstand the high ionic strength of the saturated salt solution during the crystallization procedure. On the other hand, oil-based QDs have to be transferred to the aqueous phase before they are mixed with saturated salt solutions, making a ligand exchange procedure necessary. Still, this possibly quality-affecting additional step in the preparation of mixed crystals is accepted since only oil-based synthetic approaches provide access to some QD types.

In this chapter, a short overview of synthetic approaches for different QD systems, their benefits and disadvantages will be given. In the second part, all particular measures and

approaches allowing the preparation of QD-salt mixed crystals will be discussed and compared to each other. This includes the "classical" preparation by using aqueous-based CdTe QDs and NaCl as a host as well as methods derived from this starting point. Furthermore, several ligand exchange procedures will be compared regarding their quality and applicability for mixed crystallization. In the end, section 2.4 will focus on the preparation of QD-salt composites emitting in the near-infrared (NIR) region of the electromagnetic spectrum. As mentioned above, most of the QD properties and attempts of crystallizing them are affected by stabilizing agents. Figure 2.1 provides an overview of all stabilizers used during the synthesis and ligand exchange procedures described within this work.

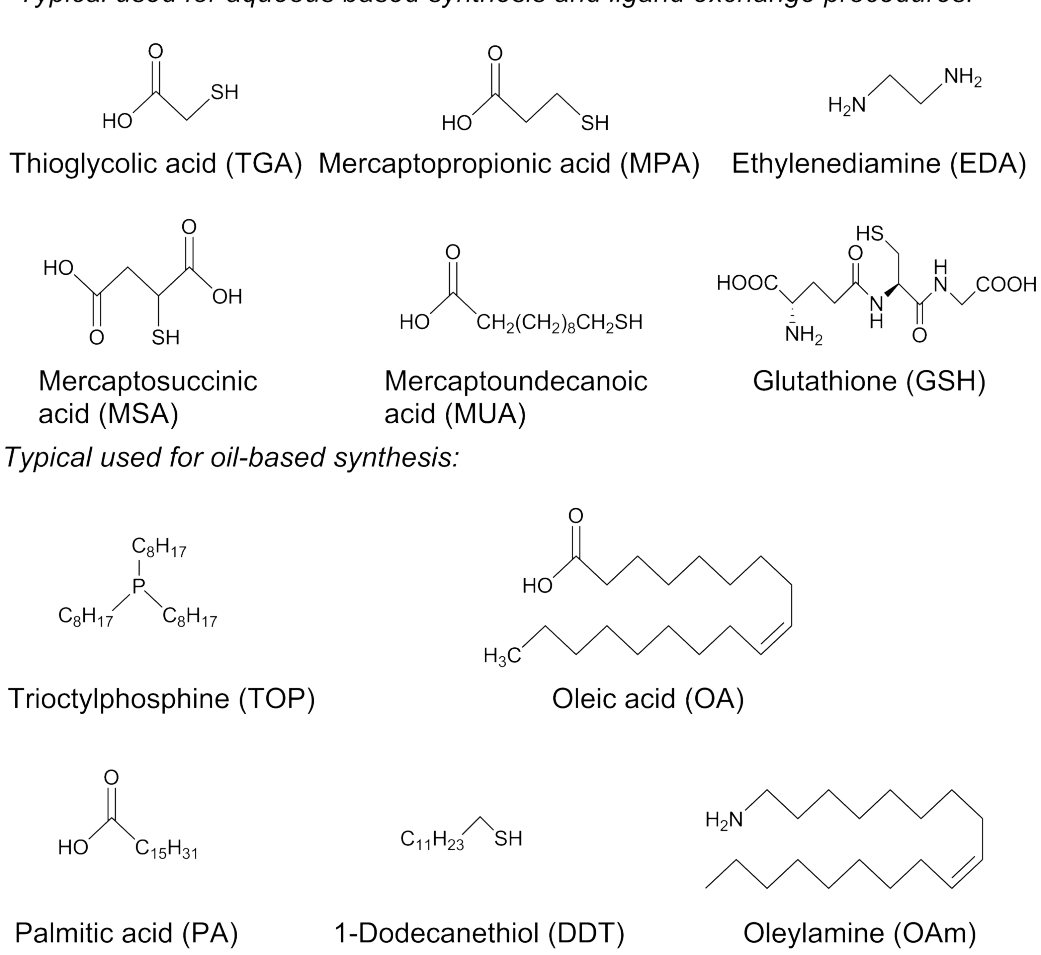

Figure 2.1.: Overview of typical stabilizing agents used for synthesizing the different QDs, the subsequent ligand exchanges and their abbreviations used in this work.

2.1.1. Synthetic Approaches in Aqueous Media

CdTe and $Cd_{1-x}Hg_xTe$ QDs were synthesized by using water as the solvent. A huge variety of stabilizing agents is known for both systems and extensively discussed in the literature. [6–9] In this work, TGA and MPA were used as the only stabilizers due to their well-known behavior, high PL-QY of the resulting QDs and the variability they offer during the synthesis. A detailed description of the synthetic procedure, based on references [10, 11], will be given in the Appendix. In both cases, the two-step synthesis separates the cluster formation and the particle growth. In the first stage, cations form a complex with the stabilizer, causing a white turbidity of the solution. The extent of this turbidity is more distinct for MPA-based and/or Hg containing systems. Subsequently, H_2Te is slowly passed through the solution which contains the stabilizer-cation complexes, causing a cluster formation and a strong color change of the solution into a brownish-red. During the second step, refluxing induces the growth of the clusters while the final size of the resulting QDs can be adjusted by keeping the solution under reflux.

In the case of MPA-stabilized CdTe QDs, the typical growth periods vary from less than one minute up to a few hours. Such synthesis yields QDs showing absorbance and PL spectra exemplarily given in Figure 2.2 with PL-QYs between 10 and 45% for green and deep red emitting fractions, respectively. The synthesis is relatively fast due to the larger size of MPA and a smaller complexation constant for Cd-thiol in comparison to TGA [12, 13], causing a weaker stabilization of small QDs and therefore a more rapid growth.

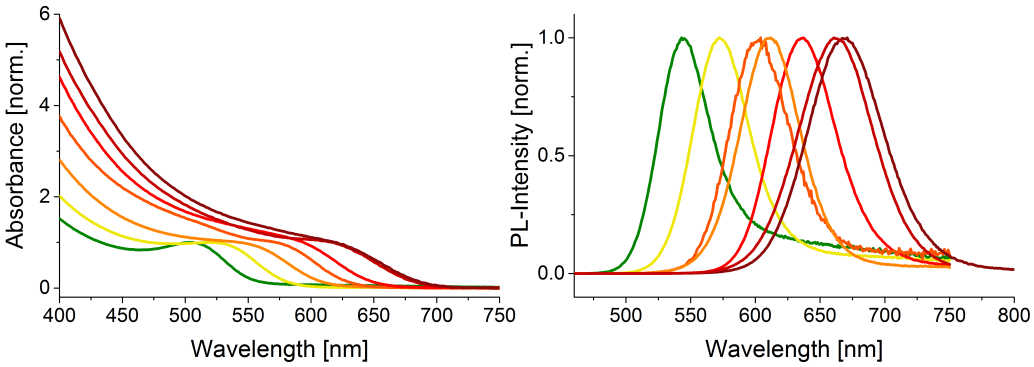

Figure 2.2.: Representative overview of absorption (left) and PL (right) spectra for MPA-stabilized CdTe QDs synthesized in water. All spectra were normalized to the first absorption peak or the emission maxima. All samples were synthesized by using the protocol given in reference [10].

Thereby, longer emission wavelengths are accessible by using MPA as stabilizing agent and also provoke a broader size distribution of the QDs. This can be seen directly in the PL spectra as large full-width-at-half-maximum (FWHM). The blurred 1s-1s transition in the absorbance spectra is typical for larger CdTe QDs due to a weaker quantum confinement effect. [14] Nevertheless, CdTe QDs stabilized with MPA emit a pure and intense color, as it can be seen in Figure 2.3

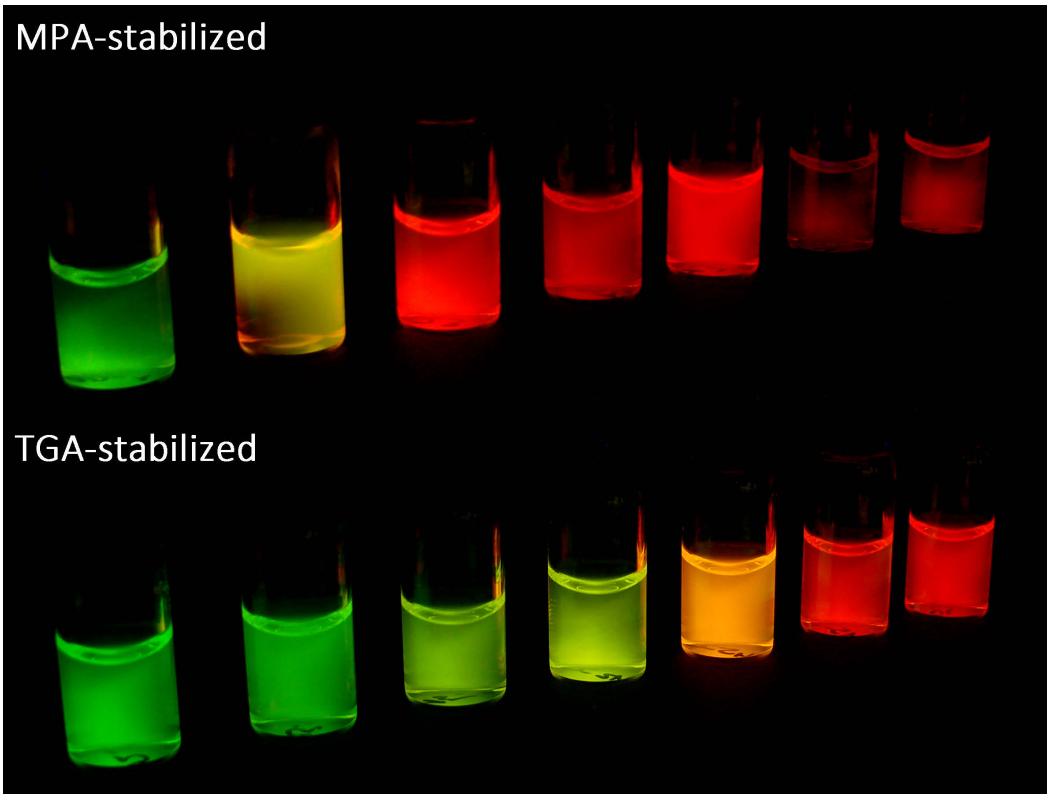

Figure 2.3.: True-color image of representative batches of CdTe QDs under 365 nm excitation. The CdTe QDs are either stabilized with MPA (top row) or TGA (bottom row), while the corresponding absorption and PL spectra can be found in Figures 2.2 and 2.4 respectively.

By using TGA as a stabilizing agent for CdTe QDs, a slightly different picture has to be drawn. The higher complexation constant and the smaller TGA size create a stronger Cd-thiol complex during the first stage of the synthesis as well as a better surface coverage of the final QDs. Both effects reduce the QDs growth rate significantly, leading to longer synthesis times but also narrower size distributions. This can be directly seen in the more distinct 1s-1s transition and the smaller FWHM in the absorbance and PL spectra, respectively, as shown in

Figure 2.4. This slower growth rate predetermines TGA-stabilized CdTe QDs to be the more suitable alternative for the green-orange region of the spectrum where PL-QYs of 30 - 60% can easily be achieved. In contrast, deep red emitting fractions of CdTe QDs stabilized by TGA can only be accessed by extensive synthesis lasting up to several days, already affecting the overall quality of the batches.
Both types, TGA- and MPA-stabilized CdTe QDs, show a generally high stability of their optical properties and a colloidal solution upon storage over long time intervals, proving their suitability as emitting centers for co-crystallization processes.

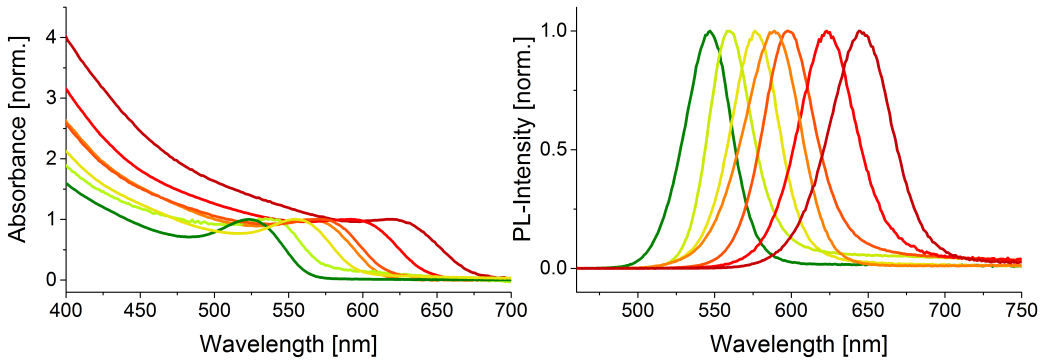

Figure 2.4.: Representative overview of absorption (left) and PL (right) spectra for TGA-stabilized CdTe QDs synthesized in water. All spectra were normalized to the first absorption peak or the emission maxima, respectively. All samples were synthesized by using the protocol given in reference [10].

Nevertheless, CdTe QDs only offer the possibility to create QDs with emission maxima up to ~850 nm. [11] Shifting their PL-emission into the NIR region can be achieved by preparing alloyed CdHgTe QDs with a molecular formula of $Cd_{1-x}Hg_xTe$, where small amounts of Cd are replaced with Hg. This exchange can be done either post-synthetic [15, 16] or during the synthesis. [11] Although both approaches provide different assets and drawbacks, the second approach was chosen for this work to avoid the necessity of a time consuming shelling procedure required for the first method. In these ternary systems and in contrast to CdTe QDs, the optical properties are not only defined by the reaction time and size, but also by the incorporation of Hg into the resulting QDs and the availability of Hg, as discussed in detail in reference [17]. All samples shown in Figure 2.5 were synthesized by using MPA as stabilizing agent and with mercury precursor amounts of 3 to 10 mol.%. MPA was chosen as a stabilizing agent because it showed the highest stability during the co-crystallization process for CdTe QDs. By varying the amounts of mercury precursors, QD batches emitting in the

range from 900 to 1100 nm could be synthesized, providing access to the so-called diagnostic windows in the NIR region. [18]

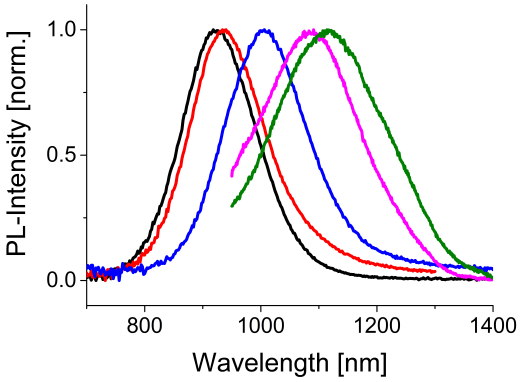

Figure 2.5.: PL spectra of $Cd_{1-x}Hg_xTe$ QDs synthesized in water with varying Hg content. The samples were synthesized by using a slightly modified procedure of reference [11].

2.1.2. Synthetic Approaches in Organic Media

As already discussed above, oil-based QD synthesis also rely on stabilizing molecules. Here, different sets of stabilizers, mainly long aliphatic chains with a functional head group, are used, as depicted in Figure 2.1, to ensure solubility and colloidal stability within the non-polar hydrophobic solvents. In contrast to water-based approaches, a larger variety of QD systems is accessible, but often core-only QDs (e.g., CdSe, CdTe, InZnP, PbS) are not long-term stable under ambient conditions and/or have only limited PL-QY. In most cases, shelling procedures were proved to be a suitable and reliable method to overcome the disadvantages. [19] In these protocols, a shell of a different inorganic material (e.g., ZnS, CdS) with a lower reactivity and a larger band gap is deposited onto the QDs. The shell serves as a chemical and electrical barrier, both reducing the tendency of core-environment reactions and confining the exciton within the core. The probably most common method to grow shells on QDs is the so-called successive ionic layer adsorption and reaction (SILAR) approach [20], in which each monolayer of the shell material is deposited consecutively. By using SILAR, discrete interfaces are created, in which lattice mismatches between the core and shell materials can induce defects, thereby potentially reducing the optical quality of the final QD system.
To avoid this potential weakness, a different approach was used for producing CdSe/ZnS QDs within this work. Since CdSe and ZnS have a large lattice mismatch, intermediate shells

of CdS would be necessary to reduce lattice strain if discrete shelling procedures were applied. Hence QDs with an alloyed shell were used, possessing in radial direction both an energy level and a composition gradient. Such alloyed structures can be prepared in a straightforward single-step synthesis where all precursors are simultaneously brought together. Earlier studies proved [21] that CdSe cores are initially formed due to the higher reactivity of the Cd and Se precursors in comparison to Zn and S precursors, respectively. Subsequently, intermediate $Cd_{1-x}Zn_xSe_{1-y}S_y$ species and a final outermost layer of nearly pure ZnS are grown. Similar to aqueous-based CdHgTe QDs, the ratios of the precursors have both an influence on the optical properties and the reaction time. Therefore a careful adjustment of these ratios yields QD batches with emission and absorption properties tunable from cyan to red, as shown in Figures 2.6 and 2.7. Especially the cyan fractions are highly interesting since these colors are not accessible via aqueous routes with a satisfactory PL-QY and stability. As described elsewhere [22], a similar approach can also be used to produce high-quality blue emitting CdS/ZnS QDs with an alloyed gradient shell which will not be discussed in the present work.

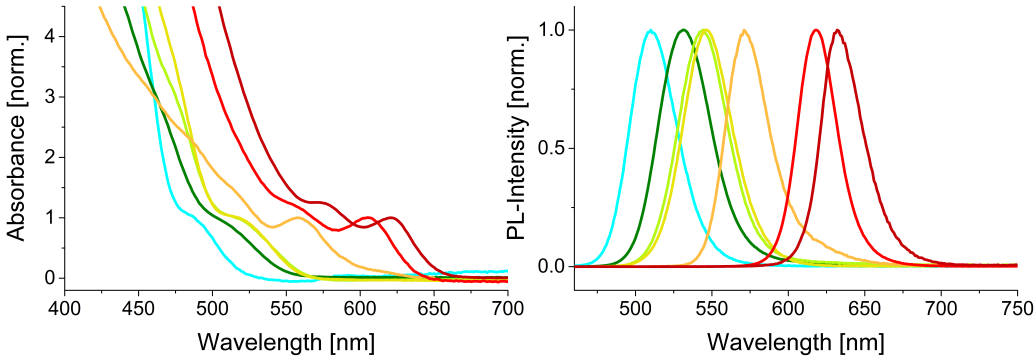

Figure 2.6.: Representative overview of absorption (left) and PL (right) spectra for CdSe/ZnS QDs with an alloyed gradient shell. All spectra were normalized to the first absorption peak or the emission maxima. These samples were synthesized in organic media by using a modified version of the protocol described in reference [23]. The red- and yellow-emitting samples shown here were kindly provided by Gordon Stachowski and Christoph Bauer.

Figure 2.7.: True-color image of CdSe/ZnS QDs with an alloyed gradient shell under 365 nm excitation. The corresponding spectra of these samples can be found in Figure 2.6.

As Cd-based materials are well analyzed but potentially highly toxic, their transfer to final applications is limited. As a potential alternative, Cd-free QDs, mainly based on In compounds, were analyzed. Two different systems, namely InZnP and Cu-doped InZnS, were chosen here. The InZnP, shelled with GaP and ZnS to protect it from environmental influences and increase the PL-QY, can easily be compared to Cd-based QDs, due to its similar exciton relaxation procedure and a direct linkage of core size and band gap. These materials, whose spectra are exemplarily shown as dotted lines in Figure 2.8, exhibit 1s-1s transitions in the absorption spectra and broad PL spectra that are typical for In-based materials. Furthermore, the inner GaP shell mitigates the lattice mismatch of the InZnP and ZnS, thereby releasing stress and reducing the risk of creating defects during the shelling procedure.
Cu-doped InZnS as the second Cd-free alternative comprises a different system of exciton relaxation also inducing a non-direct core-size to band gap connection. The absorption of the photons and thereby the exciton creation takes place in the InZnS host material with a subsequent non-radiative electron relaxation towards the Cu-level. From this point, the radiative relaxation to the host's electronic ground states occurs. Since both the host material and the dopant are involved in the exciton relaxation process, the resulting emission is mainly composition tunable instead of size-related. Nevertheless, a shelling of the crude cores with a wide band gap material (ZnS) is necessary to ensure proper stability and PL-QY, especially during the subsequent ligand exchange procedures. It should also be noticed that such dopant emission processes exhibit excitonic lifetimes of hundreds of nanoseconds.

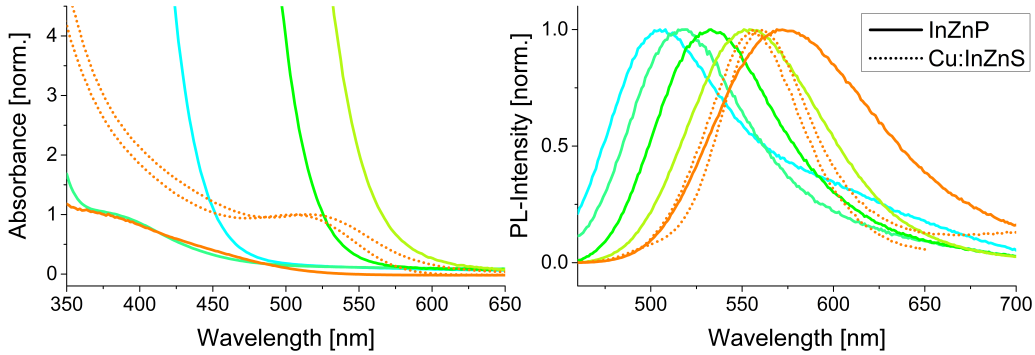

Figure 2.8.: Representative overview of absorption (left) and PL (right) spectra for Cd-free QDs. The solid lines show the spectra of Cu:InZnS/ZnS QDs while the dotted lines represent InZnP/GaP/ZnS QDs respectively. All spectra were normalized to the emission maxima and, if applicable, the first excitonic transition in the absorption spectra. Cu:InZnS/ZnS QDs were synthesized by using a modified version of reference [24] while the InZnP/GaP/ZnS QDs were prepared according to reference [25]. Five of the samples shown here were kindly provided by Josephine Lox and Christian Meerbach.

Next to the samples and batches discussed above, some of the following QD-salt mixed crystal incorporation studies were done by using QDs solely provided by other group members. This applies in detail to all subsequent discussions on PbS QDs synthesized by Dr. Stefanie Gabriel and carbon dots (C-dots) provided by Laura Kühn. Furthermore, the CdSe/CdS quantum dots for phase-transfer analyses were provided by Dr. Klaus Boldt and Dr. Christian Waurisch. Their preparation will not be discussed in this work, however, detailed information on the synthetic procedures can be found in references [26–29].

2.2. Preparation of Mixed Crystals*

This section focuses on incorporating QDs of different compositions into ionic crystals by using different approaches. Embedding QDs into polymers or inorganic matrices attracted considerable attention due to the expected increase of QD stability in the matrices and the ease of processability in conjunction with relatively low production costs. [35–38] In terms of application as devices for lighting displays, as optical gain media, photovoltaics, and color conversion materials, both the high brightness and long-term stability of such photoluminescent

*Parts of this chapter have already been published. [30–34]

solid composites are of special interest. [30, 39–41] Common organic polymers like poly(methyl methacrylate) (PMMA) and poly(styrene) (PS) as hosts can be processed easily. However, they have relatively high oxygen diffusion coefficients ($2.3 \cdot 10^{-7}$ and $3.3 \cdot 10^{-9}$ cm^2/s respectively) [42, 43] which are inappropriate to protect the QDs from photo-oxidation processes. Furthermore, rigid conditions during the polymerization process, e.g., free radicals or strong UV exposure, reduce the overall quality and long-term stability of the embedded QDs. The majority of inorganic materials, although they are probably less processable, provide on the contrary an extremely robust and airtight matrix for the embedded substances. The combination of these beneficial properties together with the tunable emission and high extinction coefficients of colloidal QDs allows us to create a new class of superior photonic materials.
Nevertheless, several actions have to be taken to provide a sufficient stability of the QDs within the saturated salt solution to ensure their proper encapsulation and the formation of non-powder-like mixed crystals. These analyses, including the control of the particles surface, the prevention of QD aggregation, the time needed for incorporation and the influences of different matrices, will be discussed in the upcoming section.

2.2.1. Mixed Crystals from Aqueous-based CdTe QDs

The preparation of QD-salt mixed crystals was demonstrated in 2012 for the first time by using CdTe QDs as emitting centers and conventional salt crystals such as NaCl, KCl, KBr, etc. [30] In contrast to long-known salts doped with semiconductor particles by using the Czochralski process, [44] the mixed crystals presented here were grown at ambient temperatures by the crystallization from saturated aqueous solutions of the respective salts additionally containing colloidally prepared, strongly photoluminescent QDs.
As described in the Appendix, the "classical" procedure for preparing mixed crystals is straight forward. Water-soluble QDs are mixed with saturated solutions of the corresponding salts and stored for periods of several days up to several weeks in which the slow evaporation of water, oversaturation and consequently crystallization take place. Alternatively, the crystallization can take place when hot saturated salt solutions are cooled down, especially in the case of salts (e.g., KBr) with a steep temperature dependence of their solubility. However, the resulting large crystallization rates (complete crystallization within less than an hour) lead to a low nanocrystal loading. All data presented in this section have therefore been obtained following the crystallization at room temperature. As seen from the images in Figure 2.9, the microcrystalline phase forming around the edges of the beakers is purely white, and therefore

QD free, while the macrocrystals formed on the bottom of the glass are significantly colored due to the incorporation of QDs.

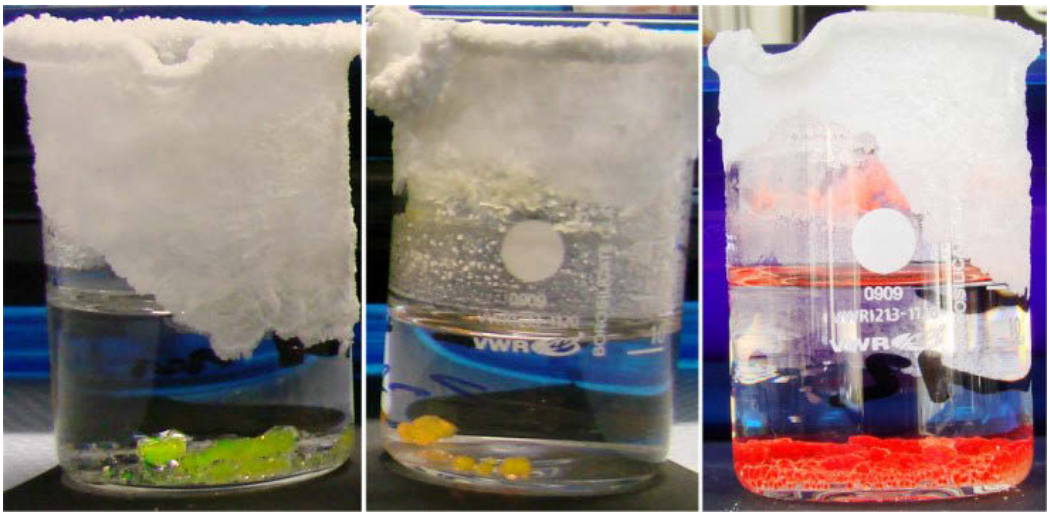

Figure 2.9.: Final stage of the NaCl crystallization in the presence of CdTe QDs of different sizes. Mixed crystals formed on the bottom of the glass appear colored due to embedded QDs. Reprinted by courtesy of Nano Lett. 2012, 12, 5348. Copyright 2012, American Chemical Society.

Before they were characterized further, the mixed crystals were taken out of the beaker and rinsed with cold water to remove residual QDs or any by-product of the synthesis precipitated or aggregated from their surface. In cases in which the QD concentration was very high or the QDs had a relatively low stability in salt media it was noticed that some precipitation of QD aggregates may emerge on the bottom of the beaker. To avoid unnecessary losses of QDs, the concentration ratio of the components in the solution for the co-crystallization should be experimentally optimized for each QD batch. The results reported below are obtained from mixed crystals prepared via optimized routes. Besides the NaCl-based materials, mixed crystals can also be prepared by using KCl, KBr and K-Na tartrate as host matrices. Examples of these combinations are presented in Figure 2.10 a) - c), however, a detailed discussion will be conducted in Chapter 2.3.

The main challenge in the preparation of mixed crystals is to achieve a reasonable long-term stability of the colloidal QDs in the presence of saturated salt solutions. Premature coagulation would indeed result in a precipitation of QD aggregates and their removal from the crystallization process.

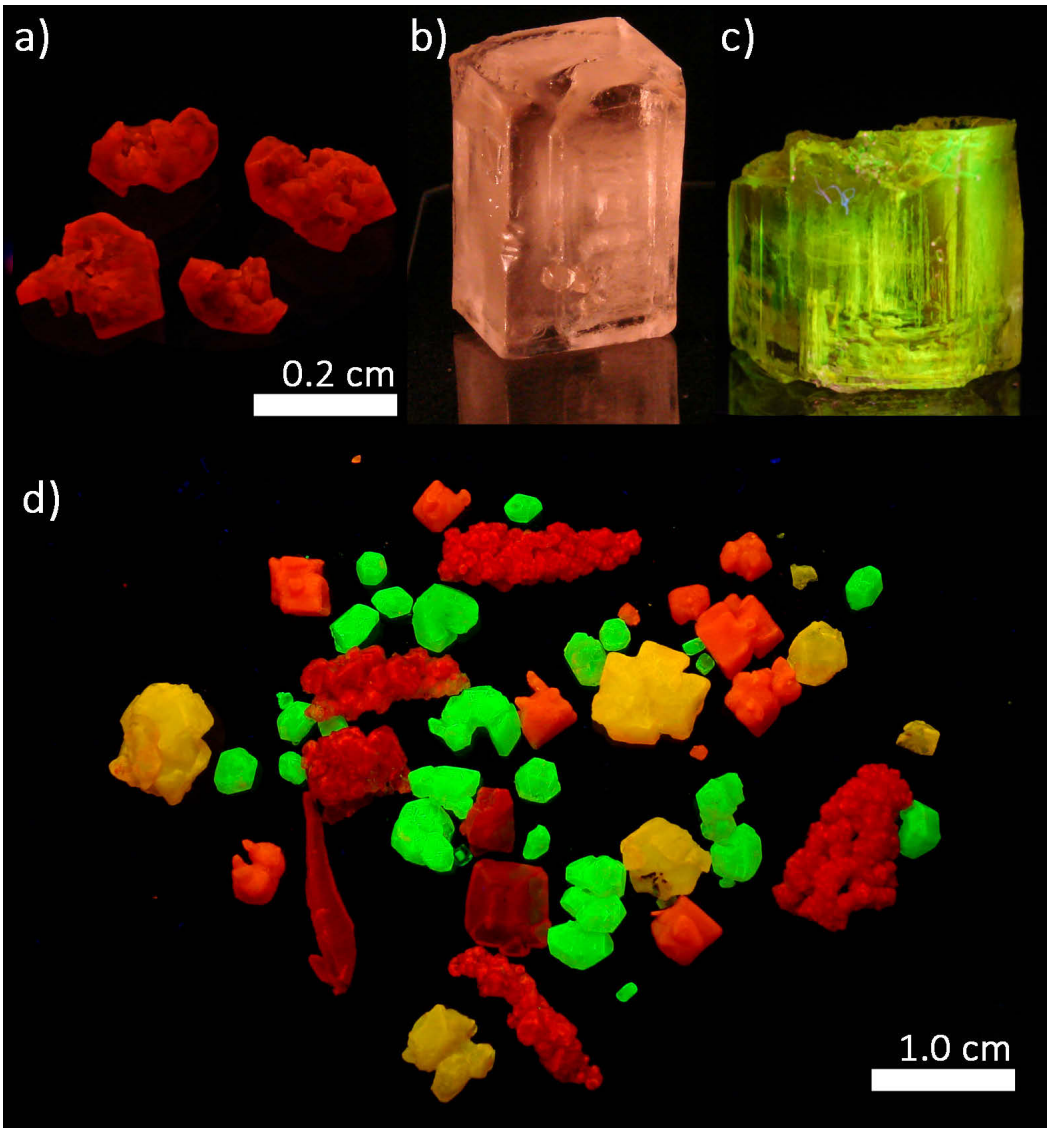

Figure 2.10.: Mixed crystals with differently emitting CdTe QDs incorporated into KCl (a), KBr (b), K-Na tartrate (c) or NaCl (d) as host matrices. Images a), c) and d) were taken under 365 nm UV-excitation, while image b) was taken under simultaneous daylight and UV-excitation. Adapted by courtesy of Nano Lett. 2012, 12, 5348. Copyright 2012, American Chemical Society.

Thus, the QDs which were directly synthesized in water in the presence of short-chain thiols are most suitable for the mixed crystallization. The required stabilization may be achieved, for example in the presence of TGA or MPA. Although both capping agents are suitable, MPA-stabilized QDs proved to be generally more stable in saturated salt solutions than

their TGA-stabilized counterparts. Therefore, TGA-stabilized QDs tend to agglomerate and precipitate earlier and more distinct, leading to more losses during the crystallization process. This behavior could be explained by mainly longer refluxing periods for TGA-stabilized QDs, causing a partial decomposition of the TGA and thereby a reduced stability of the resulting QDs in high ionic strength media. The overcoming of this disadvantage will be discussed in detail in Chapter 2.2.2.

Figure 2.10 d) shows representative images of mixed NaCl based crystals containing CdTe QDs under 365 nm excitation. As seen from this figure, the mixed crystals exhibit different but not cubic shapes which would be expected for NaCl-based crystals. This different morphology of the host material can be attributed to free stabilizing agents (TGA or MPA) within the QD-salt solution mixture. Such small and coordinating molecules are well-known to alter the shape of NaCl crystals from cubic to octahedral. [45] Thereby, the morphology of NaCl-based mixed crystals can be considered as a directed feedback regarding the amount of excess stabilizers within the parental (and thereby also the pure QDs) solution. At the same time an uniformly distributed emission from the incorporated CdTe QDs is shown. The PL spectra of the crystals cover a spectral region ranging from ca. 550 to ca. 630 nm.

As seen from Figure 2.11, the PL spectral characteristics of the mixed crystals resemble to a large extent those of the QDs in solution. A red shift of the PL maximum can be observed in the crystals and may be explained by changes in the dielectric constant of the surrounding media as well as by reabsorbing the blue part of the spectrum in optically dense samples. An energy transfer between the well-separated QDs in the composite is less probable. A sufficient difference in the PL-LTs between mixed crystal samples and the QDs in aqueous solution (Figure 2.11 b)) could indeed not be observed. This is also considered to be a direct evidence for maintaining or even a slight improvement of the initial PL-QY of the embedded QDs which will be discussed in detail in Chapter 3.1.1. The shorter PL-LT of the dissolved crystal sample is attributed to a partial aggregation of the QDs in the diluted ionic salt solution. Such a PL-LT shortening due to a non-radiative recombination of excitons is commonly observed in QD aggregates. [7, 46]

As a next step and in order to reduce the formation time of mixed crystal from several weeks to a few days, the crystallizations were conducted in an oven at slightly increased temperatures. First experiments at 30, 40 and 50 °C showed a reduction to 7, 5 and 4.5 days respectively. All temperatures significantly increased the mixed crystal formation while the gain in speed of 40 and 50 °C was less distinct in comparison to a crystallization at 30 °C. Since this temperature also involves the lowest thermal stress to the QDs, all subsequently discussed mixed crystals were produced at 30 °C in an oven. Besides that, the increased

crystallization speed offers the possibility to incorporate QDs with lower colloidal stability. Furthermore, constant conditions within the oven reduce the influence of varying ambient temperatures and therefore increase the reproducibility of the mixed crystal formation.

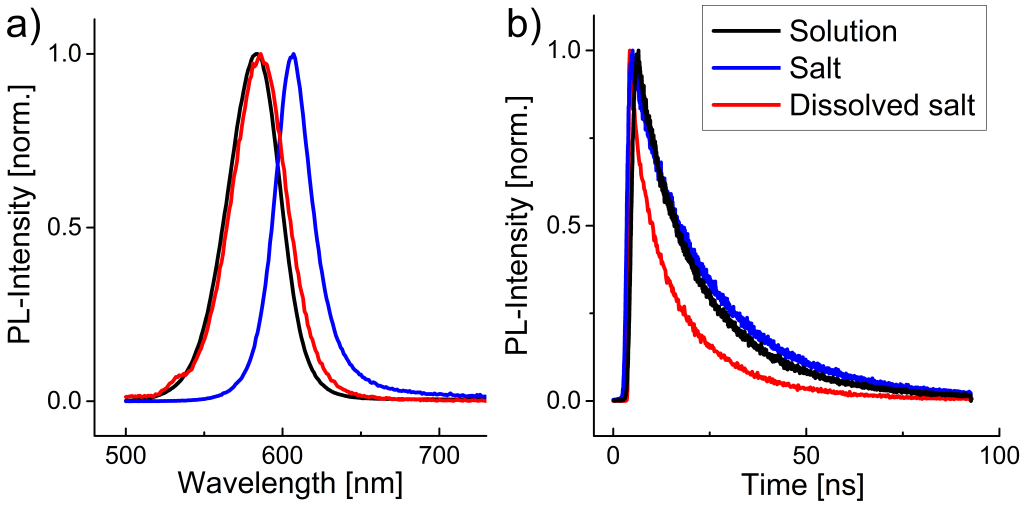

Figure 2.11.: Steady-state PL spectra (λ_{ex} = 450 nm) (a) and time-resolved (λ_{ex} = 470 nm) decay traces (b) of an initial aqueous solution of CdTe QDs (black), mixed CdTe QDs-NaCl crystals (blue) and of the aqueous solution obtained after dissolving the mixed crystal (red). Adapted by courtesy of Nano Lett. 2012, 12, 5348. Copyright 2012, American Chemical Society.

2.2.2. Influence of pH, Free Stabilizer and Type of Salt on the Embedding of TGA-stabilized QDs

As discussed in the previous section, the incorporation of MPA-stabilized CdTe QDs is a facile and easy method to prepare high-quality QD-salt mixed crystals. In comparison, the preparation of such composites by using TGA-stabilized CdTe QDs causes some difficulties, due to a limited stability of the TGA-capped QDs within the saturated salt solution. As a result, the incorporation of TGA-capped QDs into salts often resulted in low QDs loading within very small powder like crystals and undesirable agglomeration of QDs outside the crystals. However, TGA-capping provides the possibility of better synthesis control especially for CdTe QDs of relatively smaller sizes emitting in green to orange spectral regions. [47,48] Since for most applications a photoluminescence covering the whole visible range is needed, the reproducible and efficient incorporation of strongly emitting TGA-capped CdTe QDs

into salt matrices is a natural next step during the expansion of the QD-salt mixed crystal approach. These issues will be addressed in the upcoming section while providing a path for the reproducible incorporation of such high-quality CdTe QDs into NaCl and KCl salt crystals without producing powder-like, weakly emitting mixed crystals and/or a loss of large amounts of QDs due to aggregation. Therefore, different salts used as host matrix, the amount of additional free stabilizer and the pH value of the saturated salt solution were used as parameters for the optimization.

To obtain high-quality QD-salt mixed crystals, the parameters of crystallization media like the concentration of additional free stabilizer, the pH value and the host material (NaCl or KCl) were systematically varied. Additional TGA stabilizer was added to ensure a sufficiently high density of stabilizers in the direct environment of the QDs, since TGA can decompose partly during the synthesis, reducing the stabilizer amount and thus the colloidal stability. [49] The pH value of the salt solutions was varied in the range of 10-12 to ensure a full deprotonation of the stabilizer and to keep the electrostatic forces strong enough to maintain colloidal stabilization in presence of the saturated salt solutions. [50, 51]

Addition of free stabilizer

At first the ideal amount of additional free stabilizer was examined by using a freshly prepared 1 M TGA solution. The amounts of excessive stabilizer are given below as ratios to initial amounts used in the synthesis.

For mixed crystals with NaCl as host, generally small, nearly powder-like crystals are observed when no free stabilizer is added. These composites show a red shift in their emission (see Figure 2.12 a) which mainly derives from the undesired aggregation of QDs and not the matrix effects. This aggregation was verified by dissolving one of these crystals, resulting in an only weakly emitting diluted solution while the majority of QDs is still aggregated and forms a precipitate. Upon the addition of free stabilizer, regardless of the added amount, relatively large crystal monoliths are formed, as depicted in Figure 2.13. The best results were obtained with a 0.5- to 2.0-fold amount of free stabilizer. For these TGA amounts, the QD-salt mixed crystals are homogenous, as shown in Figure 2.13, and show a yellow-greenish emission which is blue shifted with respect to the initial QDs in solution. The mixed crystals with twice the amount of extra stabilizer yield the strongest luminescence. The addition of a 0.5- to 1.5-fold amount still yields strongly emitting mixed crystals, whereas excessive amounts of free TGA higher as two-fold causes PL quenching. Nevertheless, when adding free stabilizer to the crystallization solution, the PL peaks broaden in comparison to the initial colloidal solution.

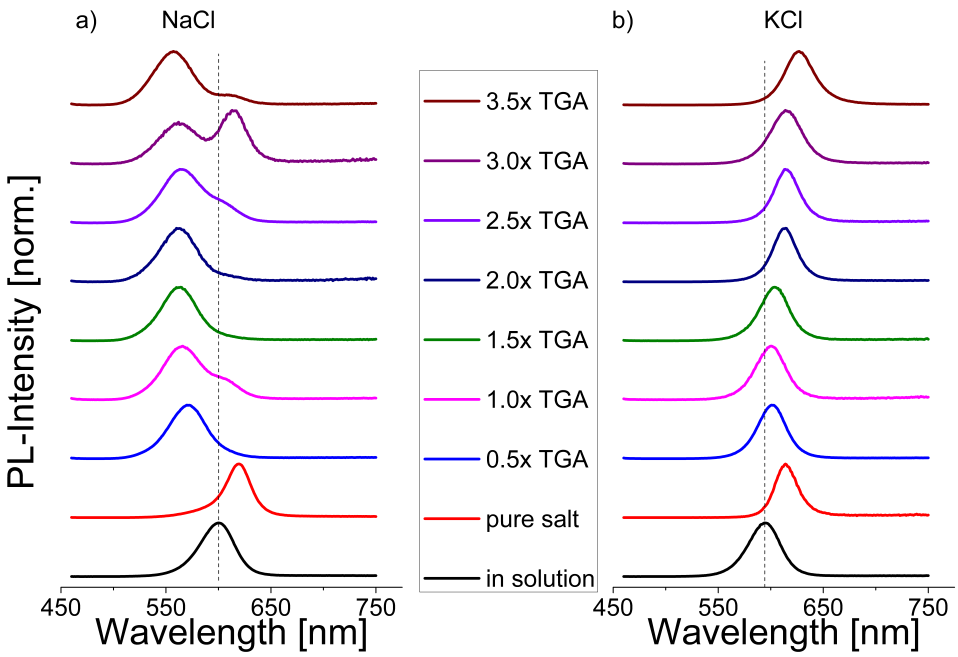

Figure 2.12.: Normalized PL spectra (λ_{ex} = 450 nm) of CdTe QDs mixed with different amounts of free stabilizer and embedded into a) NaCl or b) KCl, respectively. The spectra were stacked for more clarity and show the development of their shape and position with respect to the added amount of free stabilizer. The dotted lines in a) and b) represent the PL-maximum of the initial QD colloids. Reprinted by courtesy of Z. Phys. Chem. 2015, 229, 109. Copyright 2015, De Gruyter.

Larger amounts of free TGA are leading to a diminished emission which is shifted to higher energies, indicating a deterioration of the QD quality (see Figure 2.12 a) and Figure 2.13). Together with the reduced emission at higher stabilizer concentrations, the incorporation of aggregates might appear. For example, the appearance of an additional long-wavelength maximum for the crystal prepared in the presence of three-folds of free-stabilizer (Figure 2.12 a)) could be attributed to a red shifted emission of such aggregates. The mixed green-orange emission originating from different parts of the same crystal is also observed in the photography of the corresponding sample presented in Figure 2.13 (highlighted with an arrow).
As a second salt, potassium chloride was used as a host matrix. For these mixed crystals, the optimal amount of excessive free stabilizer is one fold of the respective amount used within the synthesis, yielding mixed crystals with an even composition. Here, the spectral blue shift upon the incorporation does indeed not appear, but a slight red shift is visible with increasing

the amount of free stabilizer, as shown in Figure 2.12 b). Furthermore, in comparison to NaCl as a host material, the PL spectra are not broadened but narrowed upon incorporation. An additional amount of 1.0- to 1.5-fold of TGA yields the best mixed crystals for KCl. By increasing the amount of free stabilizer to twice or more, the resulting mixed crystals were less homogeneous and more powder-like. If, on the other hand, no stabilizer is added, KCl also shows a stronger red shift similar to that discussed for NaCl. Due to the better predictability and reduced deterioration of the QDs, KCl was further used as the preferred host matrix for TGA-stabilized CdTe QDs.

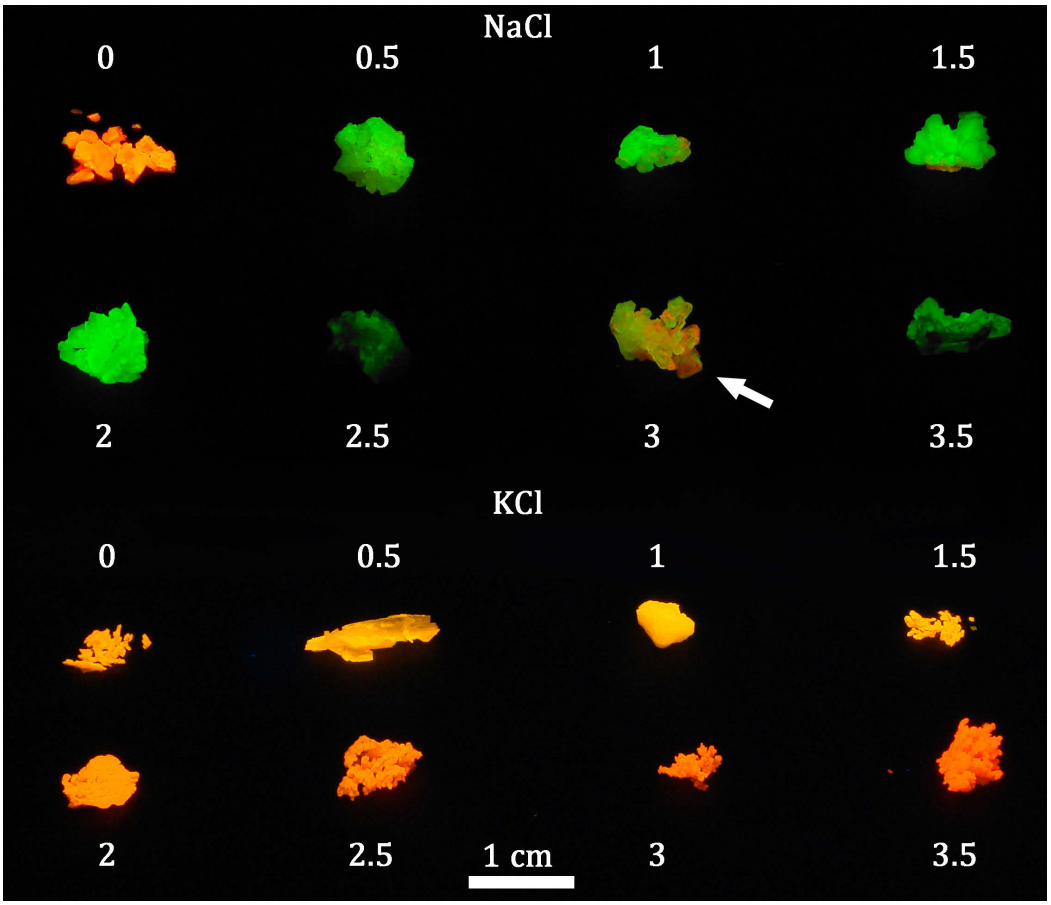

Figure 2.13.: Photography of the TGA concentration series by using NaCl (top) and KCl (bottom) as host matrix. The numbers give the amount of additionally added free stabilizer with respect to the amount used in the synthesis. In the case of the NaCl-QD mixed crystal with a threefold amount of additional stabilizer (highlighted by an arrow), two emission colors are clearly visible. Adapted by courtesy of Z. Phys. Chem. 2015, 229, 109. Copyright 2015, De Gruyter.

To evaluate the origin of the different behavior of the two salts, the evolution of the emission properties of dissolved mixed crystals was analyzed, as shown in Figure 2.14. In contrast to previous findings regarding MPA-stabilized particles, [30] dissolving the mixed crystal does not restore the PL spectrum of the initial colloidal solution. Here, the PL spectrum is blue shifted, while the overall shape stays constant. This shift, with 45 nm for NaCl and 9 nm for KCl, strongly depends on the host matrix and reveals that TGA-stabilized CdTe QDs experience a significant chemical change when getting in contact with the saturated salt solution. Such shift in the PL-maximum is generally associated with the etching of the QDs and thereby a reduction in size. [10] The stabilizing agent TGA plays hereby a divalent role. On the one hand it stabilizes the QDs, preventing their aggregation and the formation of relatively strong complexes with the etching products on the other hand (most probably Cd^{2+} which is the dominant ionic species on the surface of the QDs), favors the ongoing etching. These TGA-Cd^{2+} complexes are stronger than the equivalent complexes formed by MPA and Cd^{2+} which is a possible explanation that the etching is only observed for TGA-stabilized CdTe QDs. [12, 13] When comparing the host matrices it can be noticed that KCl and NaCl yield different evolutions of the QDs optical properties upon incorporation. Both salts crystallize in a sodium chloride structure where the cations and anions are octahedrally surrounded by their counter ions. The major difference of these salts are their lattice constants, 5.63 Å and 6.26 Å for NaCl and KCl respectively. [52] The incorporation procedure of the quantum dots into the ionic matrix has not yet been clarified in detail.

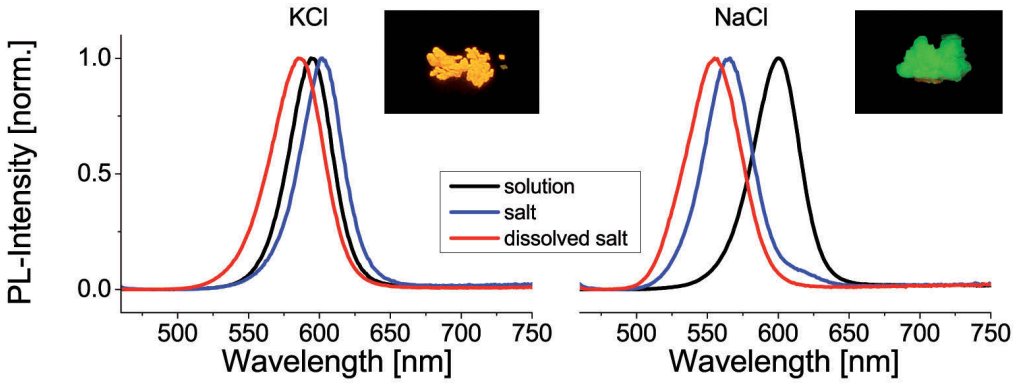

Figure 2.14.: Steady-state PL spectra (λ_{ex} = 450 nm) of an initial CdTe QDs solution (black line), mixed crystals with KCl and NaCl as host matrix (blue line) and the aqueous solution obtained after dissolving a mixed crystal (red line). The insets show the corresponding mixed crystals under UV light, emitting yellow-orange (KCl) and green (NaCl). Adapted by courtesy of Z. Phys. Chem. 2015, 229, 109. Copyright 2015, De Gruyter.

The current understanding of the process is based on the assumption that QDs injected in the concentrated salt solutions act as seeds for the crystallization with a thin salt shell being immediately formed around them. As it can be seen in Figures 2.13 and 2.14, NaCl causes a distinct blue shift of the emission while KCl keeps it nearly constant. A possible explanation for this might be the different ionic radii of Na^+ and K^+ which are 102 and 138 pm respectively, [53] making it easier for Na^+ to reach the QD surface for chemical reactions. Furthermore, the molar concentrations of saturated solutions from NaCl and KCl differ by more than 30% (KCl: 4.65 M NaCl: 6.14 M) providing a higher ionic strength and a generally higher concentration of ions that may cause chemical reactions on the surface of the QDs and result in QD aggregation.
In summary of this part, the optimum amount of free stabilizer is between 1.0- to 2.0-fold with the best quality at 2.0-fold for NaCl and 1.0-time for KCl matrices. In each case, the addition of the free stabilizer leads to a slight etching of the QD surfaces, resulting in a PL blue shift in comparison to the initial colloid. Adding a free stabilizer does not lead to mixed crystals with a powdery nature and a red shift in their emission color with respect to the solution. KCl turned out to be the better choice for TGA-capped CdTe QDs, since the observed etching is much lower resulting in higher predictability of the formed mixed crystals.

Influence of the pH value on the production of mixed crystals

Besides the amount of free stabilizing agent and type of salt, the pH value of the saturated salt solution also influences the properties of the resulting mixed crystals. Saturated salt solutions with an alkaline pH of 10, 11 or 12 were analyzed, since CdTe QD colloids possess the highest stability within this pH range. [50,51]
Additionally, optimized conditions with an 1.0- and 2.0-fold amount of free stabilizer for both salts were applied. The results are summarized in Figure 2.15. As expected, for NaCl, a strong blue shift is observed whereas for KCl the initial PL-maximum stays only slightly shifted or nearly constant upon incorporation of QDs. When the free stabilizer is not used, only relatively weak emitting powder-like crystals may be obtained at all pH values (see as an example Figure 2.16).

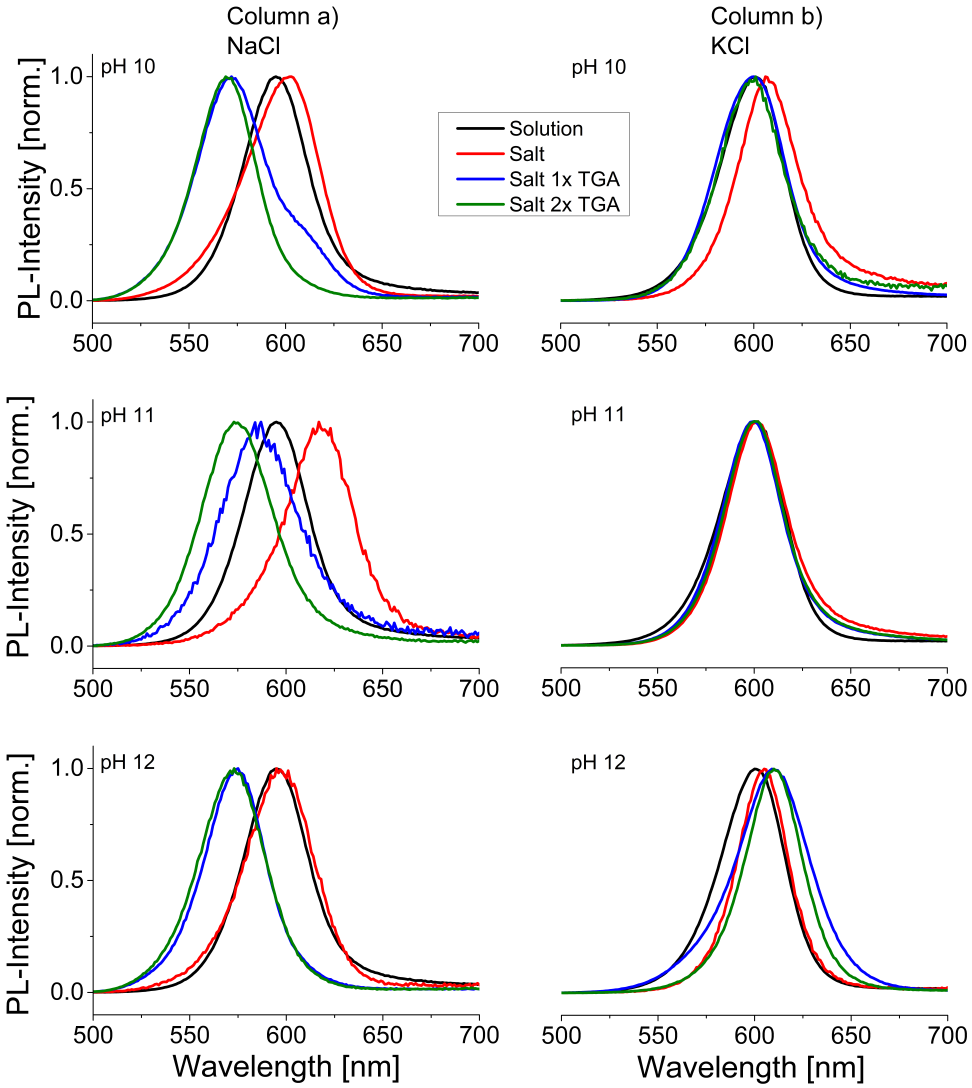

Figure 2.15.: PL spectra of similar sized TGA-capped CdTe QDs incorporated in NaCl or KCl as host. The pH of the saturated salt solutions was adjusted to the given values and for each set, mixed crystals using either pure QDs colloids or with additional stabilizer were prepared. Adapted by courtesy of Z. Phys. Chem. 2015, 229, 109. Copyright 2015, De Gruyter.

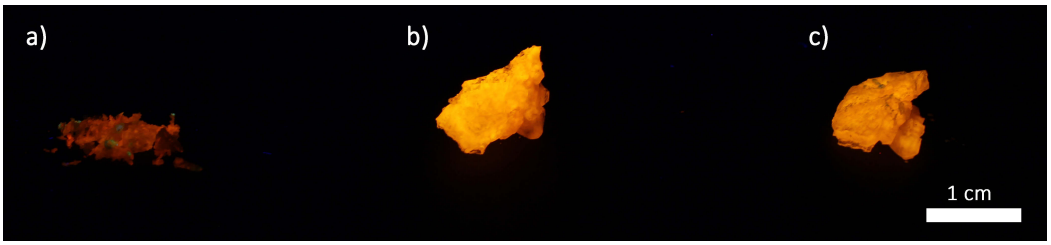

Figure 2.16.: QD-KCl mixed crystals with just a) pH adjustment, b) pH and one time excess of free TGA and c) pH and two fold excess of free TGA. Adapted by courtesy of Z. Phys. Chem. 2015, 229, 109. Copyright 2015, De Gruyter.

As evidenced from Figure 2.17, the best results for KCl were obtained at pH 11 adding a 1-fold amount of free stabilizer. The obtained mixed crystals have a very stable and strong morphology that is not powder-like, whereas an obvious shift of the PL maximum is not observed.

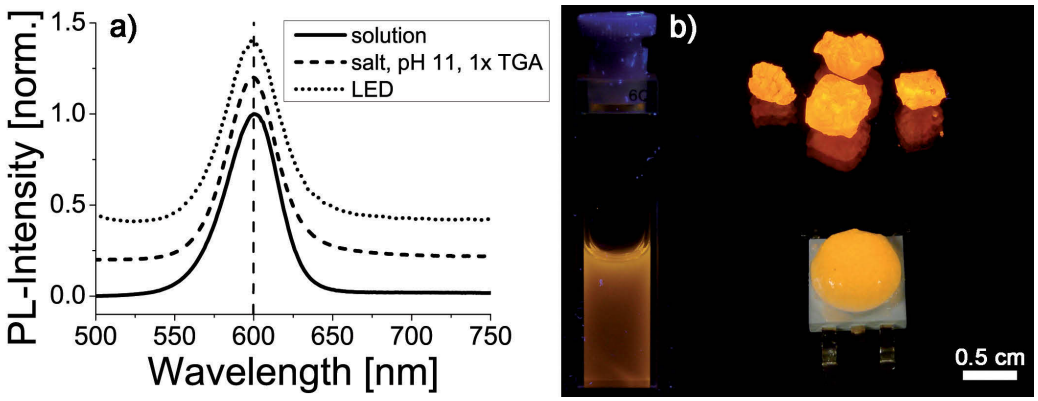

Figure 2.17.: PL spectrum (λ_{ex} = 450 nm) of mixed crystals composed of TGA-stabilized CdTe and KCl (a), dashed line) as well as the corresponding spectra of the initial colloidal solution (solid line) and the final LED (dotted line). The latter one is measured under electrical pumping of a blue emitting InGaN chip. This blue emission line of the chip is cut out for more clarity. Frame b) shows true-color images of corresponding samples, i.e., CdTe QDs in form of colloidal solution, the same QDs embedded in KCl crystals as well as the LED with color conversion layer containing these crystals. All three photographs were taken under 365 nm excitation, showing the same emission color (orange) for the solution, crystals and the conversion layer. Adapted by courtesy of Z. Phys. Chem. 2015, 229, 109. Copyright 2015, De Gruyter.

In comparison to the results presented in Figure 2.13, this is an important step toward reproducible applications in lighting technologies. These optimized mixed crystals composed of KCl and TGA-capped CdTe QDs show the same shape and position of the PL spectra compared to the initial colloidal solutions. They can be applied as color conversion materials (see Figure 2.17 a) and b)) for creating high-quality white or single color light sources. [30,54] To verify the generality of these optimized conditions, the above discussed crystallization procedure were applied to TGA-stabilized CdTe QD batches with PL-maxima at 574 nm and 633 nm. From each QD batch, mixed crystals with NaCl and KCl as host matrix were prepared by using either pure salt solutions or pH-optimized (pH 11 and 12 respectively) mixtures with a one- or two-fold amount of additional TGA. The corresponding PL spectra can be found in Figure 2.18.

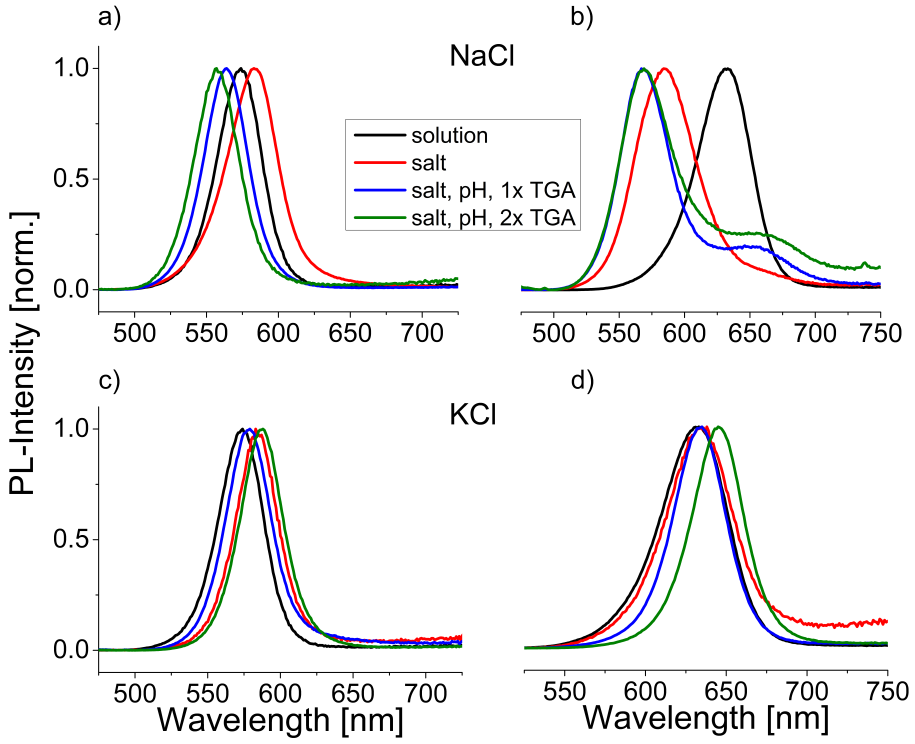

Figure 2.18.: Differently sized QDs incorporated into NaCl (top) and KCl (bottom). Frames a) and c) show the PL spectra of yellow-emitting particles whereas frames b) and d) show the corresponding spectra for red-emitting particles. Adapted by courtesy of Z. Phys. Chem. 2015, 229, 109. Copyright 2015, De Gruyter.

To summarize this section, a method for the reproducible and predictable integration of TGA-capped CdTe QDs into salt matrices was presented. The influencing parameters such

as salt type, amount of additionally added free stabilizer and pH value were varied. The adjustment of pH to an alkaline range of approximately 11 as well as the addition of a one- to two-fold amount of free stabilizer to the crystallization solution yielded the best results for KCl and NaCl respectively. However, the crystallization from saturated NaCl solutions causes a strong etching of the QDs during the crystallization process which results in an undesired blue shift of the PL spectrum upon incorporation. KCl has proven to be the better choice to be used as host matrix for TGA-capped CdTe QDs, since a deterioration of the QD quality could hardly be noticed. These optimized conditions are proven to be reproducible and to work for several different batches of similar sized as well as differently sized TGA-stabilized CdTe QDs.

2.2.3. Carbon Dots

Fluorescent materials based on carbonesceous species (carbon dots or C-dots) in the nanometer range have been attracting increasing attention since they were first discovered about one decade ago during the cleaning of carbon nanotubes. [55] Their synthetic procedures are mainly conducted in an aqueous environment from abundant precursors, making them a reasonable candidate for mixed crystallization with ionic matrices. This class of materials possesses furthermore excitation wavelength dependent PL spectra with their highest intensity in the blue region. [56, 57]

The formation of mixed crystals was conducted by using NaCl as host material and the highly concentrated as synthesized C-dot solution. As shown in Figure 2.19 a) and b), both the solution and the mixed crystals show excitation-dependent PL spectra, as expected, while there is no difference in the PL spectra when a lower or higher amount of C-dot solution is used for preparing the mixed crystals. The most obvious observation can clearly be seen in images c) and d), showing that even the mixed crystals with higher amounts of C-dots show only a pale brownish color in comparison to the initial solution. On the other hand, the mixed crystals show a bright blue emission under 254 nm UV excitation as shown in Figure 2.19 f), proving that the incorporated C-dots preserve their high emission intensity. After harvesting the crystals, a strongly colored parental solution remained which is another clear indication for the poor incorporation of these materials into the ionic host. In comparison, parental solutions of QD-salt mixed crystals were colorless after the formation was complete, proving the complete embedding of the QDs within the salt. Apart from that, the C-dots proved to be extraordinary stable within the salt solutions, allowing a recycling of the remaining parental solution. Therefore, the remaining part was refilled with a pure saturated NaCl solution which

could be repeated four times without affecting the colloidal stability or optical properties of the C-dots.

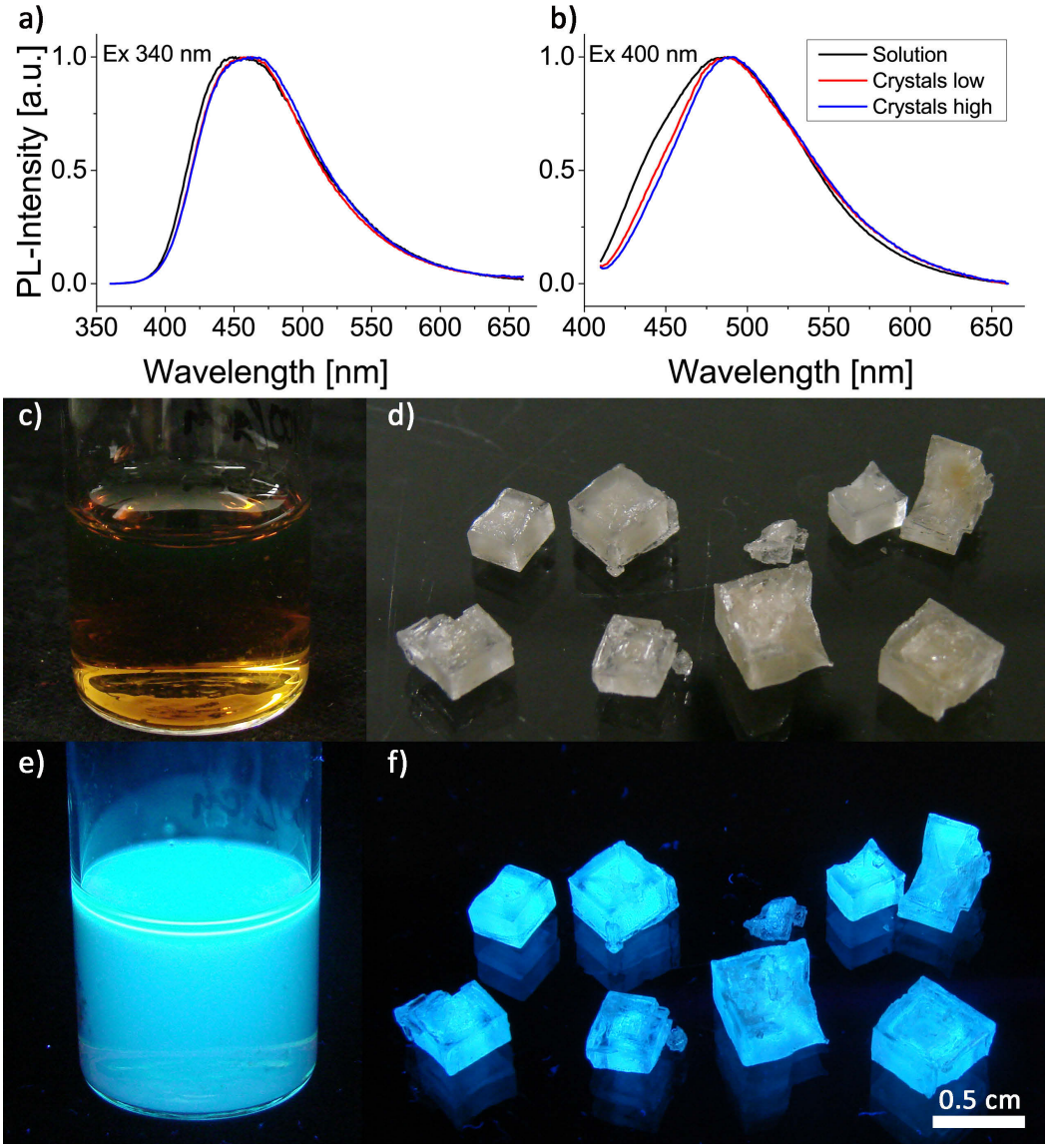

Figure 2.19.: PL spectra of C-dots embedded into NaCl at a) λ_{ex} 340 nm and b) λ_{ex} 400 nm. The black line represents the initial colloidal solution while the red and blue line are PL spectra of mixed crystals with lower or higher loading amounts of C-dots. (c-f) True-color images of C-dots in solution and the corresponding mixed crystals with higher loading amounts. Images c) and d) were taken under ambient lighting while images e) and f) was taken under 254 nm UV excitation.

Although promising results were obtained, three main weaknesses of the C-dot based mixed crystals prevent their wide application despite their presumably lower toxicity in comparison to other analyzed systems. First of all, the low loading of the mixed crystals with emitting material would require large amounts in order to form an adequately thick conversion layer. Secondly, nature and origin of the PL of these C-dots is not clear yet. And finally, a UV source emitting in the range from 300 to 400 nm would be needed to excite the blue luminescence which is not favorable in an energetic way. Therefore, upcoming work will focus on analyzing the optical properties and the stability of the composites in more detail.

2.2.4. Mixed Crystals from Oil-based QDs

Ligand Exchange Processes

Quantum dots synthesized in organic media often have a better tunability in the higher energy part of the electromagnetic spectrum and a smaller FWHM in the low energy region compared to e.g. aqueous based CdTe QDs. Unfortunately, their surfaces are covered with long-chain ligands, making them non-miscible with water-based saturated ionic salt solutions. To overcome this drawback, two main strategies can be suggested: a) utilizing macrocrystals of organic substances and b) phase transfer of QDs from nonpolar solvents to water and subsequent crystallization as discussed above. Unfortunately, the first method delivers only relatively unstable organic-based crystals that cannot be considered as strong and stable matrices for QDs suitable for lighting applications. The application of the second method is limited by a relatively high tendency of phase-transferred QDs in order to coagulate in strong ionic media. The second approach is nevertheless more promising, since the colloidal stability can be tuned more easily than the general properties of organic crystals.
The basic principle of a ligand exchange includes the replacement of the original ligands due to a higher affinity of one of the new ligands' functional groups towards the QDs surface atoms. In most cases, the thiol group of bi-functional short-chain ligands like MPA binds via Lewis acid-base interactions to Cd or Zn atoms on the surface, as depicted in Figure 2.20.
Since the new stabilizing ligands can bind to both the Cd and Zn surfaces, the question arises why CdSe/ZnS QDs with an alloyed gradient shell are utilized, whereas CdSe/CdS QDs with a distinct shell have been shown with PL-QYs reaching almost unity for several years. [58] At the first glance, these materials provide an excellent basis for high-quality color converting layers with minimal amounts of material. Unfortunately, their transfer to water is not possible without a dramatic deterioration of the initial PL-QY. [58] This behavior can be attributed to

the position of the band edge of these materials in comparison to the standard potential of most of the commonly used thiols. [59] For both the pure CdSe and the CdSe/CdS core/shell QDs, the valence band edge is below the standard potential of the used thiols causing a hole trapping on the QDs surface. Since both the hole and electron are needed for a radiative recombination, hole trapping strongly reduces the PL-QY of such systems. On the other hand, depositing a ZnS shell on the QDs strongly suppresses this mechanism. The valence band edge of ZnS is still below the thiols potential but the difference between the ZnS and CdSe band gaps is big enough to confine the electron and the hole in the core effectively.

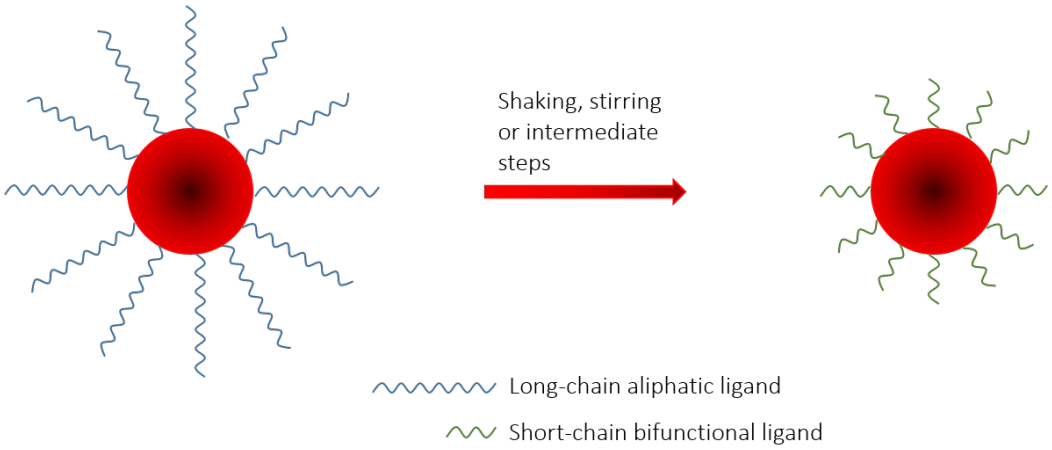

Figure 2.20.: General illustration of the replacement of oil-based QDs initial aliphatic ligands by using exchange methods with short-chain bifunctional molecules as new stabilizing agents.

To find a suitable ligand exchange process ensuring colloidal stability of the QDs in aqueous media while having only minor influence on the optical properties, several procedures were tested which will be explained experimentally in more detail in the Appendix and consecutively numbered. A brief overview of the different methods is given in Table 2.1. Procedures which do not replace the initial ligands but wrap another layer organic material around the existing stabilizing agents are generally also well-known. Unfortunately, such "wrapped QDs" are not stable in high ionic strength media at all.

Table 2.1.: Overview of the applied ligand exchange procedures

Label	Initial solvent	Initial stabilizers	New stabilizers	QDs used in orig. reference	Reference
PT1	$CHCl_3$	TOP, OA, ODE	MPA	CdSe/ZnS Alloy	[21]
PT2	Hexan	TOP, HPA	MPA	CdSe/CdS	[60]
PT3	Hexan	TOPO, OA	AMP	CdSe/CdS/ZnS	[61]
PT4	Hexan	OA	AOT	CdSe	[62]
PT5	$CHCl_3$	ODA	MPA	CdSe/ZnS	[63]
PT6	$CHCl_3$	ODA	MPA	InAs/CdSe/ZnSe	[64]
PT7	$CHCl_3$	TDPA, TOP	MPA	CdTe/CdSe and CdTe/CdSe/ZnS	[65]
PT8	$CHCl_3$	TOP, TOPO	TGA	CdSe/ZnS	[66]
PT9-11	$CHCl_3$	SA, HDA	TGA, MPA etc.	InP/ZnS	[67]
PT 12	$CHCl_3$	OA, OAm, TOP	MPA, MSA, TGA, MUA	CdSe/ZnS	[68]
PT 13	$CHCl_3$	OA	GSH	PbS	[69]

The ligand exchange procedure described in reference [21] which will be defined as PT1 (phase transfer 1) was used as the starting point. Large amounts of pure MPA as new stabilizing agent and temperatures up to 100 °C are necessary in this protocol to ensure a proper exchange. In the second step, the QDs with their new stabilizing agents are precipitated, washed and dispersed in slightly alkaline water. Figure 2.21 a) displays a representative PL spectrum of alloyed CdSe/ZnS QDs before and after the ligand exchange, proving that the position and shape of the QDs emission is nearly unaffected. Unfortunately, the PL-QY drops to 30-50% of its initial value. The resulting colloidal solution can remain stable up to several weeks in alkaline aqueous environment but tends to precipitate in contact with a saturated NaCl solution due to the high ionic strength. Some mixed crystals could nevertheless be grown by utilizing QDs that were subject to the PT1 ligand exchange procedure. Although the first results were promising, different approaches had to be analyzed in order to avoid the excessive use of MPA. Secondly, the temperature applied in the exchange procedure under ambient conditions might be harmful to the QDs. PT 2-11 were analyzed in the second step according to literary approaches. [60–67] Most procedures proved to have only a limited capability when transferring the here used QDs into the aqueous phase successfully.

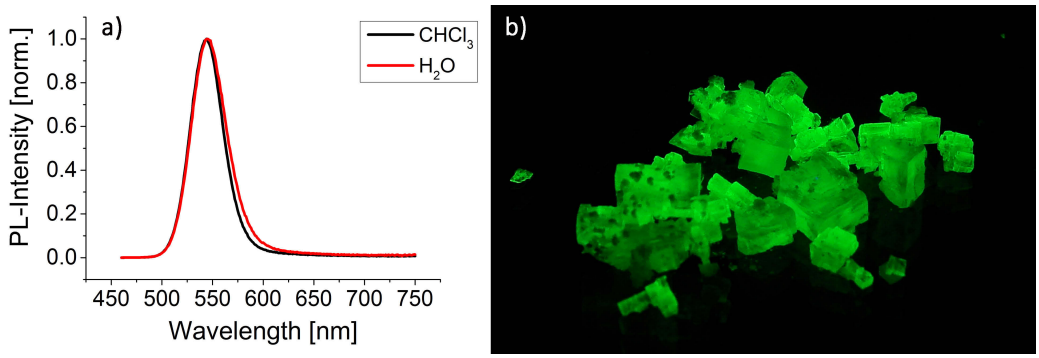

Figure 2.21.: a) PL spectrum of alloyed CdSe/ZnS QDs before (black line) and after (red line) the ligand exchange by using the PT1 procedure according to reference [21]. b) Resulting QD-NaCl mixed crystals under 365 nm excitation.

Only the method described by Reiss et al. [67] (PT9-11) showed a reproducible and stable phase transfer for CdSe/ZnS QDs with an alloyed gradient shell. By using this protocol, a highly diluted QD solution is mixed with an alkaline 0.2 M solution of the replacing ligand and vigorously shaken for four hours. Due to the two-phase system, long-chain aliphatic ligands which were removed from the QDs surface can remain in the organic phase, whereas the short-chain thiol capped QDs move to the aqueous phase, thereby separating reagent and product. In the end, the phases have to be separated and the resulting aqueous colloid can be used without further purification due to only a small access of stabilizer. The method is capable of exchanging the initial QD ligands with either TGA, MUA or MPA. All three stabilizers produce QD colloids in water, although TGA has the highest tendency to form agglomerates as well as the lowest emission intensity after the exchange. MUA on the other hand yields stable and highly emissive colloids in water, but these samples strongly agglomerate upon contact with any kind of saturated salt solution analyzed, making MPA the first choice. Such MPA-based solutions have been strongly luminescent and stable under ambient conditions and light influences for more than six months, proving the high quality and completeness of the exchange procedure. Figure 2.22 e) shows a representative PL spectrum of CdSe/ZnS QDs with an alloyed gradient shell in $CHCl_3$ and in water after the ligand exchange for which protocol PT 11 was used. As it can be seen from Figure 2.22, the QDs are transferred towards the initially colorless aqueous phase, keeping their pure color and intense emission (Figure 2.22 c) and d)). The transfer is quantitative, yielding a colorless $CHCl_3$ phase and no aggregated particles, proving the well-stabilized, ligand exchanged QDs. Both the shape and position of the PL spectra remain constant during the procedure, as it can be seen in Figure 2.22 e). No ideal surface passivation is achieved during the ligand

exchange, causing a typical decrease of the PL-QY to roughly 50% of the initial value, which means at the same time the largest drawback of the method. [67,70] It is to be noted that most of the mixed crystals discussed subsequently were prepared with QDs after their phase transfer by using this ligand exchange procedure.

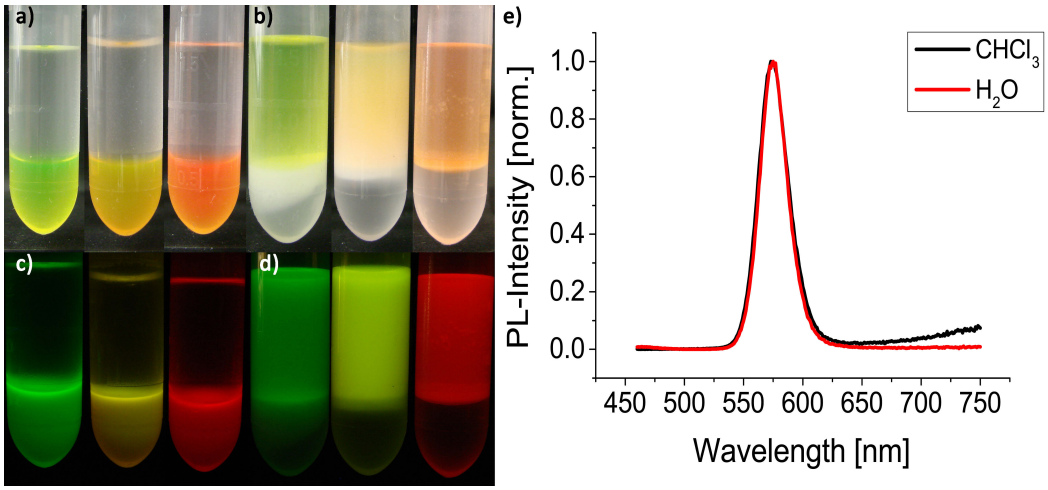

Figure 2.22.: True-color images of three different CdSe/ZnS QDs before (a and c) and after (b and d) the ligand exchange under ambient light (top) and 365 nm UV-excitation (bottom). e) PL spectra of alloyed CdSe/ZnS QDs before (black line) and after (red line) the ligand exchange by using the PT11 procedure according to reference [67]. Adapted by courtesy of ACS Appl. Mater. Interfaces 2015, DOI: 10.1021/acsami.5b08377. Copyright 2015, American Chemical Society.

To overcome the inherent drawback of the PL-QY reduction, more ligand exchange procedures were analyzed. The main reasons for the PL-QY reduction are a) low-quality inorganic shells around the emissive QD core [71,72] and b) an incomplete removal of the original ligands, causing a reduced stability of the colloids and a tendency to form agglomerates. [67,73] Furthermore, the formation of surface traps due to free bonding sites on the QD surface promotes non-radiative relaxation pathways. [74–77] To solve the latter challenges, a two-stage exchange procedure has been introduced recently. [68] In this method, the initial long-chain aliphatic ligands are stripped off by EDA in the first step. Ethylenediamine is only a weakly bonding ligand that can easily be replaced by strong binding thiol-based ligands as mercaptocarboxylic acids.
By using this approach (PT 12), both the alloyed CdSe/ZnS and the CdSe/CdS QDs were analyzed. The samples mentioned first mostly retained their optical properties during the ligand exchange and the subsequent encapsulation into borax, as it can be seen in Figure 2.23. For these only a slight dependence of the ZnS shell thickness towards retaining the initial

PL-QY was observed, with thicker ZnS shells providing a better conservation. In comparison to the previously discussed phase transfer approaches, all analyzed samples showed a higher PL-QY after the procedure, the overall stability of the samples was, however, lower. This means that the colloids were less stable during their long-term storage and in the saturated salt solution. Furthermore, as shown in Figure 2.23 a), the green-emitting QDs show a distinct red shift upon their transfer to water, while the red-emitting QDs preserve the position of their PL spectrum. The reasons for this different behavior can be manifold, from the difference in shell thickness of the ZnS, to a difference in the used stabilizers or the completeness of the ligand exchange itself. Analyzing these phenomena could spark further studies, including possible FTIR, NMR, DOSY-NMR, optical as well as Raman and SAXS analyses.

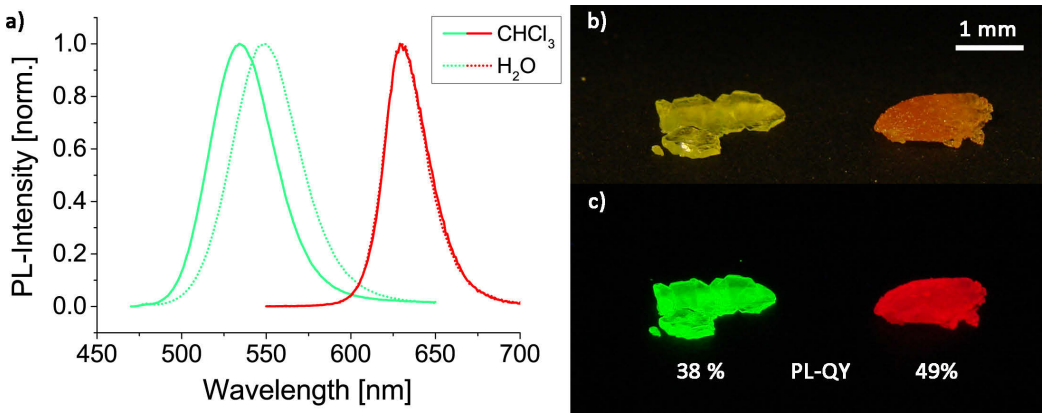

Figure 2.23.: a) PL spectra of two CdSe/ZnS QDs before (in $CHCl_3$) and after (H_2O) the ligand exchange. The subsequently grown borax-based mixed crystals are shown in b) and under ambient and c) 365 nm UV excitation respectively. Both samples retain their initial PL-QY during the ligand exchange and salt encapsulation. The values given in c) are measured for the mixed crystals.

When analyzing the second system, CdSe/CdS, it can be noted that the results differ slightly. Here, the original stabilizing ligands play major roles in retaining PL-QY upon ligand exchange. If only OA and octa-/hexadecylamine were utilized, their PL-QY is nearly completely quenched, which is to be expected according to the reasons discussed above. On the other hand, if QDs are used with OA, OAm and octadecylphosphonic acid, these samples tend to retain 80-100% of their initial PL-QY. Unfortunately, the samples are even less stable when being stored and tend to form agglomerates during the co-crystallization. Therefore, growing mixed crystals from CdSe/CdS QDs without losing most of the PL-QY for aggregation reasons was not yet possible. In summary, the EDA mediated procedure provides highly promising first results,

potentially providing access to QDs with much higher PL-QY in aqueous environment.
Due to their oil-based synthetic route, Cd-free QDs were also subject of ligand exchange processes. In the case of InZnP/GaP/ZnS, the already adopted version of reference [67] was used while Cu-doped InZnS/ZnS QDs were transferred to the aqueous phase by using a simplified version of the method described in reference [78]. In both cases, the procedures work with significant limitations and have a preliminary character. Compared to the previously discussed ligand exchanges on Cd-based QDs, the reproducibility was limited, the PL-QY decreased to ~25% or less of the initial value and the stability of the resulting water-soluble colloids was also lower than the Cd-based counterparts' one. Some of the successful phase transfers by using MPA as new stabilizing agent could nevertheless be conducted.

Mixed Crystal Formation of Ligand Exchanged QDs

As discussed above, the PT1 procedure resulted in relatively stable aqueous colloids of CdSe/ZnS QDs. Adding these colloids to a saturated solution of NaCl results in an initially clear and occasionally slightly turbid mixture. After they had been stored in an oven for about twelve hours at 30 °C, large QD portions constantly precipitated to the bottom of the beaker, while some fractions remain stable in the solution. Even the addition of free stabilizer (MPA, deprotonated as described for TGA-stabilized CdTe in Section 2.2.2) could not prevent the aggregation and sedimentation of large QDs parts. Therefore, the supernatant fluid was separated from the precipitate and the crystallization was left to proceed, until a couple of mixed crystals were formed, as depicted in Figure 2.21. These mixed crystals have a cubic shape which is a clear indicator for a lack of free stabilizing agent, being in compliance with the reduced colloidal stability of PT1-based aqueous QDs.
The subsequent procedures (PT2-8), although some partially stable colloids were formed, proved to be not suitable for a co-crystallization of QDs with salts.
On the other hand, the QDs that were transferred in accordance with the protocol for PT9-11 based on reference [67] provided promising and reproducible results. As discussed in the previous section, only the MPA-based transfer is suitable for mixed crystal formations. This can be explained by a weak emission intensity or a reduced stability in media with high ionic strength for TGA- and MUA-stabilized QDs respectively. Still, when applying MPA-stabilized CdSe/ZnS QDs for mixed crystallizations with NaCl, only mixed crystals with small loading amounts of QDs can be obtained, as shown in Figure 2.24 b) and d). Borax is used as a new host material to overcome this problem. Because of its much lower solubility in water in contrast to NaCl (0.13 mol/L compared to 6.14 mol/L respectively) [53], the ionic strength

of the saturated borax solution is much lower than for saturated NaCl solutions. Therefore, the stability of the ligand exchanged QDs is much higher within the borax solution, while on the other hand, when using the same amount of QDs (2:10 v:v QDs : saturated salt solution), the QD loading within the resulting mixed crystals is higher. Stripping voltammetry measurements showed a 3.4 times higher amount of Cd and thereby QDs within borax in comparison to NaCl-based mixed crystals prepared from the same batch of ligand exchanged QDs which can also be seen in Figure 2.24.

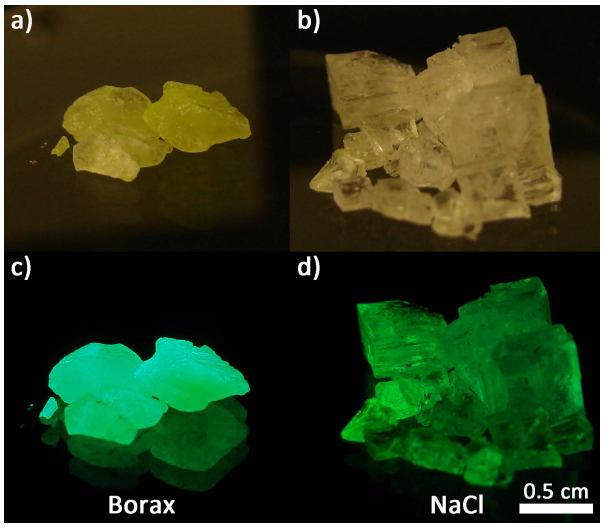

Figure 2.24.: True-color images of mixed crystals made from the same CdSe/ZnS QD batch with either borax (a and c) or NaCl (b and d) as host materials. The pictures a) and b) were taken under ambient light, c) and d) under excitation with a 365 nm UV lamp. Adapted by courtesy of ACS Appl. Mater. Interfaces 2015, DOI: 10.1021/acsami.5b08377. Copyright 2015, American Chemical Society.

As described before, the ligand exchange procedures for Cd-free QDs are at early stages of exploration with limited reproducibility. It can be noted that the results presented in Figure 2.25 cannot be considered to be generally representative for the two QD systems displayed. Image a) and PL spectrum b) show the results for Cu-doped InZnS/ZnS QDs embedded into borax. The PL-QY of this sample was below 10% in toluene and reduced further during the ligand exchange which is clearly visible due to the weak emission of the mixed crystals. Nevertheless, this sample generally proved the suitability of borax as a host matrix for such QDs, opening a new research field. The InZnP/GaP/ZnS QDs shown in c) and d) of Figure 2.25 behave in a similar way, but with better starting conditions. Here, the PL-QY was 80% for the as-synthesized QDs, preserving an intense emission of the mixed crystals despite the

demanding phase transfer as described in the previous section. As expected, both systems show a slight red shift of their emission maximum accompanied by a change in the dielectric surroundings upon incorporation. The reason why this shift is less distinct for the Cu-doped material might be found in the different excitonic recombination mechanisms of the two materials, as discussed above. It should be noted that this is just one possible hypothesis which needs to be analyzed in more detail in further studies.

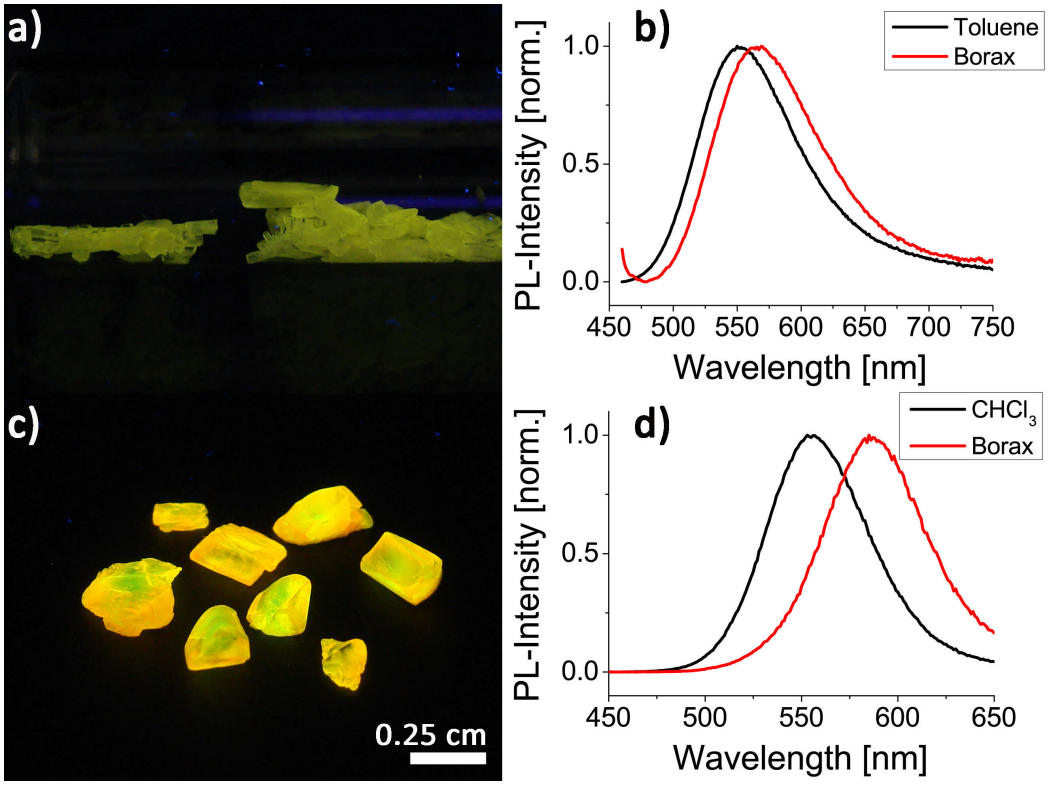

Figure 2.25.: Mixed crystals utilizing Cd-free QDs as emissive centers. a) and b) show a true-color image and PL spectrum of borax-based mixed crystals with Cu-doped InZnS/ZnS QDs. c) and d) show a true-color image and PL spectrum of InZnP/GaP/ZnS QDs embedded into borax. Both images a) and c) were taken under 365 nm excitation.

2.3. A Comparison of Different Crystallization Approaches*

2.3.1. "Classical" Crystallization Approach

The "classical" approach for forming QD-salt mixed crystals is the most analyzed one originally introduced and developed by Dr. Tobias Otto. [79] In this method, a saturated salt solution is mixed with a defined amount of aqueous colloidal QD solution and stored under ambient conditions. During the storage, water slowly evaporates, causing an oversaturation of the parental solution and inducing the crystal formation. As more water evaporates, larger and more crystallites are formed. The QDs are evenly distributed within the resulting mixed crystals which is demonstrated by their homogenous coloration and emission. During the embedding of the QDs, an alteration of the host crystal lattice is negligible, as shown in the X-ray diffractogram in Figure 2.26. This is a clear hint that the cavities within the lattices are formed to include the QDs.

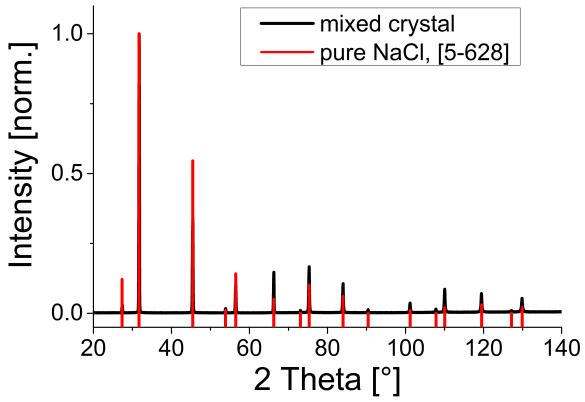

Figure 2.26.: X-ray diffractogram of a mixed crystal sample (black line) and a literature diffractogram for pure NaCl (red bars), taken from reference [80].

Due to the slow evaporation of water, crystallizations, for which this procedure is used, take 1 week in an oven at 30 °C and up to one month under ambient conditions. An extraordinary colloidal stability of the QDs within the salt solution is therefore necessary. If this high stability is reached, mixed crystals with different host matrices can be produced by using this method. As depicted in the previous chapter, NaCl-based materials are among the best characterized

*Parts of this chapter have already been published. [30, 33]

ones, but KCl, KBr, K-Na-tartrate or borax are also suitable. KCl behaves for example very similar to NaCl with slight but important differences. Especially for TGA-stabilized particles, KCl is the matrix to be chosen for forming high-quality crystals. In both cases, the size of the mixed crystals is between 0.2 and 1 cm. KBr on the other hand forms significantly larger mixed crystals, easily exceeding several cubic centimeters. These are usually loaded with a smaller QD amount, but due to their mostly faster crystallization, less stable QDs can also be used as emitting centers. The main weakness of KBr in comparison to other hosts is its distinctly higher hygroscopy which reduces the long-term stability and thus the quality of the composite materials. For K-Na tartrate, the composites show an anisotropic QD concentration which might be of interest for some special applications like lasing or for analyzing anisotropic emitting QDs. For a general application in color conversion, the non-homogenous loading and the reduced thermal stability of the K-Na tartrate is unfavorable in comparison to purely inorganic matrices. Borax was used as the last main matrix. As already discussed, this salt enables an even higher loading of the mixed crystals with QDs than with NaCl. Furthermore, and also due to its lower solubility, saturated borax solutions are a media with a lower ionic strength, enabling the use of less stable QD colloids.
Besides these salts composed of mostly monovalent ions, the possibility to form mixed crystals with multivalent ion-based salts was analyzed which will be discussed in detail in Appendix A.4.

2.3.2. Liquid-Liquid-Diffusion-Assisted Crystallization

As discussed above, one of the weakest aspects of the "classical" approach is that crystallization requires at least one week and also an extremely high QDs stability within the saturated salt solution during the long period of crystallization. Consequently, the set of QDs that can be successfully incorporated into ionic matrices is limited.
In this section, a versatile and fast method for producing high-quality QD-salt mixed crystals will be discussed, relying on the diffusion and solubility change of inorganic salts (e.g., NaCl) in solvents with various polarities. Due to the reduced solubility of NaCl in water by the interdiffusion of the worse solvent, the crystallization will be completed in less than one day. So the time needed to produce mixed crystals was reduced by more than one order of magnitude in comparison to the times reported in the references [30, 54]. The reduction of the crystallization time enables the use of even less stable QD colloids (e.g., some ligand exchanged initially oil-based QDs). Moreover, the adaptation of a two-step seed-mediated liquid-liquid diffusion-assisted crystallization (LLDC), the direct application of oil-based QDs for co-crystallization with salts without a prior phase transfer into water was achieved for the

first time. The resulting mixed crystals exhibit a stable and chemically tight matrix and can be produced by using a variety of semiconductor colloids, including Cd-free QDs, which may significantly extend the use of the QDs in photonic applications.
As mentioned above, the recently established LLDC method for preparing QD-salt mixed crystals takes approximately one day to be completed, being a distinct improvement compared to former standard crystallization approaches. [30, 32, 54, 81] The basic principle behind this method is the different solubility of NaCl in water and organic solvents with a lower polarity, as shown in Table 2.2. Due to its miscibility with water while having at the same time a much lower solubility of NaCl in comparison to water, methanol is chosen as solvent to demonstrate the concept. Furthermore, within MeOH the QDs are stable long enough for enabling the completion of the crystallization.

Table 2.2.: Solubility of NaCl in different solvents according to reference [82].

Solvent	Soluble NaCl [$g \cdot kg^{-1}$ solvent]
Water	360
Glycerin	83
Methanol	14
Ethanol	0.65

Due to their relatively high stability in saturated salt solutions, CdTe QDs were first used for preparing mixed crystals according to the LLDC approach. As schematically shown in Figure 2.27 a), a stable interface between the MeOH solution and the underlying NaCl-QD mixture instead of an instantaneous mixing is crucial for a successful crystallization. Due to the subsequent diffusion of MeOH into water and the consequently reduced solubility, NaCl crystals with incorporated CdTe QDs are formed within a few hours. Four QD-salt mixed crystal samples chosen as examples are shown in Figure 2.27 b) and c), proving their color and intense emission under daylight or UV illumination.

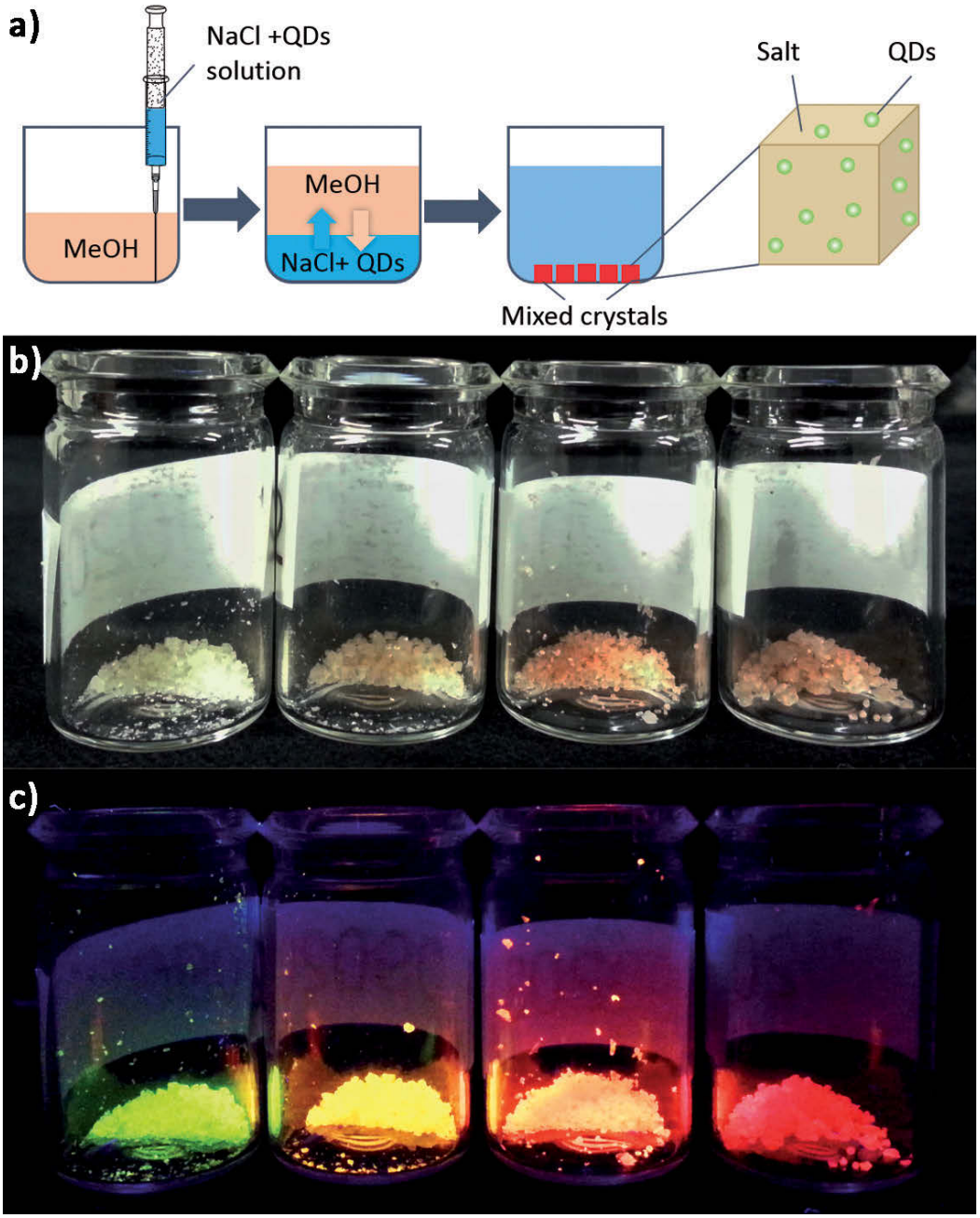

Figure 2.27.: a) Schematic illustration of the LLDC approach by using the diffusion of MeOH through a stable interface layer into an aqueous solution containing NaCl and CdTe QDs. True-color images of an exemplarily chosen set of NaCl-based mixed crystals containing differently sized CdTe QDs under b) daylight and c) 365 nm UV-illumination. Adopted by courtesy of Adv. Funct. Mater. 2015, 25, 2638. Copyright 2015, John Wiley and Sons.

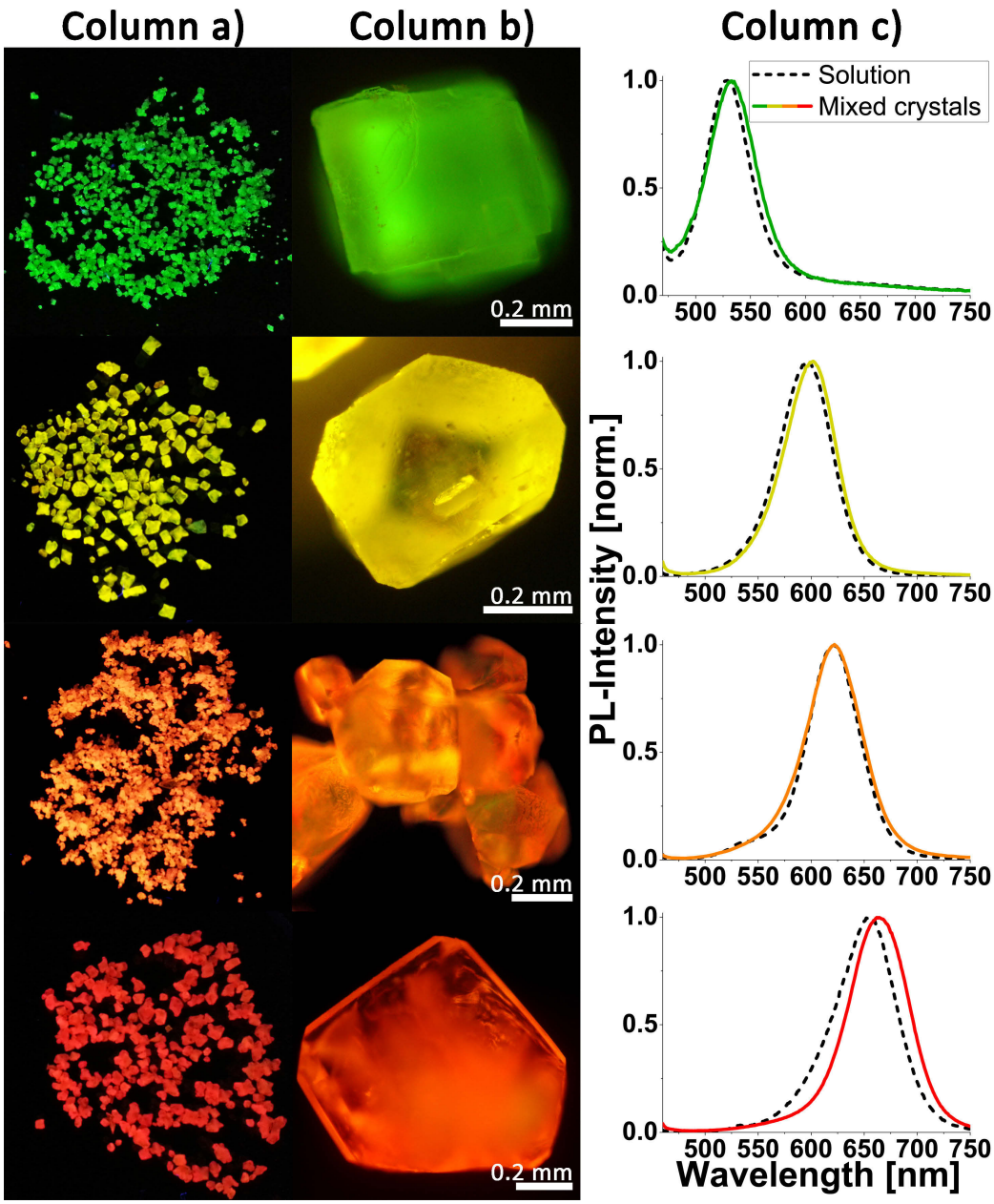

Figure 2.28.: True-color macroscopic images (column a)) and fluorescence microscopy images (column b)) of mixed crystals emitting in different colors under 365 nm UV excitation. Column c) displays the PL spectra of the initial CdTe QDs (dashed black lines) as well as the corresponding mixed crystals (colored lines). Adopted by courtesy of Adv. Funct. Mater. 2015, 25, 2638. Copyright 2015, John Wiley and Sons.

Figure 2.28 provides a magnified view of the mixed crystals. Column a) represents top view true-color images under an UV-excitation at 365 nm, whereas column b) shows fluorescence microscopic images of the green-, yellow-, orange-, and red-emitting mixed crystals. These microscopic images reveal that the QDs are evenly distributed within the mixed crystals and that the mixed crystals possess an mostly octahedral crystal shape. As discussed in Chapter 2.2.1, NaCl generally forms cubic crystals, whereas the addition of small, coordinating molecules like the stabilizing agent MPA used for the synthesis of CdTe QDs causes a change in shape towards octahedrons. [45] Therefore, an excess of free ligands exists in the parental solution. The formed mixed crystals are small, with an edge size of approximately 0.5 mm, e.g., in Figure 2.28, column b), which means a decrease in size compared to the "classical" crystallization approach presented earlier where mixed crystals with sizes larger than 1 cm are obtained. [30] These smaller crystallite sizes can be explained by a fast crystallization rate in the MeOH diffusion induced oversaturation of the NaCl solution which leads to a simultaneous formation of larger crystal seeds amounts. Furthermore, the overall reduced amount of NaCl within the system also supports the formation of smaller mixed crystals. Column c) of Figure 2.28 shows the corresponding PL spectra of the mixed crystals (colored lines) in comparison to the PL spectra of the pure QDs in solution (dashed black lines). All four samples show a minimal red shift in their emission maxima upon incorporation into the salt matrix which is related to the change of the dielectric constant of the surrounding media. [30]

When using LLDC, the production of mixed crystals can also be performed with other solvents like ethanol, and other salts such as KCl. In both cases, the resulting mixed crystals are much more powder-like, as it can be seen from Figure 2.29. This might be explained by the lower solubility of NaCl in EtOH and KCl in MeOH in comparison to NaCl in MeOH, yielding an even larger number of crystallization seeds during the diffusion of the alcohols into the underlying water phase leading therefore to the formation of more but smaller mixed crystals.

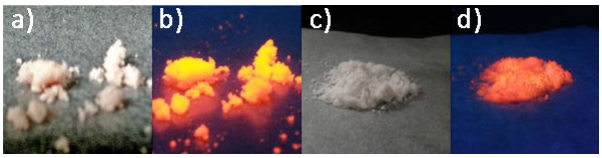

Figure 2.29.: Optical images of mixed crystals (CdTe/NaCl) made by using EtOH as the non-solvent, exposed under a) room light and b) 365 nm UV excitation. Visual images of mixed crystals (CdTe/KCl) made by using MeOH as the non-solvent, exposed under room c) light and d) UV light. Adopted by courtesy of Adv. Funct. Mater. 2015, 25, 2638. Copyright 2015, John Wiley and Sons.

Preparation of Mixed Crystals Using Oil-Based QDs After Ligand Exchange

As discussed in Chapter 2.1.2, hot injection techniques have been extensively analyzed to obtain high-quality QDs with a small size dispersion and high PL-QYs. These QDs are mainly stabilized in nonpolar solvents by long-chain alkyl phosphines (e.g., TOP/TOPO) and alkanoic acids. Exchanging the ligands on the surface with shorter polar molecules like MPA is one efficient way to make these QDs water-soluble and accessible for the co-crystallization with salt. However, this approach is limited as the stability of ligand exchanged QDs in salt solutions is moderate and therefore not always compatible with the traditionally used long-time crystallization approach. [31] At the same time, when using LLDC, the inherent drawback of the ligand exchanged QDs can be overcome as a result of the acceleration of the crystallization procedure by more than one order of magnitude. Figure 2.30 shows the results for NaCl mixed crystals containing ligand exchanged MPA-capped CdSe/ZnS core/shell QDs with an alloyed gradient shell (a-c) as well as InZnP/GaP/ ZnS core/shell/shell QDs (d-f).

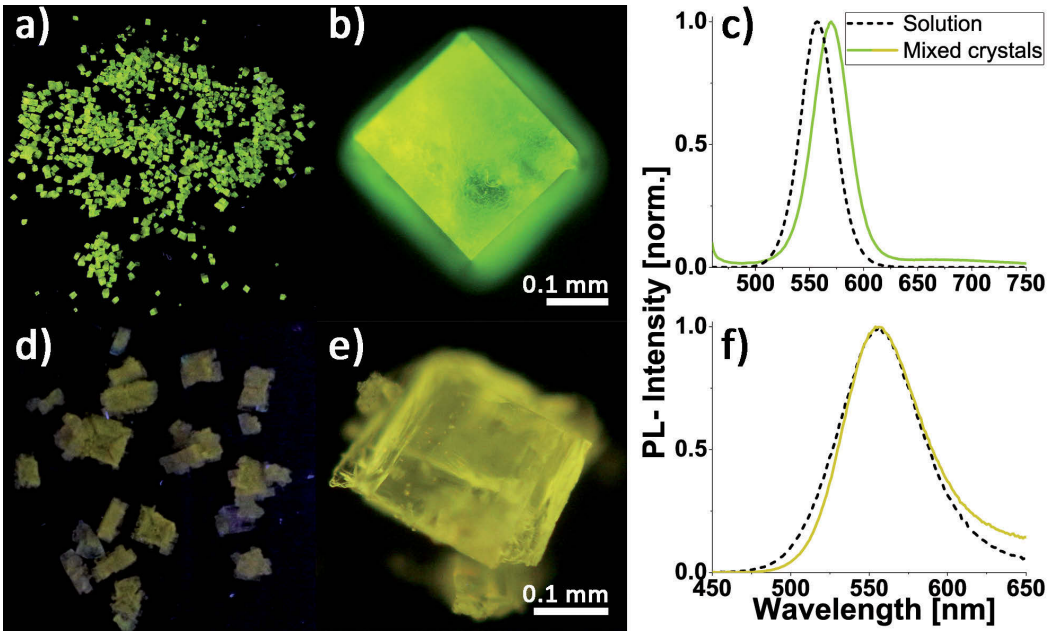

Figure 2.30.: a), d) True-color images and b), e) microscopic images under 365 nm UV-excitation as well as c), f) PL spectra of mixed crystals with a)-c) CdSe/ZnS QDs or d)-f) InZnP/GaP/ZnS QDs. The mixed crystals are prepared after replacing the long-chain ligands with MPA. Adopted by courtesy of Adv. Funct. Mater. 2015, 25, 2638. Copyright 2015, John Wiley and Sons.

At first glance, a more cubic-like structure of the mixed crystals is obtained (Figure 2.30 b) and e)), indicating a much lower amount of free MPA in the parental solution. A smaller amount of ligands on the surface is one major parameter that causes a reduced stability of the QDs in the salt solutions. By applying the LLDC method, these materials can be made accessible for a co-crystallization with NaCl without larger losses due to the shorter time needed for completing the crystallization process. The trade-off which has to be made by using ligand exchanged QDs for the incorporation into solid matrices is the inherent reduction of the PL-QY during the ligand exchange. At the exchange step, the PL-QY is reduced to 25%-50% of its initial value.

Preparation of Mixed Crystals Using Oil-Based QDs without Prior Ligand Exchange

To overcome the critical step of exchanging ligands, the LLDC method was extended to a two-step seed-mediated approach, as schematically illustrated in Figure 2.31.

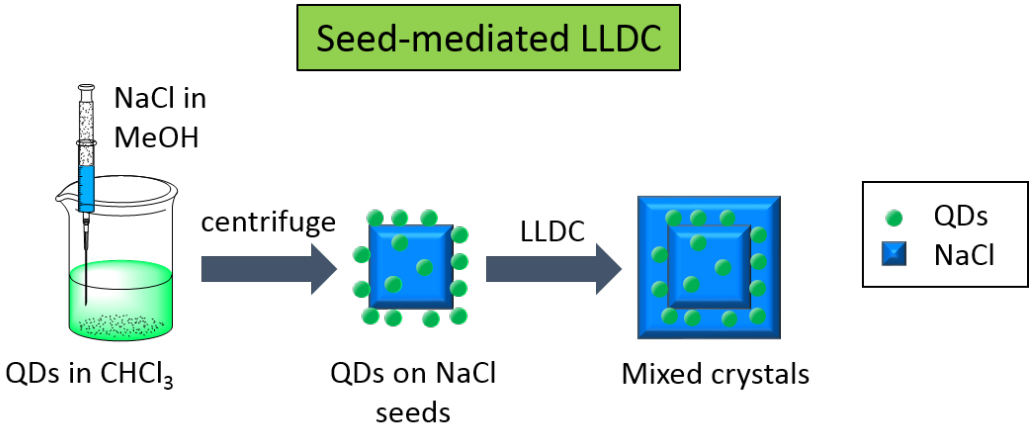

Figure 2.31.: Schematic illustration of the seed-mediated LLDC method which enables the direct usage of oil-based QDs for crystallization without a prior ligand exchange. In the first step, QDs are adsorbed on the surface of the formed NaCl seeds, while the LLDC in the second step provides a complete encapsulation of the QDs by growing the seeds to larger mixed crystals. Adopted by courtesy of Adv. Funct. Mater. 2015, 25, 2638. Copyright 2015, John Wiley and Sons.

First, the addition of the NaCl saturated MeOH solution into the diluted QD solution causes a drastically reduced solubility of NaCl, creating NaCl seed crystals (seen as turbidity in

Figure 2.32). During their formation, most of the QDs are adsorbed on the surface of the NaCl seeds to reduce the QDs surface-free energy. These small crystallites can already be used for further applications, but due to the large amount of QDs solely on the surface, these seeds do not provide a thorough protection of the QDs. However, they can ideally be used as crystal seeds for growing mixed crystals subsequently by simply repeating the LLDC approach. Afterwards, the LLDC is performed as a second step by dispersing the seeds in pure MeOH and injecting an underlying layer of the NaCl solution. MeOH is used as the mediation solvent due to its miscibility with water and nonpolar organic solvents like $CHCl_3$ being at the same time a non-solvent for the QDs.

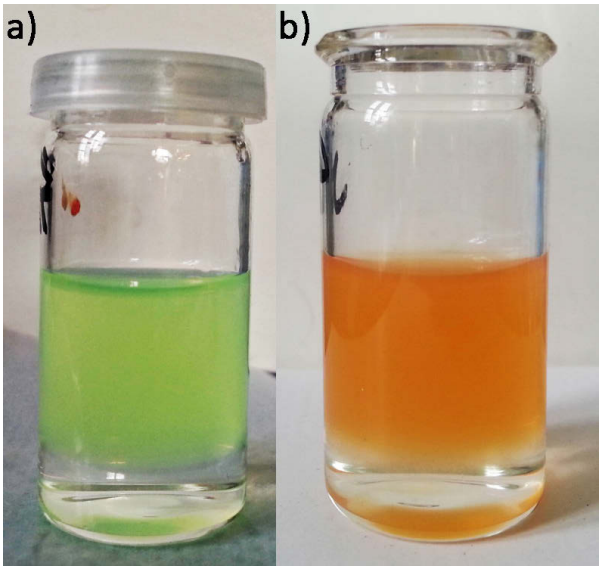

Figure 2.32.: True-color image showing the presence of a stable interface (indicated by the red arrows) between two CdSe/ZnS QD/NaCl seed solutions (a) green-emitting, b) red-emitting QDs) and the underlying MeOH solution. Adopted by courtesy of Adv. Funct. Mater. 2015, 25, 2638. Copyright 2015, John Wiley and Sons.

Figure 2.33 shows mixed NaCl-based crystals composed of either green-, yellow-, or red-emitting oil-based CdSe/ZnS QDs without a ligand exchange prepared via the seed-mediated LLDC method. As can be seen from the microscope images (Figure 2.33 a), d) and g)), the mixed crystals exhibit a pure color emission and a cubic shape. This shape is to be expected since small coordinating molecules which would alter the shape into octahedrons are not present during the complete crystallization process. In comparison to the LLDC results discussed above, the emission centers are furthermore not evenly distributed within the mixed crystals but mostly concentrated around the initial seed.

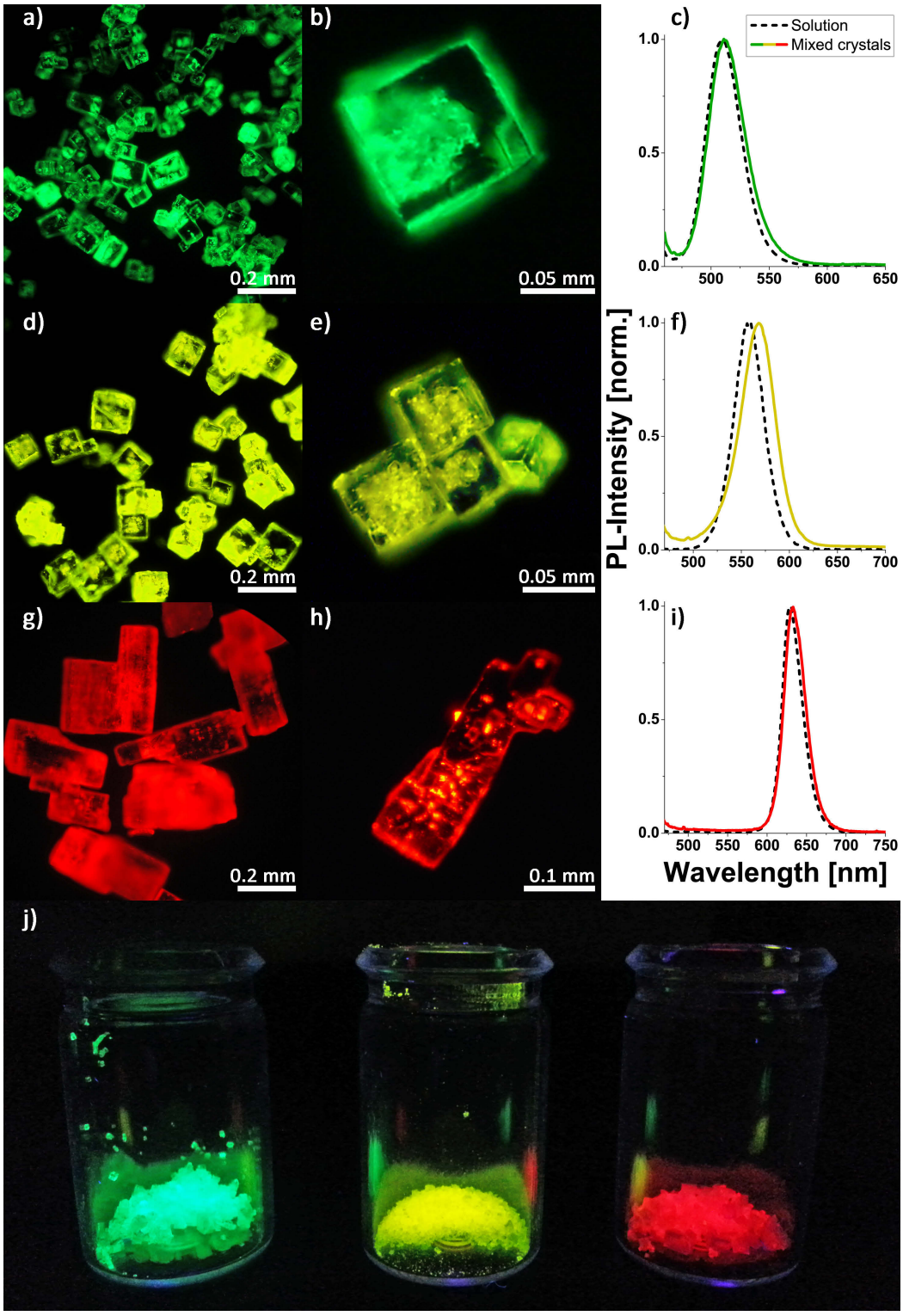

Figure 2.33.: a), d), g) Microscopic images under 365 nm UV-excitation and c), f), i) PL spectra of green-, yellow- and red-emitting CdSe/ZnS QDs incorporated into NaCl without any prior ligand exchange by using the seed-mediated LLDC approach. b), e), h) Photograph j) shows a true-color image of the corresponding mixed crystals under 365 nm UV excitation. Reprinted by courtesy of Adv. Funct. Mater. 2015, 25, 2638. Copyright 2015, John Wiley and Sons.

This confirms the concept of the QD adsorption onto the seeds in the first step and their subsequent coverage with mainly pure NaCl during the second-step LLDC, as shown in Figure 2.33 b), e) and h). The corresponding PL spectra are shown in Figure 2.33 c), f) and i). These spectra exhibit a slight red shift which can be explained by the change of the surrounding media as discussed above. No signs of aggregation like broadening, an intense red shifts or scattering effects are observed. Figure 2.33 j) shows a true-color image of the mixed crystals under 365 nm excitation, proving their intense emission.

2.4. Mixed Crystals Emitting in the Infrared Region

Mixed crystals emitting in the NIR region have main application possibilities at three different wavelength areas. As already mentioned in the synthesis section 2.1.1, two biological windows exist between 700-950 nm and 1000-1300 nm in the electromagnetic spectrum since tissues have an absorption gap due to a comparably low absorption coefficient of skin, fat and blood. [83] Furthermore, an emission wavelength around 1300 nm is an established area for telecommunication signals. [84, 85] Therefore, mixed crystals emitting in these three NIR areas are of high interest for both scientific studies and commercial application. It is noted here, that a second telecommunication window around 1550 nm can not be covered by the emission of the QDs used in present work.

First attempt, CdHgTe QDs were used as emitting centers and embedded into NaCl as host matrix according to the discussed "classical" crystallization approach. These samples were thoroughly analyzed in cooperation with our partners at the City University of Hong Kong regarding steady-state and time-resolved PL properties as well as their behavior upon temperature changes. The results from three exemplarily chosen samples emitting in the range of 900 to 1100 nm are summarized in Figure 2.34. The left column displays the PL behavior of the QDs upon incorporation and after redissolving the mixed crystals, while the right column shows the temperature stability tests.

A sample of mixed crystals emitting in the first biological window is shown in Figure 2.34 a) and b). Upon the encapsulation, the maximum of the PL is redshifted by 25 nm towards 946 nm. Such a change of the PL maximum to lower energies is expected and matches the results obtained for aqueous based pure CdTe. Again, it can be explained by the change of the dielectric constant of the surrounding media. [30] After dissolving one of the mixed crystals, the PL spectrum is blue shifted in respect of the initial solution. As discussed in Section 2.2.2, such a blue shift is an indicator for a partial etching of the QDs upon incorporation

due to salt-QD interactions and might occur when the chemical stability of the QDs is lower than usual.

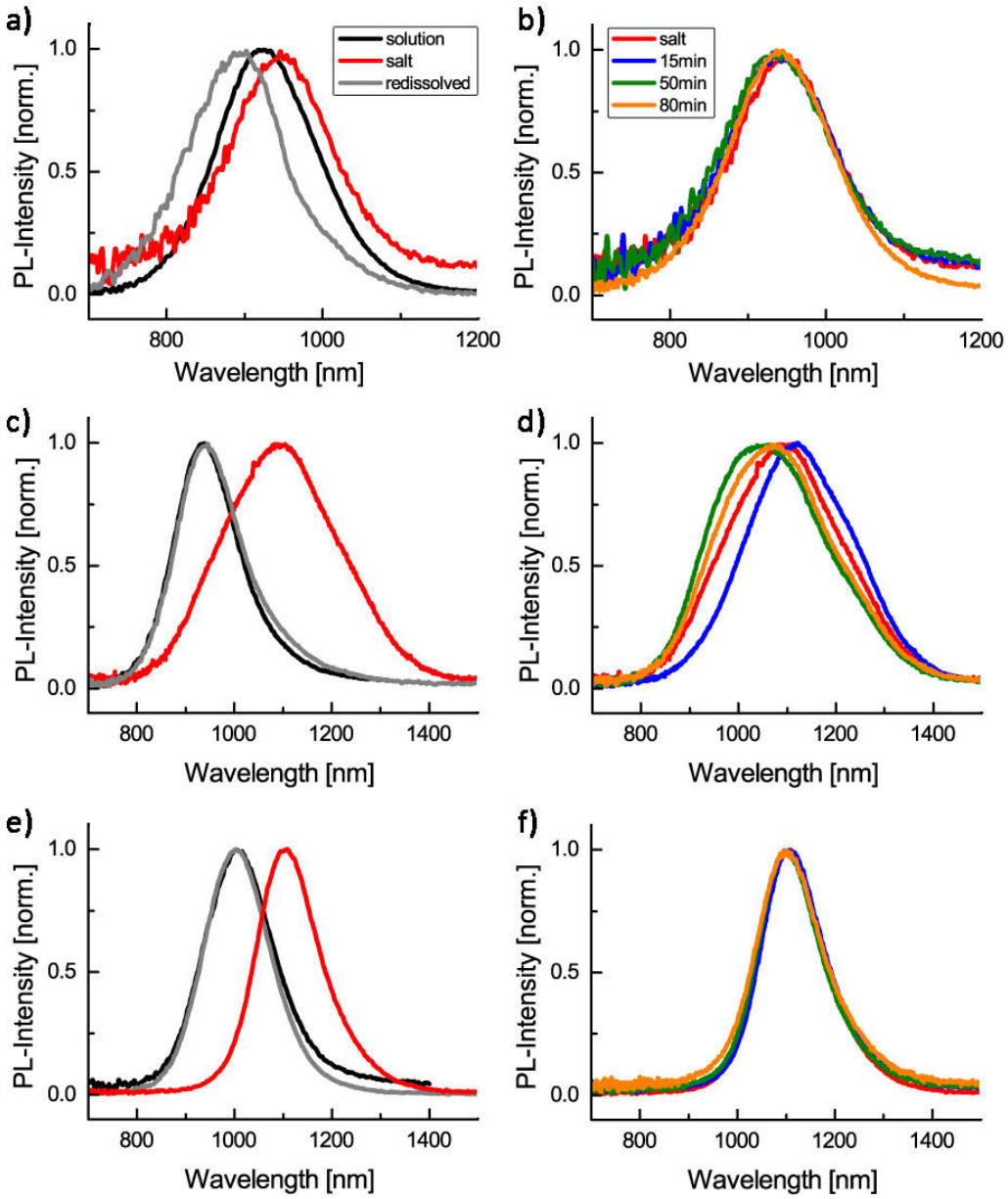

Figure 2.34.: PL spectra for three different mixed crystal sets based on aqueous $Cd_{1-x}Hg_xTe$ QDs. The left column displays the evolution of the optical properties upon incorporation of QDs into the ionic matrix and the subsequent dissolving, whereas the right column shows the optical properties of the mixed crystals after certain times kept at 70 °C.

Such reduced stability emerges when stabilizers are partially decomposed and when the sample ages over time. In the case of the QD samples used here, both events are possible. With regard to the PL-LT at the emission maximum, no significant effects (105, 98 and 89 ns in solution, salt and after dissolving respectively) occur during the incorporation and subsequent dissolution, although a slight tendency towards a reduced PL-LT is obvious. The mixed crystals have a good stability regarding steady-state and time-resolved PL features upon appropriate temperature treatments. Therefore, the QDs were heated up to 70 °C for a certain time, cooled down to room temperature and characterized afterwards. As it can be seen from Figure 2.34 b), both the position and the PL-LT (98 and 87 ns for the initial salt and after 80 min at 70 °C, respectively) of the PL remain constant during the analysis. According to the relation between PL-QY and PL-LT, drastic effects on the PL-QY can be excluded due to the constant PL-LT which is also in conformity with previous publications showing that negligible changes in PL-LT at least do not result in a reduction of PL-QY for aqueous QDs. [31] The graphs shown in Figure 2.34 c) - f) display mixed crystals and the corresponding colloids from the same synthesis but after different refluxing times and therefore distinct sizes as well as varying optical and chemical properties due to other Cd:Hg ratios. [11] Graphs c) and d) show the properties of the earlier fraction with a PL-maximum of the QDs in solution at 940 nm. The incorporation of those QDs into NaCl results in a distinct red shift of about 150 nm which can mainly be explained by an aggregation of the QDs. This hypothesis is supported by the reduction of PL-LT and the doubling of the FWHM. Nevertheless, the aggregation seems to be reversible, since dissolving the mixed crystals results in a nearly perfect restoration of the optical properties. During the temperature stability tests, this sample behaves in a very similar way as the ones discussed above, showing only minor changes in PL-LT. For the steady-state PL, a slight tendency of shifting to the high-energy region of the spectrum is observed which is still negligible.

In the case of mixed crystals prepared from the QDs with a longer refluxing time, a slightly different picture arises. First of all, no signs of severe aggregation can be derived from the optical measurements, as it can be seen from Figure 2.34 e). Both the FWHM and PL-LT remain almost constant upon incorporation into NaCl, matching the observations of the sample shown in Figure 2.34 a) and b). Here, the expected red shift of the mixed crystal's PL-maximum in comparison to the QD solution is also within the general range. On the other hand and in comparison to graphs a) and b), dissolving the mixed crystals restores the initial optical properties, showing no sign of etching induced by a contact with the saturated salt solution. This observation and the reduced tendency to form aggregates indicate a higher colloidal and chemical stability of these QDs. Such behavior is generally associated with a

better surface passivation. It should be noted that this theory is based on experiences with CdTe systems and that it has to be further analyzed in order to be understood completely and thoroughly.
Although the results discussed above are highly promising, only the range up to 1100 nm can be covered with these CdHgTe-based samples. In order to reach the telecommunication windows at 1300 nm, CdHgTe QDs with 10 mol.% mercury were synthesized, with the corresponding PL spectra shown in Figure 2.5. Unfortunately, these samples as well as some pure HgTe QDs were not stable in any analyzed salt (saturated NaCl, KCl, KBr or borax solutions). Therefore and due to the good tunability in terms of the optical properties, PbS QDs were analyzed regarding their applicability as emission centers in mixed crystals.
PbS QDs are produced by using a hot-injection method and are therefore only soluble in organic solvents, making a ligand exchange or the application of the two-step LLDC necessary. For the latter, only a complete aggregation of the QDs directly after adding MeOH to the $CHCl_3$ solution was observed, providing no possibility for forming mixed crystals when this method is used. First of all, the ligand exchange was conducted by using PT 11, as discussed in section 2.2.4 as well as a modified version of it in which the hydrophobic solution is mixed with MeOH containing MPA as a new stabilizer. In a second step, the QDs were precipitated and redispersed in water. Both attempts delivered aqueous colloidal solutions of PbS QDs which remain stable for a few hours up to several days, depending on the sample and method. When getting in contact with the saturated salt solution, a complete aggregation appeared, resulting in a clear parental solution and a black sediment of PbS aggregates within hours. Therefore, a ligand exchange according to reference [69] was used, labeled as PT 13. In this procedure, a long-chain OA is replaced by GSH in a slightly acidic aqueous environment. When using this method, PbS QDs were successfully transferred to water and were able to remain colloidal stability in the dark under ambient conditions up to three months. During the first attempts to form mixed crystals by using NaCl or borax, a sufficient colloidal stability of the QDs was observed but even after a complete evaporation of water no incorporation of the QDs into ionic matrices was achieved. As it can be seen from Figure 2.35 c), the behavior is different for KBr, where the QDs are incorporated in some cases, forming small but strongly colored mixed crystals. As depicted in graph a), such composites resemble a slightly red shifted but not broadened PL spectrum in comparison to the initial QDs in $CHCl_3$. Nevertheless, KBr is not a suitable matrix due to its high hygroscopy and the incorporation was also not reproducible for different batches of PbS QDs. Therefore, mixed crystals based on sucrose were grown according to reference [81], with a homogenous and reproducible loading of QDs, as shown in image e) of Figure 2.35. The corresponding spectra of the initial

QDs and the mixed crystals are displayed in graph b), showing an expected slight red shift but not a change in the overall spectral shape. When sucrose is used as host material, composites with an emission maxima at ca. 1050 and ca. 1320 nm could be prepared, covering both the second biological window and the telecommunication area at 1300 nm.

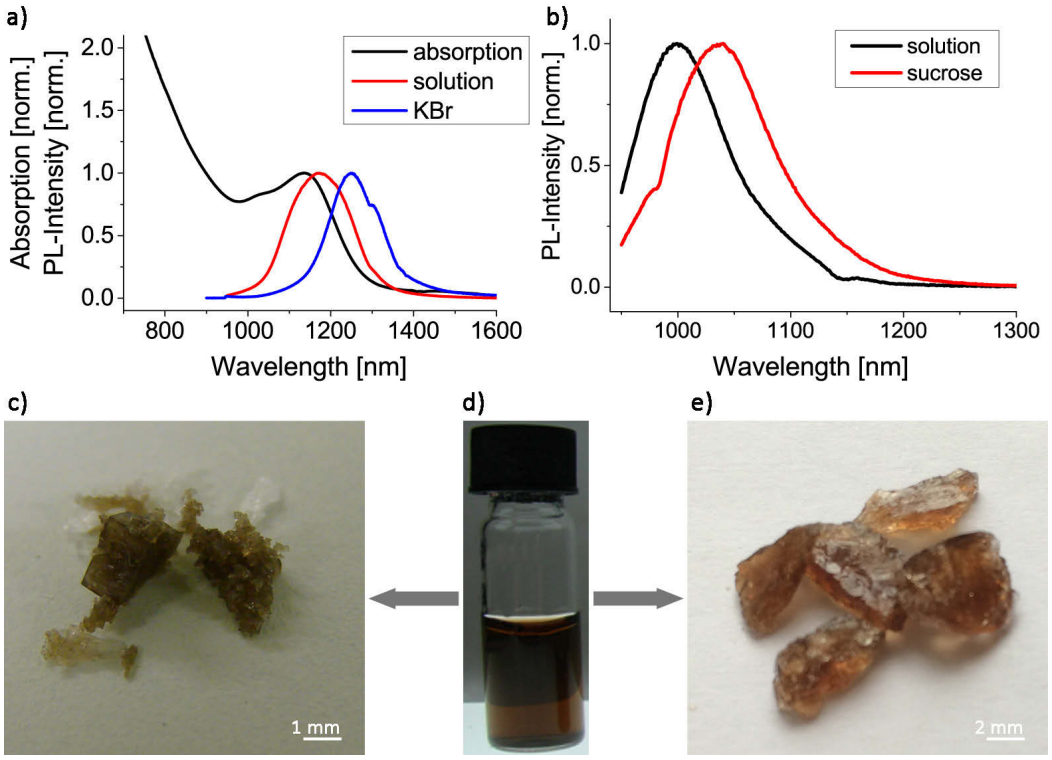

Figure 2.35.: a) Absorption (black line) and PL spectra (red line) of PbS QDs in toluene and the corresponding PL spectrum in KBr (blue line). b) PL spectra of PbS QDs in toluene (black) and after the incorporation into sucrose. c) True-color images of KBr-based mixed crystals, d) aqueous PbS QD solution and e) sucrose-based mixed crystals. It should be noted that these images were chosen exemplarily and that the different mixed crystals were not grown from the same batch of PbS QDs.

As a proof-of-concept system, the IR emitting mixed crystals based on CdHgTe QDs embedded into NaCl were blended onto a blue-emitting LED as excitation source. The corresponding PL spectra of the initial solution, the mixed crystal and the resulting device can be found in Figure 2.36. The graph clearly shows that upon embedding the mixed crystal powder into the silicone on top of the excitation source, no change in the optical properties occurs as expected. Such a light source could be used for external bioimaging processes or as an excitation source

for upconversion materials. Furthermore, the use as an IR light guide for automated surgeries as well as other in vivo bioimaging processes with these crystals as conversion material on top of fiber optics are possible.

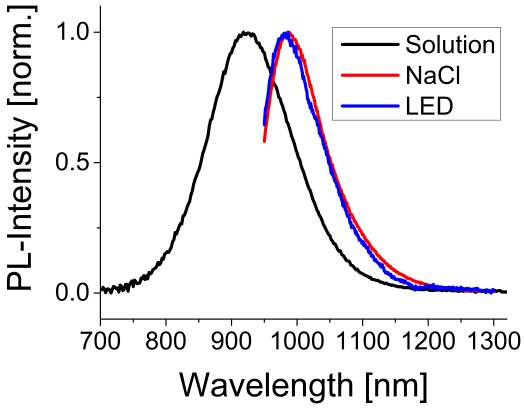

Figure 2.36.: PL spectra of CdHgTe QDs in solution (black line) after incorporation into NaCl (red line) as well as powderized mixed crystals blended on top of a blue emitting 1 W InGaN LED as excitation source (blue line).

2.5. Summary

Briefly, a short overview of the synthetic procedures of the used QDs was given in the first part of this chapter. In the second part, approaches for the mixed crystal preparation were discussed. For aqueous CdTe, the "classical" crystallization method as well as the optimizations based on this initial versatile and simple route are presented. One main aspect was to generate a protocol for embedding TGA-stabilized CdTe QDs due to their better tunability in the green-yellow part of the visible spectrum. Oil-based QDs, as the second main system of QDs, had to be phase transferred to make them compatible with the co-crystallization which was successfully demonstrated. Their embedding into the ionic matrix proved to be less straight forward and was accomplished by using either borax as the host matrix or applying the LLDC method for a rapid crystallization. Finally, QDs emitting in the two biological windows as well as the first telecommunication window were successfully embedded into different matrices and a proof-of-principle device utilizing them as down-conversion material was presented.

References

[1] A. Henglein, *Berichte der Bunsengesellschaft für Physikalische Chemie*, **1982**, *86*(4), 301.

[2] T. Rajh, O. I. Micic, and A. J. Nozik, *The Journal of Physical Chemistry*, **1993**, *97*(46), 11999.

[3] C. B. Murray, D. J. Norris, and M. G. Bawendi, *Journal of the American Chemical Society*, **1993**, *115*(19), 8706.

[4] S. Qu, X. Wang, Q. Lu, X. Liu, and L. Wang, *Angewandte Chemie International Edition*, **2012**, *51*(49), 12215.

[5] W. Zhang, H. Zhang, Y. Feng, and X. Zhong, *ACS Nano*, **2012**, *6*(12), 11066.

[6] S. Leubner; *On the ligand shell complexity of strongly emitting , water-soluble semiconductor nanocrystals;* Dissertation, TU Dresden, **2015**.

[7] V. Lesnyak, S. V. Voitekhovich, P. N. Gaponik, N. Gaponik, and A. Eychmüller, *ACS Nano*, **2010**, *4*(7), 4090.

[8] N. Gaponik, S. G. Hickey, D. Dorfs, A. L. Rogach, and A. Eychmüller, *Small*, **2010**, *6*(13), 1364.

[9] A. L. Rogach, Eds., *Semiconductor Nanocrystal Quantum Dots;* Springer Vienna, Vienna, 2008.

[10] N. Gaponik, D. V. Talapin, A. L. Rogach, K. Hoppe, E. V. Shevchenko, A. Kornowski, A. Eychmüller, and H. Weller, *The Journal of Physical Chemistry B*, **2002**, *106*(29), 7177.

[11] V. Lesnyak, A. Lutich, N. Gaponik, M. Grabolle, A. Plotnikov, U. Resch-Genger, and A. Eychmüller, *Journal of Materials Chemistry*, **2009**, *19*(48), 9147.

[12] I. Turyan and D. Mandler, *Electrochimica Acta*, **1995**, *40*(9), 1093.

[13] M. A. Vairavamurthy, W. S. Goldenberg, S. Ouyang, and S. Khalid, *Marine Chemistry*, **2000**, *70*(1-3), 181.

[14] L. Zou, Z. Gu, N. Zhang, Y. Zhang, Z. Fang, W. Zhu, and X. Zhong, *Journal of Materials Chemistry*, **2008**, *18*(24), 2807.

[15] M. T. Harrison, S. V. Kershaw, M. G. Burt, A. Eychmüller, H. Weller, and A. L. Rogach, *Materials Science and Engineering B*, **2000**, *69-70*, 355.

[16] A. L. Rogach, M. T. Harrison, S. V. Kershaw, A. Kornowski, M. G. Burt, A. Eychmüller, and H. Weller, *physica status solidi (b)*, **2001**, *224*(1), 153.

[17] S. Leubner, R. Schneider, A. Dubavik, S. Hatami, N. Gaponik, U. Resch-Genger, and A. Eychmüller, *Journal of Materials Chemistry C*, **2014**, *2*(25), 5011.

[18] J. R. Allport and R. Weissleder, *Experimental Hematology*, **2001**, *29*(11), 1237.

[19] C. B. Murray, C. R. Kagan, and M. G. Bawendi, *Annual Review of Materials Science*, **2000**, *30*(1), 545.

[20] J. J. Li, Y. A. Wang, W. Guo, J. C. Keay, T. D. Mishima, M. B. Johnson, and X. Peng, *Journal of the American Chemical Society*, **2003**, *125*(41), 12567.

[21] W. K. Bae, K. Char, H. Hur, and S. Lee, *Chemistry of Materials*, **2008**, *20*(2), 531.

[22] W. K. Bae, M. K. Nam, K. Char, and S. Lee, *Chemistry of Materials*, **2008**, *20*(16), 5307.

[23] W. K. Bae, J. Kwak, J. Lim, D. Lee, M. K. Nam, K. Char, C. Lee, and S. Lee, *Nano Letters*, **2010**, *10*(7), 2368.

[24] W. Zhang, Q. Lou, W. Ji, J. Zhao, and X. Zhong, *Chemistry of Materials*, **2014**, *26*(2), 1204.

[25] S. Kim, T. Kim, M. Kang, S. K. Kwak, T. W. Yoo, L. S. Park, I. Yang, S. Hwang, J. E. Lee, S. K. Kim, and S.-W. Kim, *Journal of the American Chemical Society*, **2012**, *134*(8), 3804.

[26] K. Boldt, N. Kirkwood, G. A. Beane, and P. Mulvaney, *Chemistry of Materials*, **2013**, *25*(23), 4731.

[27] S. Gabriel; *Assessment of Lead Chalcogenide Nanostructures as Possible Thermoelectric Materials;* Dissertation, TU Dresden, **2013**.

[28] L. Kühn; *Synthese und Charakterisierung fluoreszierender Kohlenstoffnanopartikel;* Forschungspraktikum, TU Dresden, **2013**.

[29] C. Waurisch; *Thermodynamic and kinetic investigations into the syntheses of CdSe and CdTe nanoparticles;* Dissertation, TU Dresden, **2012**.

[30] T. Otto, M. Müller, P. Mundra, V. Lesnyak, H. V. Demir, N. Gaponik, and A. Eychmüller, *Nano Letters*, **2012**, *12*(10), 5348.

[31] M. Müller, M. Kaiser, G. M. Stachowski, U. Resch-Genger, N. Gaponik, and A. Eychmüller, *Chemistry of Materials*, **2014**, *26*(10), 3231.

[32] M. Adam, R. Tietze, N. Gaponik, and A. Eychmüller, *Zeitschrift für Physikalische Chemie*, **2015**, *229*(1-2), 109.

[33] M. Adam, Z. Wang, A. Dubavik, G. M. Stachowski, C. Meerbach, Z. Soran-Erdem, C. Rengers, H. V. Demir, N. Gaponik, and A. Eychmüller, *Advanced Functional Materials*, **2015**, *25*(18), 2638.

[34] M. Adam, T. Erdem, G. M. Stachowski, Z. Soran-Erdem, J. Lox, C. Bauer, J. Poppe, H. V. Demir, N. Gaponik, and A. Eychmüller, *ACS Applied Materials & Interfaces*, **2015**, *DOI: 10.1021/acsami.5b08377*.

[35] J. Lee, V. C. Sundar, J. R. Heine, M. G. Bawendi, and K. F. Jensen, *Advanced Materials*, **2000**, *12*(15), 1102.

[36] N. Gaponik and A. L. Rogach, *Physical Chemistry Chemical Physics : PCCP*, **2010**, *12*(31), 8685.

[37] D. V. Talapin, S. K. Poznyak, N. P. Gaponik, A. L. Rogach, and A. Eychmüller, *Physica E: Low-dimensional Systems and Nanostructures*, **2002**, *14*(1-2), 237.

[38] H. Zhang, Z. Cui, Y. Wang, K. Zhang, X. Ji, C. Lü, B. Yang, and M. Gao, *Advanced Materials*, **2003**, *15*(10), 777.

[39] E. F. Schubert, *Light-Emitting Diodes;* Cambridge University Press, Cambridge, 2 ed., 2006.

[40] R. Mueller-Mach, G. O. Mueller, M. R. Krames, and T. Trottier, *IEEE Journal of Selected Topics in Quantum Electronics*, **2002**, *8*(2), 339.

[41] H. V. Demir, S. Nizamoglu, T. Erdem, E. Mutlugun, N. Gaponik, and A. Eychmüller, *Nano Today*, **2011**, *6*(6), 632.

[42] E. I. Hormats and F. C. Unterleitner, *Journal of Physical Chemistry*, **1965**, *69*(11), 3677.

[43] Y. Gao and P. R. Ogilby, *Macromolecules*, **1992**, *25*(19), 4962.

[44] B. Boudine, M. Sebais, O. Halimi, R. Mouras, A. Boudrioua, and P. Bourson, *Optical Materials*, **2004**, *25*(4), 373.

[45] H. J. Meyer, *Kristallisation;* Number Bd. 16. Bibliographisches Institut, 1909.

[46] S. Mayilo, J. Hilhorst, A. S. Susha, C. Höhl, T. Franzl, T. A. Klar, A. L. Rogach, and J. Feldmann, *The Journal of Physical Chemistry C*, **2008**, *112*(37), 14589.

[47] A. Shavel, N. Gaponik, and A. Eychmüller, *The Journal of Physical Chemistry B*, **2006**, *110*(39), 19280.

[48] A. L. Rogach, T. Franzl, T. A. Klar, J. Feldmann, N. Gaponik, V. Lesnyak, A. Shavel, A. Eychmüller, Y. P. Rakovich, and J. F. Donegan, *The Journal of Physical Chemistry C*, **2007**, *111*(40), 14628.

[49] A. L. Rogach, *Materials Science and Engineering B*, **2000**, *69*(0), 435.

[50] S. Xu, C. Wang, H. Zhang, Z. Wang, B. Yang, and Y. Cui, *Nanotechnology*, **2011**, *22*(31), 315703.

[51] H. Zhang, Z. Zhou, B. Yang, and M. Gao, *The Journal of Physical Chemistry B*, **2003**, *107*(1), 8.

[52] A. Neuhaus and T. H. Darmstadt, *Angewandte Chemie*, **1941**, *54*(51-52), 527.

[53] D. R. Lide, *Handbook of Chemistry and Physics;* CRC Handbook of Chemistry and Physics. Taylor & Francis Group, 89 ed., 2008.

[54] S. Kalytchuk, O. Zhovtiuk, and A. L. Rogach, *Applied Physics Letters*, **2013**, *103*(10), 103105.

[55] X. Xu, R. Ray, Y. Gu, H. J. Ploehn, L. Gearheart, K. Raker, and W. A. Scrivens, *Journal of the American Chemical Society*, **2004**, *126*(40), 12736.

[56] X. Jia, J. Li, and E. Wang, *Nanoscale*, **2012**, *4*(18), 5572.

[57] S. Sahu, B. Behera, T. K. Maiti, and S. Mohapatra, *Chemical Communications*, **2012**, *48*(70), 8835.

[58] A. B. Greytak, P. M. Allen, W. Liu, J. Zhao, E. R. Young, Z. Popović, B. J. Walker, D. G. Nocera, and M. G. Bawendi, *Chemical Science*, **2012**, *3*(6), 2028.

[59] S. F. Wuister, C. de Mello Donegá, and A. Meijerink, *The Journal of Physical Chemistry B*, **2004**, *108*(45), 17393.

[60] T. Otto, P. Mundra, M. Schelter, E. Frolova, D. Dorfs, N. Gaponik, and A. Eychmüller, *Chemphyschem: a European Journal of Chemical Physics and Physical Chemistry*, **2012**, *13*(8), 2128.

[61] L. Liu and X. Zhong, *Chemical Communications*, **2012**, *48*(46), 5718.

[62] H. G. Bagaria, G. C. Kini, and M. S. Wong, *The Journal of Physical Chemistry C*, **2010**, *114*(47), 19901.

[63] R. Xie, U. Kolb, J. Li, T. Basché, and A. Mews, *Journal of the American Chemical Society*, **2005**, *127*(20), 7480.

[64] A. Aharoni, T. Mokari, I. Popov, and U. Banin, *Journal of the American Chemical Society*, **2006**, *128*(1), 257.

[65] W. Zhang, G. Chen, J. Wang, B.-C. Ye, and X. Zhong, *Inorganic Chemistry*, **2009**, *48*(20), 9723.

[66] W. C. Chan and S. Nie, *Science*, **1998**, *281*(5385), 2016.

[67] S. Tamang, G. Beaune, I. Texier, and P. Reiss, *ACS Nano*, **2011**, *5*(12), 9392.

[68] M. Q. Dai and L. Y. L. Yung, *Chemistry of Materials*, **2013**, *25*(11), 2193.

[69] A. N. Jumabekov, F. Deschler, D. Bohm, L. M. Peter, J. Feldmann, and T. Bein, *The Journal of Physical Chemistry C*, **2014**, *110*(10), 5142.

[70] V. V. Breus, C. D. Heyes, and G. U. Nienhaus, *The Journal of Physical Chemistry C*, **2007**, *111*(50), 18589.

[71] J. McBride, J. Treadway, L. C. Feldman, S. J. Pennycook, and S. J. Rosenthal, *Nano Letters*, **2006**, *6*(7), 1496.

[72] A. M. Munro, I. Jen-LaPlante, M. S. Ng, and D. S. Ginger, *The Journal of Physical Chemistry C*, **2007**, *111*(17), 6220.

[73] M. Thiry, K. Boldt, M. S. Nikolic, F. Schulz, M. Ijeh, A. Panicker, T. Vossmeyer, and H. Weller, *ACS Nano*, **2011**, (6), 4965.

[74] H. Borchert, D. V. Talapin, N. Gaponik, C. McGinley, S. Adam, A. Lobo, T. Möller, and H. Weller, *The Journal of Physical Chemistry B*, **2003**, *107*(36), 9662.

[75] S. K. Poznyak, N. P. Osipovich, A. Shavel, D. V. Talapin, M. Gao, A. Eychmüller, and N. Gaponik, *The Journal of Physical Chemistry B*, **2005**, *109*(3), 1094.

[76] N. P. Osipovich, A. Shavel, S. K. Poznyak, N. Gaponik, and A. Eychmüller, *The Journal of Physical Chemistry B*, **2006**, *110*(39), 19233.

[77] V. V. Matylitsky, A. Shavel, N. Gaponik, and A. Eychmüller, *The Journal of Physical Chemistry C*, **2008**, page 2703.

[78] W. Zhang and X. Zhong, *Inorganic Chemistry*, **2011**, *50*(9), 4065.

[79] T. Otto; *Herstellung und Charakterisierung von Nanokristall-Lichtemitterdioden;* Dissertation, TU Dresden, **2011**.

[80] United States National Bureau of Standards, *Circular;* Number Nr. 530,Bd. 1 Nr. 539,Bd. 2. U.S. Govt. Print. Off., Michigan, 1953.

[81] T. Erdem, Z. Soran-Erdem, P. L. Hernandez-Martinez, V. K. Sharma, H. Akcali, I. Akcali, N. Gaponik, A. Eychmüller, and H. V. Demir, *Nano Research*, **2015**, *8*(3), 860.

[82] J. Burgees, *Metal ions in solution;* Ellis Horwood, 1981.

[83] A. M. Smith, M. C. Mancini, and S. Nie, *Nature Nanotechnology*, **2009**, *4*(11), 710.

[84] A. L. Rogach, A. Eychmüller, S. G. Hickey, and S. V. Kershaw, *Small*, **2007**, *3*(4), 536.

[85] S. V. Kershaw, M. Harrison, A. L. Rogach, and A. Kornowski, *IEEE Journal of Selected Topics in Quantum Electronics*, **2000**, *6*(3), 534.

3. Optical and Structural Analyses

In the previous chapter, different ways for producing QD-salt mixed crystals were discussed, while an overview of the possibilities they offer was also provided. However, an in-depth understanding of the processes occurring during the QD incorporation and their impact on the optical properties of the resulting mixed crystals is necessary. The determination of both optical and structural peculiarities of the mixed crystals provides the basis for their specific design. This information can be gathered by using TEM, chemical and optical stability tests as well as time-resolved and steady-state photoluminescence measurements which will be discussed in the upcoming chapter.

To allow the use as color conversion materials, high PL-QY as well as reproducible and stable emission spectra are among the essential requirements. Consequently, a systematic study allowing to interpret changes in the luminescence behavior of the QD colloids upon incorporation into the ionic matrices was performed. In order to understand the origin of the bright emission of QD-salt composites and to aim at an efficient matrix control of their PL-QY, the PL behavior of these fascinating materials was studied in more detail. Therefore, differently sized parent CdTe QDs with two different thiol capping ligands, TGA and MPA as well as CdTe QDs with low and high PL-QY in an aqueous solution were focused. The resulting QD-salt composites were characterized by the absolute measurements of their PL-QY and studies of their PL decay kinetics. Additionally, the PL behavior of different CdSe/ZnS QDs with an alloyed gradient shell and a stabilization by OA and MPA was analyzed. They were incorporated into different matrices according to the "classical" and the LLDC approach in order to understand the influence of the salt matrix on the PL properties of the embedded QDs better.

The production of a high-performance optical material based on QDs embedded into a matrix is only possible when the QDs are well separated within the host, preventing prominent self-quenching mechanisms. TEM measurements grant the possibility to evaluate the mixed crystals on a nanometer scale and to check if the different preparation methods yield non-aggregated QDs within the matrix.

Besides superior initial optical properties, potential color conversion materials need to provide a sufficient durability in terms of photo-oxidation and chemical stability. These studies will be discussed in section three of this chapter.

3.1. Photoluminescence Quantum Yield Measurements*

Over the last decades, fluorescence spectroscopy became a major tool for determining and analyzing a variety of samples, including classical organic dyes [4,5], rare-earth doped oxides [6,7], upconversion materials [8,9] and QDs [10,11]. Apart from the position and shape of the fluorescence spectra, the PL-QY ϕ is one of the key factors allowing to evaluate and classify all the above mentioned samples. ϕ is defined as the ratio of emitted to absorbed photons and is therefore a straight measure of the fluorophores' luminescence efficiency, playing an important role in applications as fluorescent labels [5,12,13], dye-sensitized solar cells [14–16], color conversion materials [1,17] and in biological assays [18–20].
The measuring of the PL-QY is usually carried out in two possible ways, although other measurement procedures are known requiring more sophisticated setups. [21–23] Both methods have advantages and disadvantages which are briefly summarized in Table 3.1. [24]

Table 3.1.: Main differences of relative and absolute quantum yield measurements

Relative determination	Absolute determination
Suitable for liquid, non-scattering samples	Suitable for all (non-)scattering samples
Measured by using a fluorescence standard emitting in the same spectral region	No standard needed
Sample optical density (OD) must match the OD of the standard	Sample OD more variable, lower ODs are easier to measure
Excitation wavelength mainly determined by the fluorescence standard used	Excitation wavelength variable, only limited by the instrument itself
No blank sample needed	Blank sample needed
Roughly 20 min per measurement	Roughly 20 min per measurement
Easy to perform with most common fluorescence spectrometer setups	More sophisticated setup including an integrating sphere

*Parts of this chapter have already been published. [1–3]

The first option is based on a relative measurement [25] in comparison to a fluorescent standard of a known fluorescence quantum yield. In the second attempt, an absolute measurement with an integrating sphere setup [26] is applied. As shown in Table 3.1 and Figure 3.1, relative PL-QY measurements require only a common laboratory equipment, e.g., a standard absorption and fluorescence spectrometer. On the other hand, the main drawback of this method is the need for a reliable and spectrally matching fluorescence standard of known ϕ.

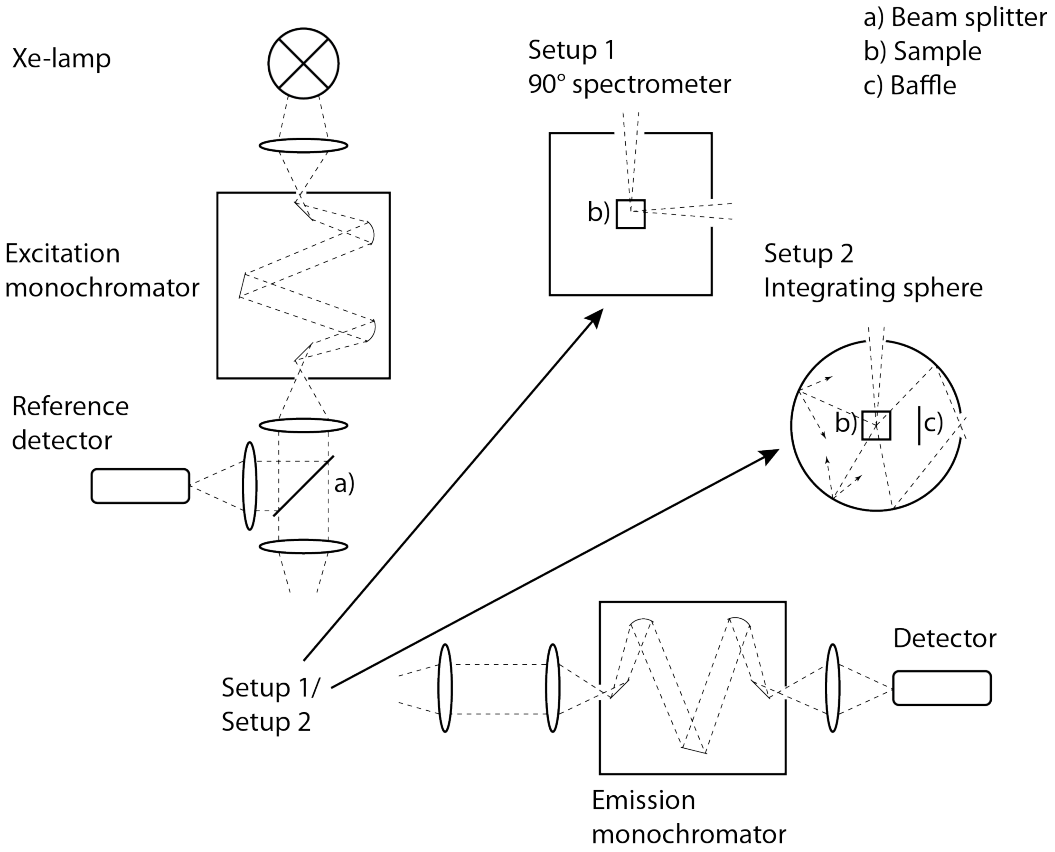

Figure 3.1.: Schematic illustration of a fluorescence spectrometer. [26] By using setup 1, all measurements are carried out in a 90° measurement geometry, capable of measuring relative quantum yields of non-scattering samples. The more sophisticated setup 2 includes an integrating sphere as sample chamber, providing the possibility of an absolute quantum yield determination and the reliable measurement of scattering samples. It should be noted that in the case of the 90° geometry, polarizes could be equipped before and after the sample chamber, enabling anisotropy fluorescence measurements. Adapted by courtesy of Macmillan Publishers Ltd: Nature Protocols 8, 1535-1550, copyright 2013.

Absolute measurements spare the need for a fluorescence standard but require more sophisticated setups which are not yet available everywhere. Furthermore, an optically matching blank is needed to correct matrix effects in the case of absolute PL-QY measurements. The main reason for the different requirements of the two methods originate is that, within an integrating sphere, all emitted photons are collected, whereas in a 90° fluorescence spectrometer only a small portion of the samples' emitted photons is collected. This share cannot be determined for sure, since it depends on many factors, including emission wavelength, scattering of the sample, sample geometry, refractive index of the solvent, etc. [24] Therefore, the sample has to be compared to a known standard with closely matching optical properties.

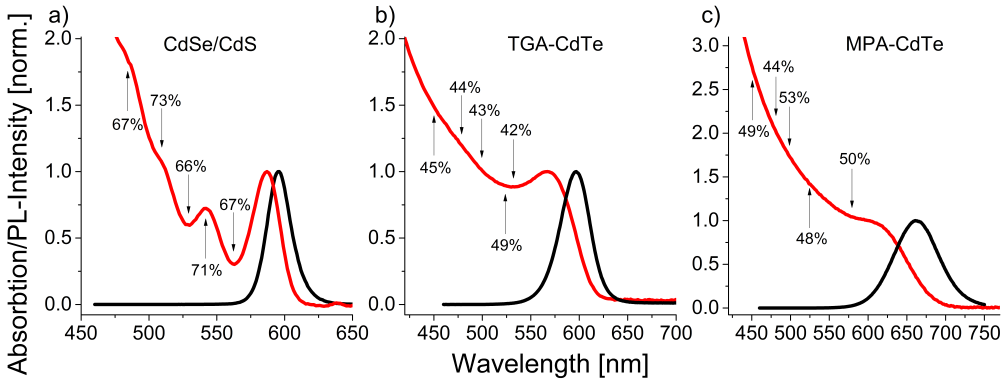

Figure 3.2.: PL (black) and absorption (red) spectra of a) CdSe/CdS, b) TGA-stabilized CdTe and c) MPA-stabilized CdTe. Arrows mark the chosen excitation wavelengths for PL-QY measurements and the corresponding PL-QY. For this study, all measurements were conducted at least twice and the average is shown here.

While the excitation wavelength is strongly predetermined by the fluorescence standard in the case of relative measurements, it can be freely chosen for an absolute determination. Therefore, possible λ_{ex} dependencies of the PL-QY need to be considered when the latter method is used. In case of relative measurement, dependencies can hardly be evaluated due to the restricted λ_{ex}, predetermined by the fluorescence standard used. As reported in the literature [27], PL-QY of both core and core/shell QDs may vary depending on the chosen excitation wavelength, especially in the higher energy excitation range. In Figure 3.2, both absorption and PL spectra of three different QD systems are displayed. PL-QYs were measured at five different wavelengths, where the absorbance spectrum showed defined features in the case of CdSe/CdS, displayed in graph a). For the CdTe systems in graphs b) and c), no clearly resolved transitions with the exception of the 1s-1s can be derived from the absorbance spectra. Therefore, wavelengths generally used for absolute PL-QY measurements

(480 and 450 nm) or relative measurements by using the most common dyes Rhodamine 6G and 101 (500 and 525 nm) were chosen. The fifth λ_{ex} for these systems was selected to be within the energetically higher depression following the 1s-1s transition. As it can be seen from Figure 3.2, the measured PL-QYs fluctuate mainly within the systematical error of the procedure, determined to be lower than 7% [28] in the analyzed spectral area. Still, a general independence of the PL-QYs from the λ_{ex} for these three QD systems cannot be excluded. Therefore, all of the following measurements were conducted at a fixed excitation wavelength of 480 nm, unless this would overlap with the QDs emission in the case of cyan samples. In those cases, 450 nm were chosen as λ_{ex} to ensure that the measured results can be compared to each other.

Nevertheless, in case of both absolute and relative determinations, PL-QY measurements are nontrivial and may be influenced by a large amount of potential error sources. Some of the most common errors as well as how they can be avoided are discussed in the subsequent paragraph.

The equipment shall be thoroughly cleaned, especially the cuvettes used. They should be made of the same material (quartz is mandatory for measurements at wavelengths $<$ 400 nm), have four polished windows and identical dimensions. Only spectroscopy grade purity is recommended as solvents and standard dyes, since even small amounts of impurity may affect the measured results. While the sample and standard solution are prepared, ca. 15 min of equilibration time is recommended to ensure a proper dispersion of the sample in the cuvette and to dissolve aggregates of solid samples. This can be monitored by measuring the absorbance spectra within a short time interval of 10-15 minutes. If the measured spectra differ, longer equilibration times are needed to ensure valid measurements. Secondly, the absorbance of the analyte and (if applicable) the standard have to be below 0.1 ($<$ 0.05 for absolute measurements) at the desired excitation wavelength to minimize reabsorption effects. On the other hand, the concentration should not be too low, since otherwise the measurements may be distorted by poor signal intensities and concentration dependencies of the PL-QY. [29] Therefore, absorbance ranging from 0.01 to 0.1 (0.05 in case of absolute measurements) are recommended. Before the measurements are started, the calibration of the monochromators of the spectrometers shall be checked by using standard procedures provided by the manufacturer. Additionally, the amount and position (in case of, e.g., hydrogels) of the analyte solution in the cuvette shall be selected to ensure that the excitation beam hits the sample. Proper excitation wavelengths and emission ranges need to be used for the measurements as well as an optically matching blank in order to correct matrix influences. Furthermore, appropriate temperature conditions are necessary, since a variety of samples

shows temperature-dependent PL-QYs. A comprehensive knowledge of the samples' behavior is also required to ensure that no sample-solvent or sample-excitation light interaction may corrupt the conducted measurements.
Finally, Table 3.2 displays four different widely used fluorescence standard materials for the visible range of the electromagnetic spectrum. These materials meet the standards defined in a technical note by the IUPAC [30] and can be purchased with a reliable purity at reasonable prices. They can furthermore be used without special conditions like purification steps, inert atmosphere or uncommon solvents, making them easily applicable.

Table 3.2.: Selected known fluorescence standards, their emission and absorption ranges, solvents and fluorescence quantum yields. [24]

	Solvent	Absorbance [nm]	Emission [nm]	Fluorescence quantum yield
Quinine sulfate	0.105 M $HClO_4$	270 - 400	385 - 700	0.59
Fluorescein	0.1 M NaOH	400 - 550	490 - 690	0.89
Rhodamine 6G	Ethanol	425 - 575	505 - 750	0.91
Rhodamine 101	Ethanol	475 - 620	540 - 750	0.915

3.1.1. PL-QY Measurements on QDs and Mixed Crystals

All samples, both parental colloidal QD solutions as well as mixed crystals were prepared according to the methods described in Chapter 2. Due to the variety of facets and shapes of the mixed crystals, they were ground to a fine powder prior to the measurements to ensure a reproducible scattering behavior of the different samples. Subsequently, the PL properties of the pure powders and the powders incorporated into silicone, a common matrix for the hybridization of color conversion layers with LEDs (as shown in Figure 3.3), were studied in comparison to those of the parent QD solutions. The photoluminescence quantum yield of the QDs in solution, the QD-salt crystals, and the QD-salt crystal silicone composites were absolutely determined either with a custom-designed integrating sphere setup [31] or by using a commercial FluoroLog-3 spectrofluorometer (Horiba Jobin Yvon) fitted with a Quanta-Φ integrating sphere. Further information on both setups regarding sample placing, excitation wavelengths, etc., can be found Appendix A.7. and A.8.
The luminescence decays of the QDs in solution, in the crystal matrices and in the silicon pellets were measured with identical instrument settings to obtain comparable values, e.g., similar

excitation wavelengths, detection at the emission maximum, identical detection/excitation band passes, and repetition rates (0.5 or 1 MHz). To evaluate the data, the PL-LTs of these multiexponential decays were set equal to the time when the intensity corresponds to 10,000/e of the initial intensity.

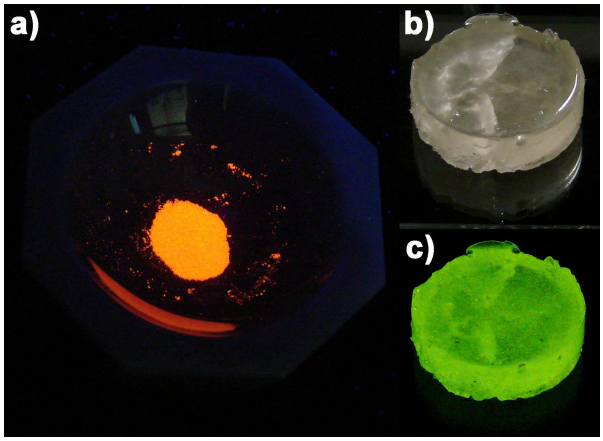

Figure 3.3.: Photograph of an exemplarily chosen QD-salt composite a) after grinding and another exemplarily chosen QD-salt composite sample (b),c) after grinding and incorporating into silicone. The photographs were taken under room light (b) and UV light (a), c). Adopted by courtesy of Chem. Mater. 2014, 26, 3231. Copyright 2014, American Chemical Society.

At first, the concentration of the QD-salt crystals embedded in silicone was optimized for the PL studies. Therefore, three QD-salt silicone composites of an exemplarily chosen QD-salt batch were prepared, varying the amount of the QD-salt powder to determine a concentration range suitable for accurate PL-QY measurements with a minimum reabsorption contribution. The concentrations were chosen to be 5, 10, and 20 mg of powder per 500 μL silicone, as it can be seen in Table 3.3.

Table 3.3.: PL-QY and absorption of a set of silicone pellets containing different amounts of the same QD-salt batch. Reprinted by courtesy of Chem. Mater. 2014, 26, 3231. Copyright 2014, American Chemical Society.

Concentration	PL-QY	Absorption
2.5 mg/mL	0.28	8.8%
5 mg/mL	0.30	27%
10 mg/mL	0.23	49%

Spectroscopic measurements of these samples revealed matching absorption and emission spectra, an increase in absorption with an increasing sample concentration as well as PL-QY values of 28%, 30% and 23%. The decrease in PL-QY found for the highest QD-salt concentration was attributed to reabsorption. Therefore, only 10 mg of powder were used for the subsequently prepared samples. The results of these first measurements also showed the considerable challenge of determining the PL-QY of these strongly scattering, asymmetrically faceted materials with acceptable uncertainties.

The PL-QY and PL-LT of various CdTe QD systems (parent QD, QD-salt crystal, and QD-salt crystal in silicone) were studied to achieve a better understanding of the PL behavior of the QD-salt crystal composites, to confirm the occurrence of matrix-induced PL enhancements and to obtain prerequisites for a PL enhancement. [32, 33] To ensure representative results, various CdTe QDs sample series were systematically studied including QDs of different sizes, QDs stabilized with either TGA or MPA as well as QDs having relatively low and relatively high PL-QY in a parent solution. Exemplarily chosen emission spectra are shown in Figure 3.4 for these materials.

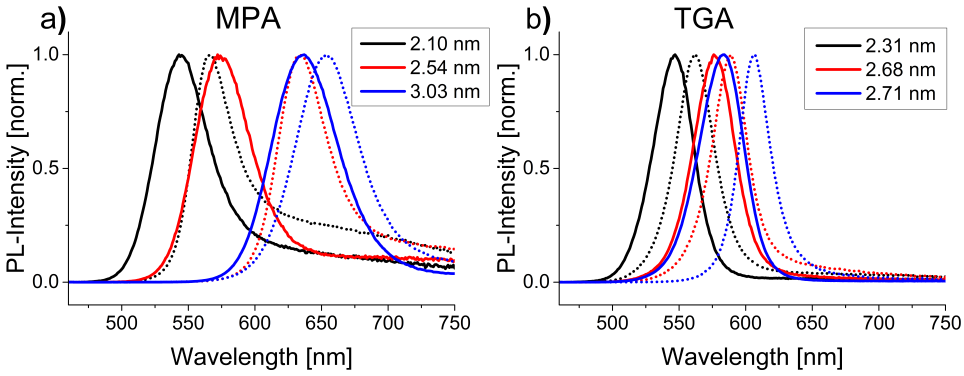

Figure 3.4.: Representative emission spectra of the used CdTe QDs. Graph a) shows the emission spectra of MPA-stabilized CdTe QDs with different sizes in solution (solid lines) and within the NaCl matrix (dotted lines). In graph b), the emission spectra of differently sized TGA-stabilized CdTe QDs in solution (solid lines) or within NaCl (dotted lines) are shown. All spectra were normalized for better comparison. The sizes were determined by using the 1s-1s transition maximum, following the method of Rogach et al. [34] Reprinted by courtesy of Chem. Mater. 2014, 26, 3231. Copyright 2014, American Chemical Society.

In order to clarify the influence of the QD-NaCl interface, salt composites of CdSe/ZnS QDs with Zn atoms on their surface as well as CdTe QDs incorporated into a halogen-free matrix

of borax were evaluated additionally. An overview of all samples discussed in the following sections can be found in Appendix A.8. These tables include information on the QDs, the stabilizing agent as well as PL-QY data and the decay behavior in solution, in the salt matrices and the corresponding enhancement factors.

Influence of the Mixed Crystal Incorporation into Silicone

As discussed in detail earlier, many potential applications of solid QD-salt mixed crystals, e.g., in the production of LEDs, require an incorporation of the QD-salt composites in an additional matrix such as silicone. Hence, mixed crystals from the same or comparable batches were studied both with and without silicone encapsulation. The overall goal was to ensure that the incorporation into silicone does not affect the beneficial optical properties of the solid QDs and to guarantee comparability of the measurements conducted on pure mixed crystals and silicone encapsulated ones. The matching PL-QY of a CdTe-NaCl mixed crystal batch measured in silicone and without silicone encapsulation (size of ~3 nm) and the very similar PL decay behavior (see Appendix A.8.) emphasize the negligible influence of such an additional polymer matrix. The immediate QD environment is obviously not affected by silicone when micrometer-sized QD-salt composites are used.

Influence of PL-QY of the Parent QD on the PL-Properties of QD-Salt Mixed Crystals

In order to understand the influence of the PL-QY of the parent QDs on the PL-QY of the resulting QD-salt composites better, the PL properties of mixed crystals made from CdTe QDs with high (ca. 50% in solution) and low (ca. 10% in solution) PL-QY were compared. The PL-QYs of four different CdTe QDs in solution and in a NaCl matrix are shown in Figure 3.5 a). The two samples originating from QDs with low PL-QY in solution showed a very promising PL enhancement of more than 2.5 times, thereby considerably exceeding the PL increase reported in reference [33] for CdTe QDs with comparable PL-QY. The composites derived from parent QDs, which already in solution have a stronger emission, revealed only an increase in PL-QY by a factor up to 1.3 after the incorporation into NaCl crystals. Nevertheless, the PL-QYs of the analyzed CdTe salt crystal composites were on average between 30% and 80% (see Appendix A.8.). This emphasizes the remarkable potential of this simple strategy to obtain highly emissive solids of QDs. PL-LT measurements performed with the samples revealed multiexponential decay kinetics for both the CdTe solution and the CdTe salt composites, as

it was expected for these rather heterogeneous systems (see Figure 3.5). The corresponding lifetimes are summarized in Appendix A.8. together with the PL-QY data. As shown in Figure 3.5 b), despite the considerable PL enhancement, the PL-LT and the decay kinetics of the QDs incorporated into the NaCl salt crystals change only slightly in comparison to the parent QD solutions.

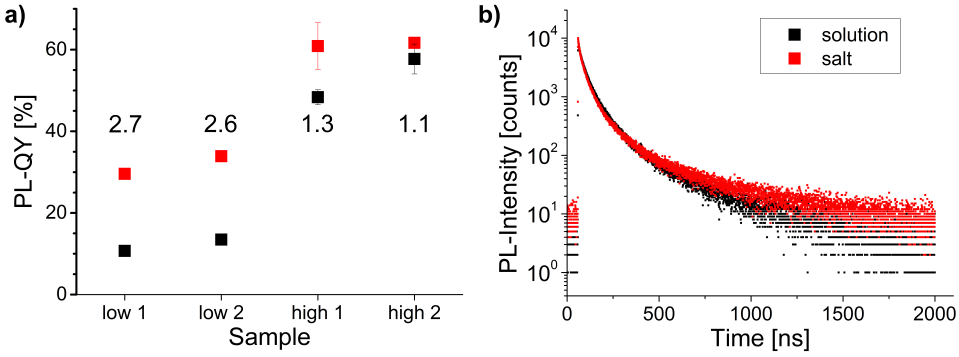

Figure 3.5.: a) PL-QY of four exemplarily chosen CdTe QD samples with relatively low (low 1, 2) and high (high 1, 2) PL QYs of parent solutions. The black squares show the PL-QY of the QDs in solution and the red ones the PL-QY of the QDs in the NaCl crystals. The numbers in the panel provide the salt-induced PL-QY enhancement factor of the QDs as compared to their solution values. b) PL-LT decay curve of the CdTe sample "low 1" in solution (black squares, PL-LT of 16.9 ns) and within the salt crystals (red squares, PL-LT of 14.6 ns). Reprinted by courtesy of Chem. Mater. 2014, 26, 3231. Copyright 2014, American Chemical Society.

To correlate PL-QY and PL-LT, it must furthermore be considered that the presented data arise from ensemble measurements of QDs and from QDs revealing multiexponential decay kinetics. These ensemble data reflect most likely a broad distribution in PL-QY, the distribution of trap states on the QD surface or core/shell interface and the heterogeneous QD environment. Moreover, an energy transfer from smaller to larger QDs is also possible, as suggested by the red shift in emission observed for nearly all nanocrystal-salt systems. The PL-QY ensemble data equal the number of photons emitted per absorbed photon of the QD ensemble studied, with the sample-specific fraction of dark QDs contributing only to the absorption measurement. A correlation between the PL-QY and the ratio of bright to dark QDs was for example shown by Ebenstein et al. [35] for CdSe/ZnS nanocrystals by single particle measurements of QD ensembles of varying PL-QY. PL-LT data of QD ensembles are usually dominated by the decay behavior of the strongest luminescent QDs, with no or

very little contribution from weakly emitting (or dark) QDs. Although PL-QY and PL-LT are straight correlated for molecular emitters showing usually monoexponential decay kinetics in a homogeneous environment, [36] a straightforward and stringent correlation for PL-QY and the decay behavior of QD ensembles has not yet been reported. For such systems, only similar tendencies of both parameters can be observed usually, with changes in PL-QY often exceeding the corresponding changes in the decay behavior. [27, 37] A possible explanation was given by Bawendi et al. showing with single particle measurements that fluctuations of the decay rates can be caused by changes in emission intensities of single QDs. [38] Rogach et al. who similarly reported multiexponential decay kinetics for their materials could not find a clear correlation between both quantities for their QD-salt systems. [33] One explanation for the stronger changes in PL-QY compared to those in the decay behavior, even when considering the respective changes in radiative rate constants caused by a change of the surrounding matrix, presented in the literature, [1] could be the following. An improved surface passivation of the QDs in the salt crystal especially enhances the PL-QY of weakly-emissive nanocrystals causing their PL-LT to reach similar values, as already observed for stronger emissive QDs. In summary, the observed PL changes seem to arise from both changes in refractive index and changes in the radiative and non-radiative rate constants.

Influence of QD Size on the Luminescence Behavior of CdTe-NaCl Composites

Afterwards, the influence of the parent QD size (and QD size-related PL-QY) on the luminescence properties of the resulting CdTe salt composites was studied. The evolution of PL-QY for a set of differently sized MPA-stabilized CdTe QDs is shown in the left part of Figure 3.6, revealing an enhancement in PL-QY with increasing particle size (from 2.1 to 3.0 nm) in solution. This is due to the improved crystallinity and, hence, a diminished number of surface defects evoking through a longer growing time as well as a reduced surface-to-volume ratio. [34] After the incorporation of the MPA-stabilized QDs into the NaCl matrix, the PL-QY increased for all sizes, yet in a particle size-specific manner, thus yielding size-dependent enhancement factors ranging from 1.1 to 2.8. This is consistent with the behavior of the samples shown in Figure 3.5. A similar tendency can be observed for the TGA-stabilized samples shown in the right part of Figure 3.6. For this ligand, the differences in the enhancement factors of the differently sized QDs (2.3-2.7 nm) are less distinct, ranging from 1.1 to 1.6. Nevertheless, it can be concluded that the tendency of size-specific PL-QY enhancement does not depend on the QD's stabilizing agent. Figure 3.6 also emphasizes the stronger PL-QY enhancement found here in comparison to the effects reported by the

authors of reference [33]. These favorable effects can be attributed to the different synthetic methods given in references [39, 40] (i.e., in the ratios of the precursors) applied for producing the CdTe QDs within reference [33] and this work, respectively. The observed variations might also be ascribed to different amounts of QDs incorporated into the salt matrix yielding different ratios of reabsorption.

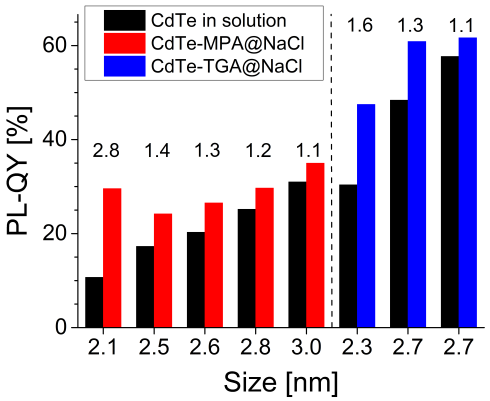

Figure 3.6.: PL-QY of thiol-stabilized CdTe QDs before (black) and after (red or blue) the incorporation into the salt matrix with the respective enhancement factors given as numbers. An increase of the particle size leads to a higher PL-QY in solution and a smaller PL-QY enhancement factor for both thiol ligands. The two TGA-stabilized samples with a radius of 2.7 nm differ slightly in size and, thus, also in the position of their absorption and emission maxima. Reprinted by courtesy of Chem. Mater. 2014, 26, 3231. Copyright 2014, American Chemical Society.

Influence of Surface-$CdCl_x$ on PL-QY

The increase in PL-QY upon incorporation of CdTe into NaCl crystals also agrees with the findings of Sargent and co-workers regarding the influence of halide ions on the emission intensity of PbS QDs. [41, 42] This enhancement was attributed to the formation of a thin $PbCl_x$ or $CdCl_x$ layer, as depicted in Figure 3.7 a), which seems to passivate dangling bonds on the QD surface. This results in a reduction of the non-radiative relaxation routes and an increase of PL-QY. While comparing the measured PL-QY enhancement factors for the samples shown in Figure 3.7 b) with their corresponding change in the PL emission maxima, a clear correlation was found. As shown in Appendix A.8., all samples exceeding the model-predicted PL-QY enhancement factors show a slightly larger red shift in their emission maximum than the samples which are within the predicted range of the models discussed in reference [1].

These findings indicate that the formation of a $CdCl_x$ shell might be a reason for the PL-QY enhancement reaching beyond the model predictions. Indeed, a proper shell formation usually causes a red shift in the emissions of QDs which was also observed by Sargent et al. for QDs with $CdCl_x$ shells. [41]

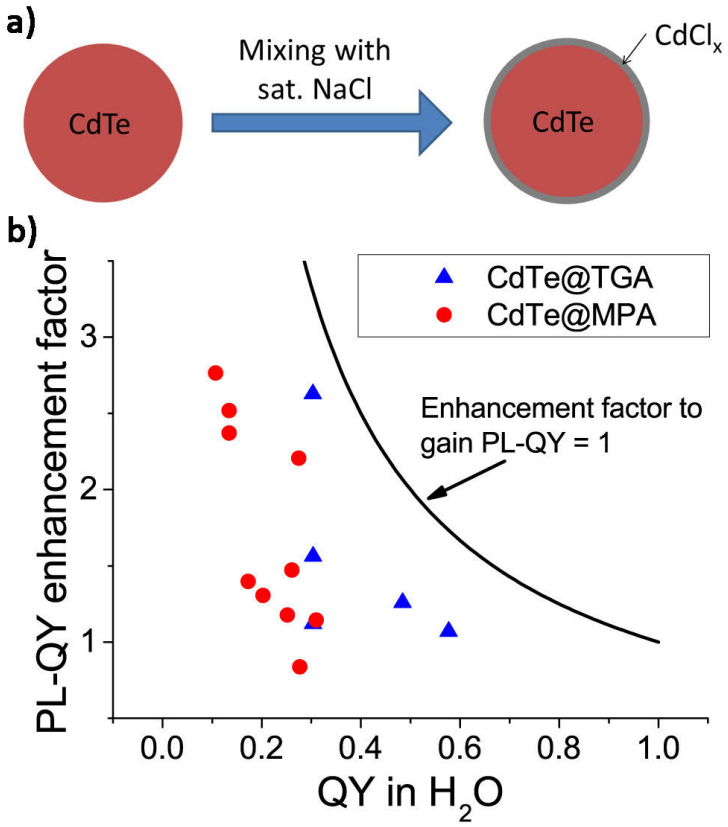

Figure 3.7.: a) Formation of a thin $CdCl_x$ layer on the surface of a CdTe-QDs after mixing the QD solution with the saturated NaCl solution. b) Enhancement of PL-QY values arising from the incorporation of thiol-stabilized CdTe into a NaCl matrix for differently sized CdTe (radii of 2-3 nm) QDs. For better orientation, enhancement factors allowing a gain of PL-QYs = 1 are shown as solid line. Adopted by courtesy of Chem. Mater. 2014, 26, 3231. Copyright 2014, American Chemical Society.

To verify the hypothesis of surface defect curing related to the formation of a chloride layer and the binding of chloride to surface Cd atoms, comparative studies of CdSe/ZnS QDs embedded in NaCl crystals and CdTe QDs in $NaB_4O_7 \cdot 10\ H_2O$ (sodium tetraborate or borax), were performed respectively. In both cases, $CdCl_x$ cannot be formed on the QD surface. According to Figure 3.8, CdSe/ZnS QDs show a typical drop in PL-QY during the

ligand-exchange mediated phase-transfer from organic media (OA-capped) to H_2O (MPA-capped) [43,44] which remains almost unaffected by the incorporation into the NaCl host. In the case of borax-encapsulated CdTe, the PL-QY of the QDs increases only slightly upon incorporation in the salt matrix (see Figure 3.8 b) and the Appendix A.8.). Changes of PL-QY which are below the expected refractive index-induced changes, indicate an increase of non-radiative processes. This suggests that the formation of $CdCl_x$ at the QD surface which can occur for CdTe in NaCl possibly contributes to the salt-crystal induced PL enhancement. Also PL-QY values with different QD-NaCl systems shown in Appendix A.8. emphasize the assumption of a salt-induced curing of Cd atom-related surface defects.

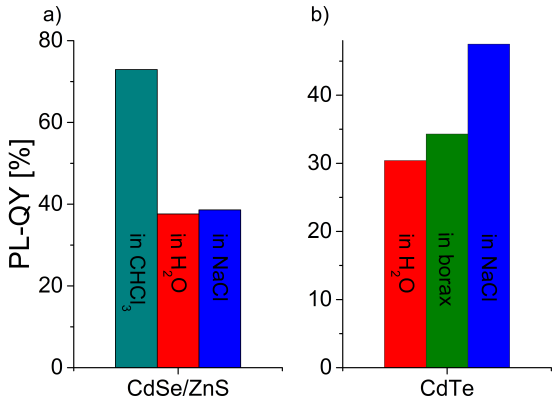

Figure 3.8.: a) Relative PL-QY of CdSe/ZnS and the respective QD-salt mixtures. OA-capped CdSe/ZnS QDs were phase transferred from $CHCl_3$ to H_2O by a ligand exchange using MPA as a new stabilizing ligand, resulting in a PL-QY drop, whereas subsequent incorporation into NaCl causes only a negligible change in PL-QY. (b) CdTe QDs from one batch were incorporated into either $NaB_4O_7 \cdot 10\ H_2O$ or NaCl crystals, yielding almost no change for the former but a strong increase by a factor of 1.5 in the case of the NaCl host. Adopted by courtesy of Chem. Mater. 2014, 26, 3231. Copyright 2014, American Chemical Society.

Influence of the Crystallization Time: LLDC vs. "Classical" Approach

As discussed in the second chapter, the LLDC is an extremely fast method for forming CdTe-NaCl mixed crystals. To figure out if such rapid crystallization rates have an influence on forming a passivating $CdCl_x$ shell, these samples were analyzed regarding their PL-QY evolution. By using CdTe QDs as emission centers, the PL-QY did not change in the course of transferring them from the parent solution to the NaCl crystals by using the LLDC. This

suggests that the fast crystallization procedure does not allow to form a complete passivating $CdCl_x$ shell since this should result in an increase of the PL QY as discussed in the previous sections.

Influence of ZnS-Shell Thickness on the Luminescence Behavior for CdSe/ZnS QD-Salt Mixed Crystals

As shown in Figure 3.8 a), the PL-QY of alloyed CdSe/ZnS QDs decreases upon ligand exchange as expected to ca. 50% of its initial value. According to reference [45], the one-pot synthesis used yields QDs with different emission colors by adjusting the ratios of the precursors while the overall size of the QDs remains almost constant. Therefore, adjusting the precursor ratios only changes the ratio of core size to shell thickness which might have a significant influence on the behavior of the QDs upon ligand exchange and the subsequent incorporation into the ionic matrix. To evaluate this influence, these QDs were characterized regarding their PL-QY and PL-LT properties after the incorporation into NaCl by using the two-step LLDC as well as the "classical" approach with borax as ionic matrix.

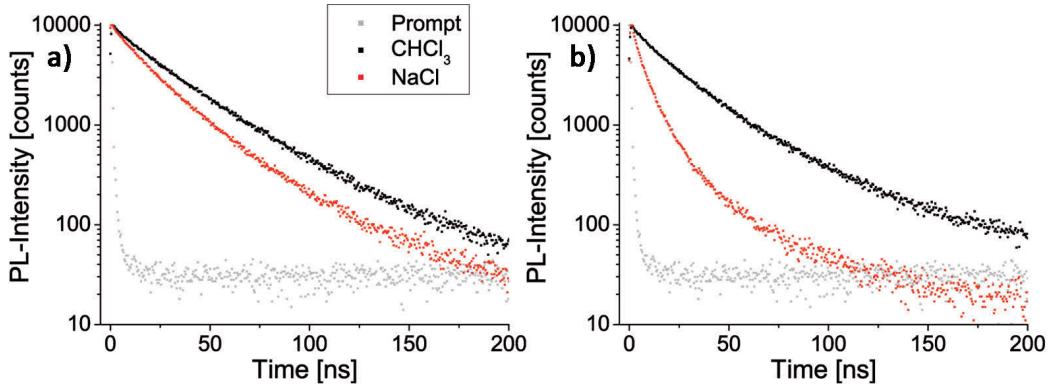

Figure 3.9.: Photoluminescence decay rates of a) green-emitting CdSe/ZnS alloy QDs and b) red-emitting CdSe/ZnS alloy QDs in chloroform (black squares) and after their encapsulation into NaCl (red squares) by using the two-step LLDC method. The light grey squares represent the prompt measurement. Reprinted by courtesy of Chem. Mater. 2014, 26, 3231. Copyright 2014, American Chemical Society.

Red- and green-emitting samples shown in Figure 2.33 were chosen as representative examples for the LLDC approach. The measurements shown in Figure 3.9 proved that the PL-LT dropped from 27.65 ns in $CHCl_3$ to 20.04 ns in NaCl and from 23.34 to 7.45 ns for the green- and red-emitting QDs respectively. At the same time, the decrease in the PL-QY was relatively

lower in both cases, i.e., from 42.2% in $CHCl_3$ to 34.7% in NaCl and from 36.5% to 16.2% for the green and the red samples respectively. This observation is in good agreement with the conception mentioned in Section 2.3.2 that the QDs are mainly concentrated around the initial crystallization seeds formed in the first step. A close proximity between the individual QDs in such a shell results in a higher risk of self-quenching. In this respect, a stronger decrease in PL-QY for the red-emitting QDs can be explained by the thinner protecting ZnS shell on their surfaces, making it easier for charge carriers to reach the surface for any kind of environment-related quenching process. On the other hand, the green-emitting QDs used have a thicker ZnS shell, confining the charge carriers stronger within the core and reducing the possibility for environment-related quenching processes to happen. [46] To test this hypothesis, mixed crystals were prepared by using the two-step LLDC approach with bare, non-shelled CdSe QDs as emitting centers. As expected, these samples showed a complete loss of PL upon incorporation into NaCl crystals.

Green-, yellow- and red-emitting CdSe/ZnS QDs with an alloyed gradient shell were used for the "classical" mixed crystallization approach with borax as host matrix. PL-LT and PL-QY measurements were conducted in $CHCl_3$, H_2O and borax for all samples; the corresponding results are given in Figure 3.10. As expected from recent studies on mixed crystals, [1, 2, 33] all samples show a stronger change in the PL-QY than PL-LT at all stages (and thereby during the change of the surrounding media) while both figures exhibit similar trends. This behavior was previously discussed in the literature, [37] and Chapter 3.1.1 considering the fact that both PL-QY and PL-LT data arise from ensemble measurements of QDs revealing multiexponential decay kinetics. Secondly, the results are in good agreement with the findings of the recent mixed crystal PL-QY study. [1] An encapsulation of CdSe/ZnS QDs into an ionic matrix does result in a significant increase in PL-QY, since no passivating $CdCl_x$ can be formed on the QDs surface.

A comparison of LLDC-based mixed crystals with the "classical" approach based on borax as host matrix reveals that both methods cause comparable reductions in PL-QY and PL-LT. Although a ligand exchange is not necessary for the LLDC-based samples, the partial aggregation and close proximity of the QDs within the mixed crystals is responsible for the relatively low PL-QY.

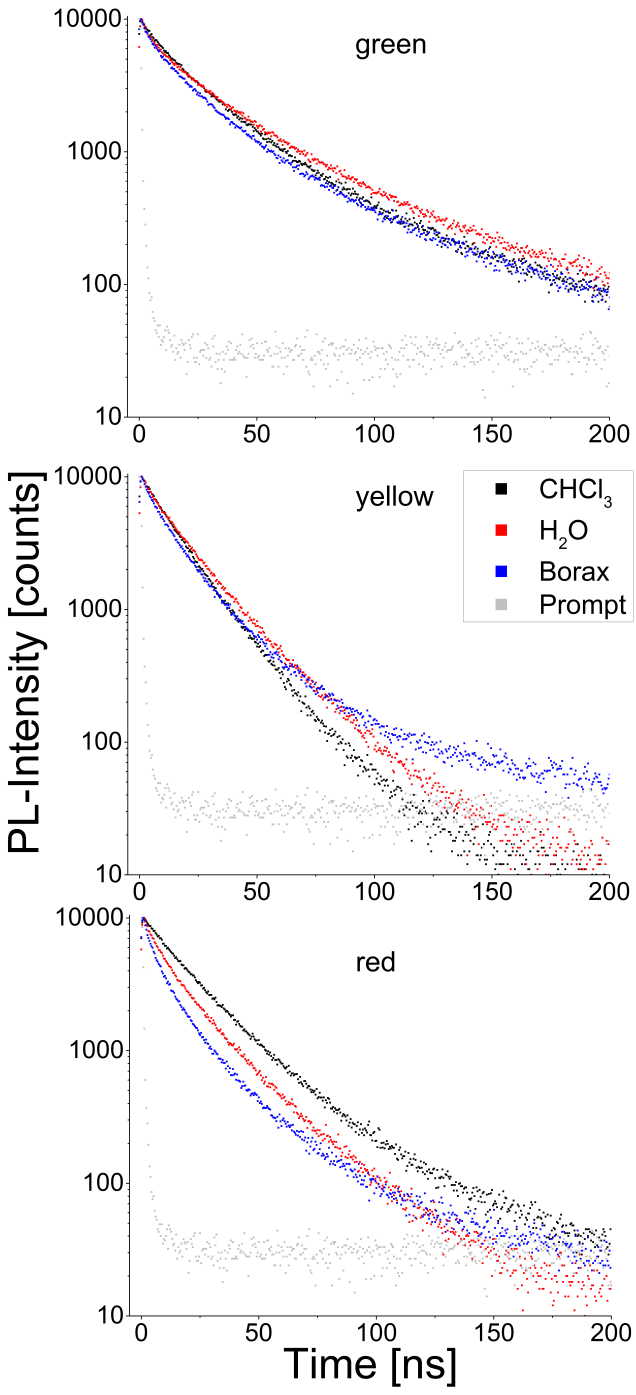

τ in $CHCl_3$	21.9 ns
τ in H_2O	21.2 ns
τ in Borax	17.6 ns
PL-QY in $CHCl_3$	38.5%
PL-QY in H_2O	23.8%
PL-QY in Borax	30.2%

τ in $CHCl_3$	16.5 ns
τ in H_2O	17.4 ns
τ in Borax	14.1 ns
PL-QY in $CHCl_3$	40.3%
PL-QY in H_2O	16.6%
PL-QY in Borax	15.7%

τ in $CHCl_3$	21.6 ns
τ in H_2O	14.7 ns
τ in Borax	9.9 ns
PL-QY in $CHCl_3$	42.6%
PL-QY in H_2O	17.6%
PL-QY in Borax	14.0%

Figure 3.10.: PL decay spectra of three different CdSe/ZnS QDs in $CHCl_3$ (black squares), H_2O (red squares) and after embedding into borax (blue squares). The grey squares represent the measured prompt. The corresponding average PL-LTs and PL-QYs for three QDs in different media are given within the tables. PL-QY values were measured three times and on average. Adapted by courtesy of ACS Appl. Mater. Interfaces 2015, DOI: 10.1021/acsami.5b08377. Copyright 2015, American Chemical Society.

3.2. Transmission Electron Microscopy Imaging*

When using TEM, samples can be imaged down to an atomic resolution, allowing to analyze their nanometer structure. At first, TEM images of pure QDs were obtained directly from the solution. Representative CdTe QD samples were imaged for the aqueous systems, as shown in Figure 3.11 a) and d). Image a) clearly shows that the QDs are non-aggregated, whereas image d) with a larger magnification reveals the spherical shape of the QDs with a narrow size distribution. CdSe/ZnS QDs with an alloyed gradient shell and different emission colors are displayed in Figure 3.11 b) - f). While images b) and e) correspond to a green-emitting sample, c) and f) represent a red-emitting batch. It is obvious that both batches show a similar size which is in good agreement with the results in the literature. [45,47] There, the authors stated that for the synthetic procedure, a change of the precursor ratios does not affect the overall size of the QDs but solely the core-shell ratio including thinner shells for red- and thicker shells for green-emitting fractions.

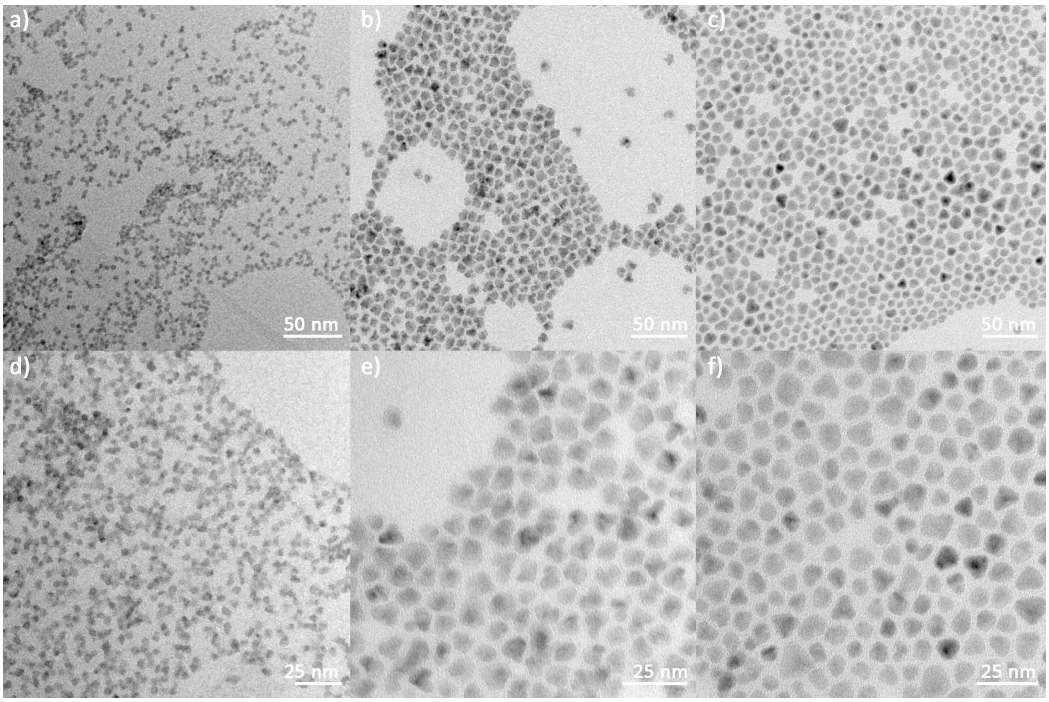

Figure 3.11.: TEM images of CdTe (a and d) as well as green- (b and e) and red-emitting (c and f) CdSe/ZnS QDs with an alloyed gradient shell.

*Parts of this chapter have already been published [2,3,32]

Due to the charging and melting upon electron beam exposure, a subsequent detailed and especially high-resolution TEM characterization of the mixed crystals is difficult. Figure 3.12 shows a set of images taken from the same small piece of a NaCl crystal containing CdTe QDs. As seen from the images, although separate QDs are not visible in the bulk crystal (Figure 3.12 a)), they may be recognized very well after the melting process has started (Figure 3.12 b)-d)). Separate crystalline QDs are seen in the high-resolution TEM image of the melting process (inset to Figure 3.12 d)). It was also observed that not aggregated but well-separated QDs dominate the crystals (e.g., see Figure 3.12 b) and c)). A partial aggregation as seen in Figure 3.12 d) occurs mainly during the melting process.

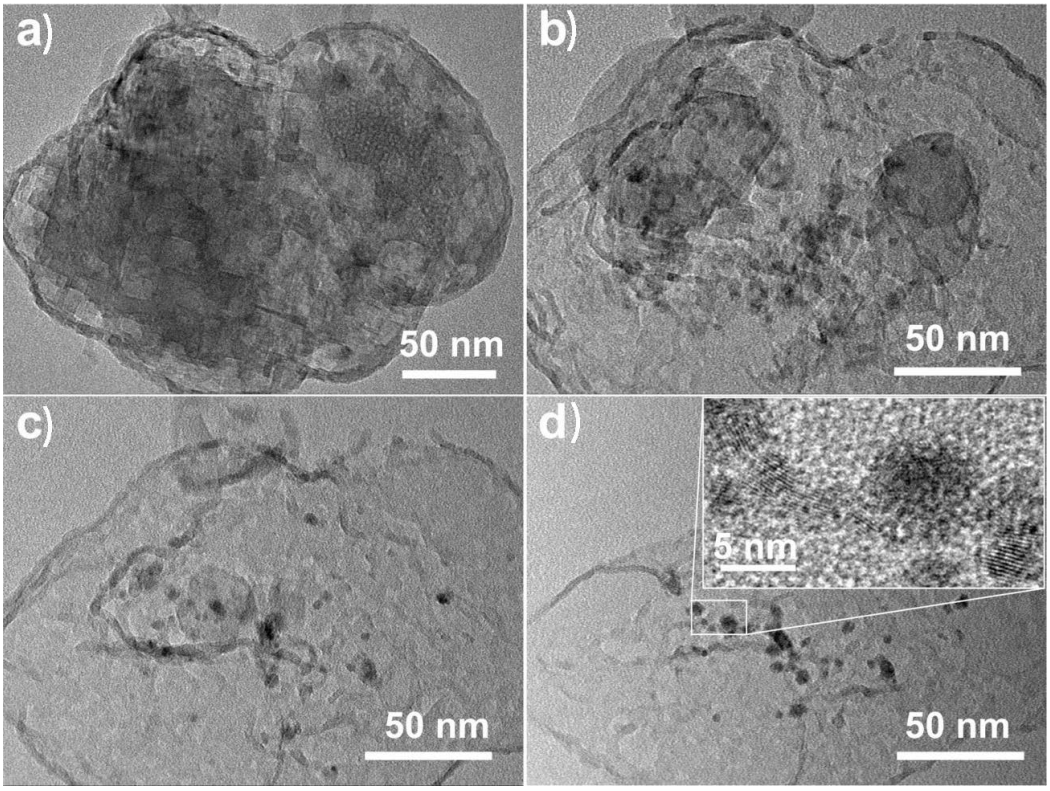

Figure 3.12.: Representative TEM (a-d) and high-resolution TEM (inset) images of a mixed crystal sample (NaCl + CdTe QDs). Images were taken from the very same part of the sample. The evolution of the appearance of the sample (from a) to d) is due to the melting of the ionic crystal under the electron beam. Reprinted by courtesy of Nano Lett. 2012, 12, 5348. Copyright 2012, American Chemical Society.

A probable crystallization mechanism of the mixed crystals can be suggested based on this data. When injecting the QDs into the saturated salt solution, individual nanoparticles play the role of seeds for crystallizing the salt and are immediately "wrapped" by small crystallites of the respective salt. This salt shell protects the QDs from aggregation and the small crystallites can merge and grow further finally yielding macrocrystals. It is noted that the separation of the individual QDs in the matrix is a very important step for maintaining their original PL. Both the observation and the proposed crystallization mechanism match well with the results obtained during the PL-QY characterizations.
As discussed above, charging of the mixed crystals under an electron beam is a severe problem that prohibits a detailed TEM analysis. To solve this problem, a composite of resin and mixed crystals was prepared for the TEM measurements. The composite was cut into sheets with a thickness of 200 nm by using ultramicrotomy in order to enable the transmission of the electron beam while the surrounding resin may protect the mixed crystals from melting for at least a few minutes. The detailed procedure of the composite formation is described in Appendix A.7. A TEM image of the mixed crystal within such a thin sheet is shown in Figure 3.13.

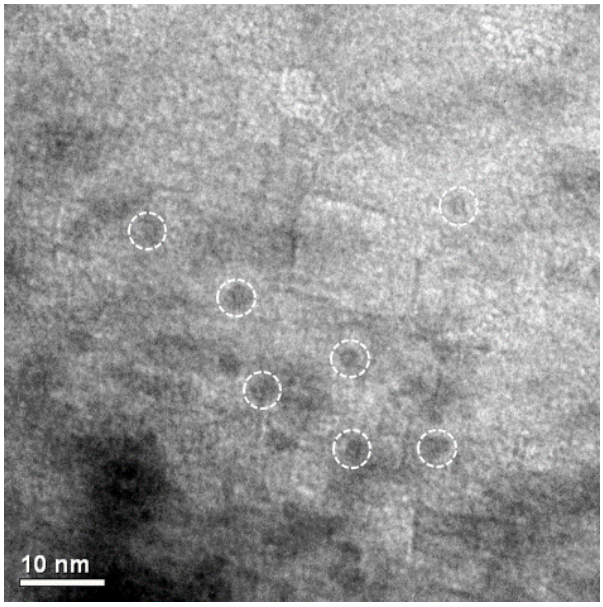

Figure 3.13.: TEM image of CdTe QDs embedded in a NaCl crystal applying LLDC (sample shown in Figure 3.16 c)) and using ultramicrotomy to prepare thin slides embedded in a protective resin sheet. Some of the QDs are highlighted with a white circle as a guide for the eye. Reprinted by courtesy of Adv. Funct. Mater. 2015, 25, 2638. Copyright 2015, John Wiley and Sons.

The TEM confirms the successful incorporation and a relatively uniform and non-aggregated distribution of the CdTe QDs in the NaCl matrix, although the LLDC process is fast. The observation of the separated integration of the QDs into the salt matrix matches the optical studies showing only a slight shift in the PL spectrum from the dispersion into the solid salt. Besides LLDC-based mixed crystals, borax-based ones were also utilized as thin sheets for TEM analyses. The images in Figure 3.14 show reasonably well-separated and non-aggregated CdSe/ZnS QDs in the salt matrix which is in good agreement with the results obtained from the optical characterization methods. It should be emphasized that an imaging of the QDs in an inorganic crystal matrix at atomic resolution while showing the crystallographic planes of the QDs at the same time is only possible when these thin sheets are used. Although, as discussed above, a similar approach was used for QDs within NaCl-based mixed crystals, only borax proved to be suitable as a stable matrix under electron beam exposure, allowing these high magnifications.

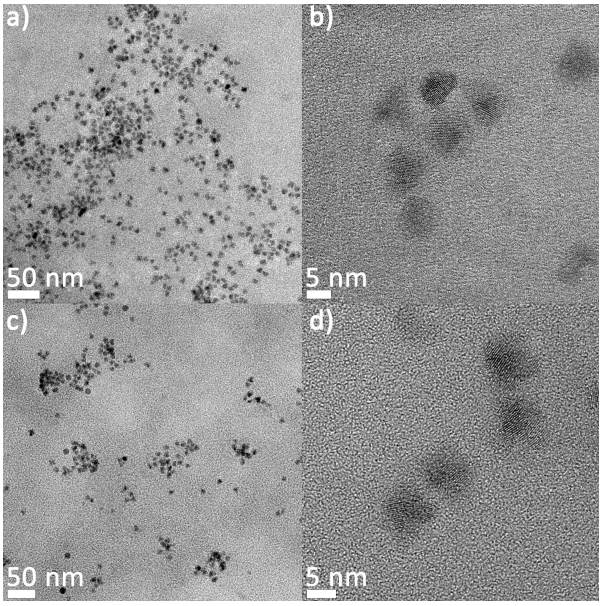

Figure 3.14.: TEM images of the green- (a) and b) and red-emitting (c) and d) mixed crystals shown in Figure 4.8 a) and g). The overviews a) and c) as well as the highly magnified images b) and d) of the samples prove non-aggregated and well-distributed QDs in the matrix. Adapted by courtesy of ACS Appl. Mater. Interfaces 2015, DOI: 10.1021/acsami.5b08377. Copyright 2015, American Chemical Society.

3.3. Analysis of the Mixed Crystals' Stability*

Even when having exceptional initial properties, no material without a short- and long-term stability will deploy its application potential. For this purpose, the mixed crystals discussed in the previous sections were subject to optical and chemical stability analyses.
The ionic salt is expected to provide an exceptionally tight matrix for the embedded QDs. It is indeed very unlikely that ambient oxygen could penetrate through the salt into the encapsulated QDs. The QDs should consequently offer high photostability when they are protected from the environment. To perform the photostability tests, the mixed crystal samples were placed in the focal point of a 1000 W xenon lamp fitted with a water filter for cutting off the NIR part of the spectrum.

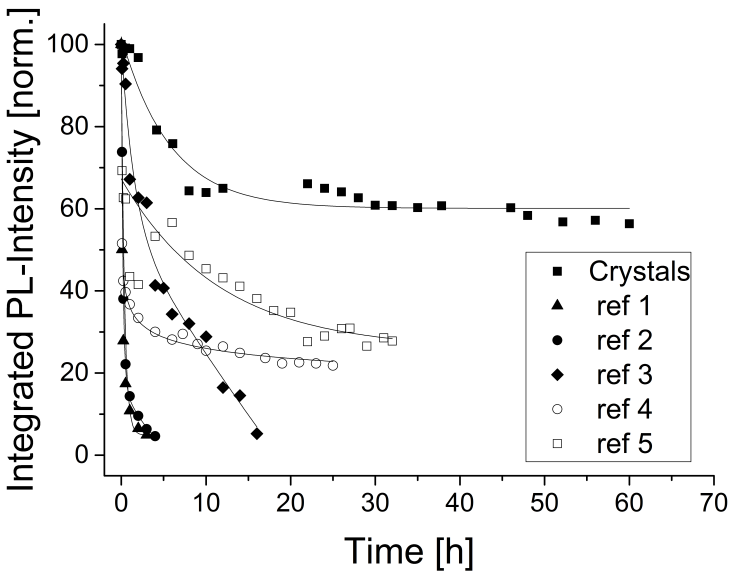

Figure 3.15.: Evolution of the integral PL intensity of CdTe QDs-NaCl mixed crystals and several reference samples containing the same QDs in different matrices or mixtures under ca. 1.0 W/cm^2 light intensity generated in the focal point of a 1000 W xenon lamp with a luminance of ca. 1800 cd/cm^2. Reference samples are: mixtures of CdTe QD powders with PMMA-powder (ref 1), NaCl powder (ref 2), and glass powder (ref 3) as well as CdTe QDs embedded in bulk polymers: PMMA/PS (ref 4) and PS (ref 5). Solid lines are solely provided as a guide to the eye. Reprinted by courtesy of Nano Lett. 2012, 12, 5348. Copyright 2012, American Chemical Society.

*Parts of this chapter have already been published [2, 32]

The light intensity that had an effect on the sample in the focal point was approximately 1.0 W/cm^2. CdTe QDs embedded in polymers (PS and a mixture of PS/PMMA), mixtures of QD powder with NaCl crystal powder, with glass powder and with PMMA powder were used as reference samples. All of the reference samples were carefully prepared to achieve optical densities comparable with the mixed crystal sample as described in detail in Appendix A.6. To monitor the stability, the PL spectra of the samples were measured in the course of the phototreatment. As it can be seen from Figure 3.15, the harsh conditions of the illumination used in the tests are indeed harmful to all of the reference samples. Even the CdTe QDs embedded in common bulk polymer matrices like PMMA and PS lost more than half of their initial PL intensity after the first ten hours of illumination. Unprotected QD mixtures with various powders totally degraded on time scales from minutes to several hours. Nevertheless, the mixed crystal sample showed a remarkable PL stability of more than 60 hours. The initial drop of 30-40% in the emission intensity may be assigned to degradation processes involving water and oxygen entrapped in the mixed crystals during the crystallization procedure, for example as inclusions in hydrate shells around the colloidal nanocrystals. The degradation of the QDs associated with the surface of the mixed crystal may also contribute to this initial emission drop. It should be emphasized that only changes of the integral PL intensity were observed. The shape and position of the PL spectra were not affected by this intensive phototreatment. Some irregular changes of the PL intensity observed in the data may be explained by slight temperature deviations during the phototreatment and the measurements. Besides the photometric durability a high level of chemical stability is also crucial. While it was already shown that the incorporation of QDs into mixed crystals increases the photometric stability under illumination signisficantly, [32] the mixed crystals need to prove that their formation results in rigid composites. Analyses of the chemical tightness of the host were performed on both classically prepared and LLDC-based mixed crystals. For the stability tests, mixed crystals containing CdSe/ZnS QDs as well as pure QDs were exposed to benzoyl peroxide solutions in toluene. In the presence of the strong oxidant, the emission of the CdSe/ZnS QDs was fully quenched after 24 hours (Figure 3.16 a) and b). The LLDC-based mixed crystals made of NaCl and containing either aqueous CdTe or oil-based CdSe/ZnS QDs were strong enough to withstand the oxidation in benzoyl peroxide solution under identical conditions (Figure 3.16 c) and d). Their emission intensity was almost unaltered during the oxidation test, showing a stability which is comparable to the mixed crystals made by the "classical" crystallization, as it can be seen in Figure 3.16 e)-h).

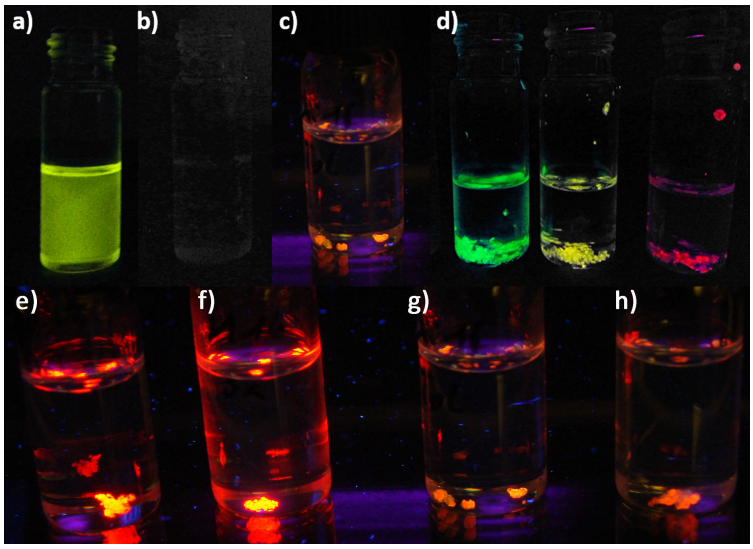

Figure 3.16.: True-color images of the stability test of mixed crystals by using benzoyl peroxide as oxidizing agent under 365 nm UV excitation. A solution of CdSe/ZnS QDs in toluene a) before and b) after the addition of benzoyl peroxide for 24 h; mixed crystals containing c) CdTe QDs and various d) CdSe/ZnS QD after the addition of benzoyl peroxide in toluene for 24 h. QD-salt mixed crystals from the same CdTe QD batch prepared in accordance with the standard crystallization approach (e and f) and the LLDC method (g and h). The images were taken after the mixed crystals had been stored for 24 h in pure toluene (f and h) and for 24 h in a solution of benzoyl peroxide (e and g). The images clearly reveal that the emission intensity is not diminished upon exploiting the mixed crystals, either prepared by the "classical" crystallization or the LLDC approach, towards benzoyl peroxide. Adopted by courtesy of Adv. Funct. Mater. 2015, 25, 2638. Copyright 2015, John Wiley and Sons.

3.4. Summary

A detailed discussion on the structure-property relationship of the mixed crystals was given in this chapter. It was demonstrated with absolute quantum yield measurements that the PL-QY of CdTe QDs can be increased upon incorporation of QDs into a salt matrix by using the "classical" crystallization procedure. The resulting PL enhancement factors strongly depend on the change of the refractive index of the surrounding matrix and on the PL-QY of the parent QDs, with the incorporation of QDs with small PL-QY and, thus, a higher number of surface defects, favoring non-radiative decay processes, yielding higher enhancement

factors. Time-resolved PL measurements revealed that the PL decay behavior of the QD-salt crystals and the silicone composites do not correlate with the changes in PL-QY of the parent QDs upon salt incorporation. The observed changes were attributed to contributions from refractive index related changes of the radiative rate constants and to QDs which are initially weakly emitting (or even dark) in solution and turn bright upon crystal incorporation, thereby influencing PL-QY and the PL decay kinetics in a different manner. The observed PL enhancement is ascribed to the curing of surface defects, most likely due to the formation of a thin passivation layer of $CdCl_x$. This hypothesis is supported by studies with CdSe/ZnS showing a Cd-free surface incorporated into NaCl as well as CdTe QDs incorporated into borax, where the crystal-induced PL-QY increase fell below the values expected for the respective change of the refractive index. It is additionally noted that the mixed crystals display a superior environmental stability. Their PL-QY was reduced by only a few percent of the initial intensity after being stored under ambient conditions for more than one year.
TEM analyses revealed that the QDs are well-dispersed within the mixed crystals, while it was shown that using an ultramicrotome for the TEM sample preparation is crucial. Only then the mixed crystal sample remain stable and can be analyzed by using high-resolution techniques. Both the photo- and the chemical stability analyses proved the applicability of the mixed crystals for highly demanding optical applications like color conversion. The fast LLDC procedure did furthermore not alter the protective properties of the inorganic matrices.

References

[1] M. Müller, M. Kaiser, G. M. Stachowski, U. Resch-Genger, N. Gaponik, and A. Eychmüller, *Chemistry of Materials*, **2014**, *26*(10), 3231.

[2] M. Adam, Z. Wang, A. Dubavik, G. M. Stachowski, C. Meerbach, Z. Soran-Erdem, C. Rengers, H. V. Demir, N. Gaponik, and A. Eychmüller, *Advanced Functional Materials*, **2015**, *25*(18), 2638.

[3] M. Adam, T. Erdem, G. M. Stachowski, Z. Soran-Erdem, J. Lox, C. Bauer, J. Poppe, H. V. Demir, N. Gaponik, and A. Eychmüller, *ACS Applied Materials & Interfaces*, **2015**, *DOI: 10.1021/acsami.5b08377*.

[4] L. D. Lavis and R. T. Raines, *ACS Chemical Biology*, **2008**, *3*(3), 142.

[5] U. Resch-Genger, M. Grabolle, S. Cavaliere-Jaricot, R. Nitschke, and T. Nann, *Nature Methods*, **2008**, *5*(9), 763.

[6] P. Schlotter, R. Schmidt, and J. Schneider, *Frontiers in Neuroscience*, **1997**, *418*, 417.

[7] M. R. Krames, O. B. Shchekin, R. Mueller-Mach, G. O. Mueller, L. Zhou, G. Harbers, and M. G. Craford, *Journal of Display Technology*, **2007**, *3*(2), 160.

[8] H. S. Mader, P. Kele, S. M. Saleh, and O. S. Wolfbeis, *Current Opinion in Chemical Biology*, **2010**, *14*(5), 582.

[9] M. Haase and H. Schäfer, *Angewandte Chemie International Edition*, **2011**, *50*(26), 5808.

[10] N. Gaponik, S. G. Hickey, D. Dorfs, A. L. Rogach, and A. Eychmüller, *Small*, **2010**, *6*(13), 1364.

[11] C. B. Murray, D. J. Norris, and M. G. Bawendi, *Journal of the American Chemical Society*, **1993**, *115*(19), 8706.

[12] A. Waggoner, *Current Opinion in Chemical Biology*, **2006**, *10*(1), 62.

[13] J. O. Escobedo, O. Rusin, S. Lim, and R. M. Strongin, *Current Opinion in Chemical Biology*, **2010**, *14*(1), 64.

[14] B. O'Regan and M. Grätzel, *Nature*, **1991**, *353*(6346), 737.

[15] L. Etgar, T. Moehl, S. Gabriel, S. G. Hickey, A. Eychmüller, and M. Grätzel, *ACS Nano*, **2012**, *6*(4), 3092.

[16] M. Grätzel, *Nature Materials*, **2014**, *13*(9), 838.

[17] J. M. Phillips, M. E. Coltrin, M. H. Crawford, A. J. Fischer, M. R. Krames, R. Mueller-Mach, G. O. Mueller, Y. Ohno, L. E. S. Rohwer, J. A. Simmons, and J. Y. Tsao, *Laser & Photonics Review*, **2007**, *1*(4), 307.

[18] K. E. Sapsford, L. Berti, and I. L. Medintz, *Angewandte Chemie International Edition*, **2006**, *45*(28), 4562.

[19] Y. Wang, J. Y.-J. Shyy, and S. Chien, *Annual Review of Biomedical Engineering*, **2008**, *10*, 1.

[20] H. Kobayashi, M. R. Longmire, M. Ogawa, and P. L. Choyke, *Chemical Society Reviews*, **2011**, *40*(9), 4626.

[21] K. Rurack; Fluorescence quantum yields-methods of determination and standards; In Ute Resch-Genger, Eds., *Standardization and Quality Assurance in Fluorescence Measurements I: Techniques*, chapter Fluorescen. Springer Science & Business Media, 2008.

[22] J. Olmsted, *The Journal of Physical Chemistry*, **1979**, *83*(20), 2581.

[23] E. P. Tomasini, E. S. Román, and S. E. Braslavsky, *Langmuir*, **2009**, *25*(10), 5861.

[24] C. Würth, M. Grabolle, J. Pauli, M. Spieles, and U. Resch-Genger, *Nature Protocols*, **2013**, *8*(8), 1535.

[25] M. Grabolle, M. Spieles, V. Lesnyak, N. Gaponik, A. Eychmüller, and U. Resch-Genger, *Analytical Chemistry*, **2009**, *81*(15), 6285.

[26] J. C. de Mello, H. F. Wittmann, and R. H. Friend, *Advanced Materials*, **1997**, *9*(3), 230.

[27] J. Hoy, P. J. Morrison, L. K. Steinberg, W. E. Buhro, and R. A. Loomis, *The Journal of Physical Chemistry Letters*, **2013**, *4*(12), 2053.

[28] C. Würth, M. Grabolle, J. Pauli, M. Spieles, and U. Resch-Genger, *Analytical Chemistry*, **2011**, *83*(9), 3431.

[29] S. Leubner, S. Hatami, N. Esendemir, T. Lorenz, J.-O. Joswig, V. Lesnyak, S. Recknagel, N. Gaponik, U. Resch-Genger, and A. Eychmüller, *Dalton Transactions*, **2013**, *42*(35), 12733.

[30] U. Resch-Genger and P. C. DeRose, *Pure and Applied Chemistry*, **2010**, *82*(12), 2315.

[31] C. Würth, M. G. González, R. Niessner, U. Panne, C. Haisch, and U. Resch-Genger, *Talanta*, **2012**, *90*, 30.

[32] T. Otto, M. Müller, P. Mundra, V. Lesnyak, H. V. Demir, N. Gaponik, and A. Eychmüller, *Nano Letters*, **2012**, *12*(10), 5348.

[33] S. Kalytchuk, O. Zhovtiuk, and A. L. Rogach, *Applied Physics Letters*, **2013**, *103*(10), 103105.

[34] A. L. Rogach, T. Franzl, T. A. Klar, J. Feldmann, N. Gaponik, V. Lesnyak, A. Shavel, A. Eychmüller, Y. P. Rakovich, and J. F. Donegan, *The Journal of Physical Chemistry C*, **2007**, *111*(40), 14628.

[35] Y. Ebenstein, T. Mokari, and U. Banin, *Applied Physics Letters*, **2002**, *80*(21), 4033.

[36] J. R. Lakowicz, *Principles of Fluorescence Spectroscopy;* Springer, 3 ed., 2009.

[37] P. D. Wadhavane, R. E. Galian, M. A. Izquierdo, J. Aguilera-Sigalat, F. Galindo, L. Schmidt, M. I. Burguete, J. Pérez-Prieto, and S. V. Luis, *Journal of the American Chemical Society*, **2012**, *134*(50), 20554.

[38] B. R. Fisher, H.-J. Eisler, N. E. Stott, and M. G. Bawendi, *The Journal of Physical Chemistry B*, **2004**, *108*(1), 143.

[39] S. Wu, J. Dou, J. Zhang, and S. Zhang, *Journal of Materials Chemistry*, **2012**, *22*(29), 14573.

[40] A. Shavel, N. Gaponik, and A. Eychmüller, *The Journal of Physical Chemistry B*, **2006**, *110*(39), 19280.

[41] Z. Ning, Y. Ren, S. Hoogland, O. Voznyy, L. Levina, P. Stadler, X. Lan, D. Zhitomirsky, and E. H. Sargent, *Advanced Materials*, **2012**, *24*(47), 6295.

[42] J. Tang, K. W. Kemp, S. Hoogland, K. S. Jeong, H. Liu, L. Levina, M. Furukawa, X. Wang, R. Debnath, D. Cha, K. W. Chou, A. Fischer, A. Amassian, J. B. Asbury, and E. H. Sargent, *Nature Materials*, **2011**, *10*(10), 765.

[43] V. V. Breus, C. D. Heyes, and G. U. Nienhaus, *The Journal of Physical Chemistry C*, **2007**, *111*(50), 18589.

[44] S. Tamang, G. Beaune, I. Texier, and P. Reiss, *ACS Nano*, **2011**, *5*(12), 9392.

[45] W. K. Bae, K. Char, H. Hur, and S. Lee, *Chemistry of Materials*, **2008**, *20*(2), 531.

[46] M. Grabolle, J. Ziegler, A. Merkulov, T. Nann, and U. Resch-Genger, *Annals of the New York Academy of Sciences*, **2008**, *1130*, 235.

[47] W. K. Bae, J. Kwak, J. Lim, D. Lee, M. K. Nam, K. Char, C. Lee, and S. Lee, *Nano Letters*, **2010**, *10*(7), 2368.

4. Lighting Applications of Mixed Crystals

4.1. Luminaire Science or How We Perceive Colors

Light sources or luminaires are a major contributor to both human evolution and energy consumption as discussed in the introduction. To reduce the latter negative aspect, alternatives to replace standard luminaires currently used for residential and industrial lighting are in the focus of research. Incandescent bulbs which were banned recently in the EU [1] have a limited efficiency due to their filament temperature. These light sources would reach up to 95 lm/W$_{opt.}$ at 6600 K [2] where the spectrum of these black-body radiators matches the human visual response perfectly, while their operating temperature is practically limited to 2700-3000 K resulting in only 16 lm/W$_{opt.}$. [3] Fluorescent and high-intensity discharge (HID) light sources as the first generation replacement have a luminous efficiency of 25 up to 115 lm/W$_{elect.}$, but they have a lower color rendering index than their incandescent counterparts. [3] Furthermore, the barely encapsulated mercury vapor that is often used in these systems raises concerns about safety regulations, leading to the point of treating them as hazardous waste. Secondly, the mercury is also a reason for reduced efficiency, since its main emission wavelength at 254 nm needs to be down-converted to the visible region, resulting in a loss of at least 45 and 60% of the injected energy for blue and red photons respectively. Today, inorganic solid-state-lighting (SSL) based technologies are often seen as the most prominent replacement for currently used luminaires. Developed about 50 years ago [4–7], red-orange-emitting LEDs were first used for signal lighting only, due to their low intensity. About 30 years later, high-brightness blue-emitting LEDs based on GaN were presented by Shuji Nakamura [8], opening the field for effective down-conversion w-LEDs. Nakamura as well as his colleagues Isamu Akasaki and Hiroshi Amano were awarded the Nobel Prize for Physics in 2014. [9]

Both in science and industry, the first down-conversion w-LEDs were produced by blending

yellow-emitting YAG:Ce onto a blue LED, forming an efficient but bluish w-LED due to the lack in photons emitted in the red spectral region. [10, 11] The resulting devices could be used well for different commercial reasons, but due to the bluish or cold white they were often not accepted as residential lighting by the consumers. Several measures were suggested to overcome this issue, including the addition of a second conversion material emitting in the red spectral region. These materials as well as the YAG:Ce are based on rare earth ions as emission centers with high PL-QY. Due to monopolistic suppliers, companies will, however, face great uncertainties concerning their accessibility in the long term. Furthermore, these materials have a relatively broad emission spectrum reducing the overall efficiency of the devices, as discussed in Section 4.1.3. Semiconductor QDs can be considered as suitable alternative due to their adjustable size, relatively narrow PL spectra and high PL-QY.

4.1.1. The Human Eye and its Visual Response to Incident Light

All electromagnetic radiation, no matter if it is emitted by a luminaire, the sun or reflected by an object, needs to be detectable with our eyes in order to be seen as light. Therefore, our eye response function for different wavelengths (see Figure 4.1) comprehensively defines how we see our environment. This response function differs depending on the amount of light hitting the eye. As depicted in Figure 4.1, light with a wavelength of 555 nm is detected with the highest sensitivity if the illumination intensity is above 3 cd/m^2 which is the case for daylight or in illuminated rooms.

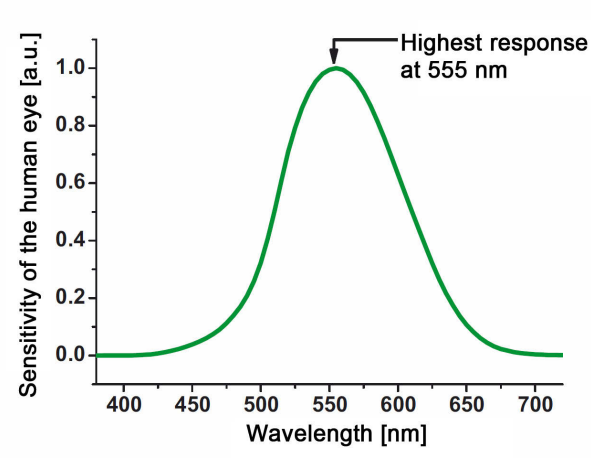

Figure 4.1.: Response function of the human eye to light of different wavelength. This function is valid during the photoscopic vision with light intensities above 3 cd/m^2.

Then, three different cones for red, blue and green are facilitating the human vision, which will be the assumed setting for the subsequent discussions. This curve was originally introduced by the *Commision Internationale de l'Eclairage* (CIE) in 1931 [12] and revised in 1978 by Wyszecki and Stiles. [13] The revision was necessary since the original response functions underestimated the sensitivity in the blue region around 460 nm. If the light intensities fall below 3 cd/m^2, the sensitivity curve shifts to lower wavelengths, since the vision is then mediated by a mixture of cones and rods. Rods have in comparison to cones a higher sensitivity in the blue-cyan region but are not capable of differentiating colors resulting in a grey vision at night.

4.1.2. The CIE Diagram

Together with the eye sensitivity curve, the CIE adopted the color matching functions derived from a test based on the idea of John Guild and David Wright for calculating the intensity of different colors within the XYZ color system. Detailed information about this system, its sources, variations and uncertainties can be found in the corresponding literature. [14–16] Derived from these premises, the CIE 1931 chromaticity diagram was introduced, as shown in Figure 4.2.

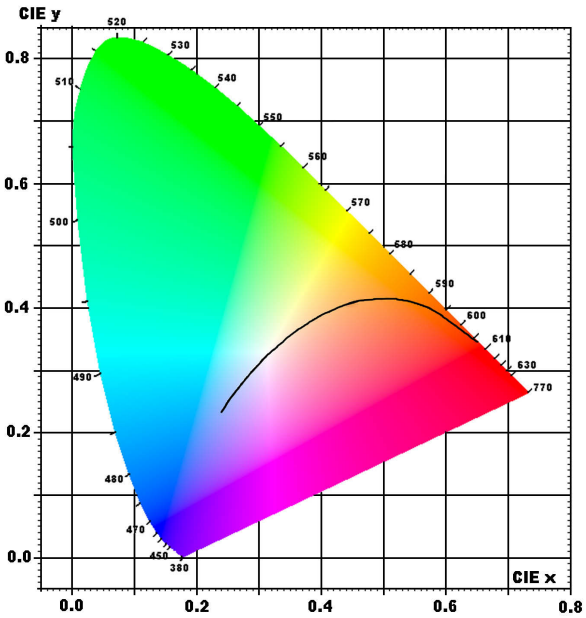

Figure 4.2.: CIE chromaticity diagram together with the Planckian locus (black line) representing a black-body radiator.

This diagram displays all colors in maximum intensity that can be perceived by the human eye. It is limited at the lower end by the purple boundary, while the horseshoe-shaped outer line shows spectrally pure, fully saturated colors within the range of 380-770 nm. At the center, at the x-; y-coordinates 1/3;1/3, the white point displays a mixture of all, but completely unsaturated colors. A straight line between two points (resembling two different colors) in the diagram shows all accessible mixed colors that can be generated from the starting ones. On the other hand, three or more points open a color gamut spanning again all colors that can be accessed by mixing the starting values. In relevance to the initially discussed w-LEDs based on a blue chip and yellow-emitting phosphor, it becomes clear that this combination can only represent a very limited area of the colors visible to the human eye or rather a straight line in the CIE diagram. The addition of a third or fourth color opens the gamut for significantly more colors and therefore a much better tunability of the resulting devices' hue.
The Planckian locus (shown in Figure 4.2 as a black line) represents the emission color of a black-body radiator at different temperatures. While temperatures below 3000 K cause a more yellow-red emission, temperatures above 5000 K become blue-dominated. During the evaluation of luminaires, the Planckian locus evolved to a reference concerning their correlated color temperature which will be discussed in the next section.

4.1.3. Metrics for the Evaluation of Luminaires

Correlated color temperature (CCT): The CCT is defined as the temperature of a black-body radiator at a position along the Planckian locus with the closest proximity towards the evaluated emitter within the CIE diagram. Therefore, the CCT is directly associated with the hue of the emitter or luminaire, making it one of the two directly visible metrics discussed here. Reliable CCTs can only be derived if the position of the evaluated emitter is generally in close proximity to the Planckian locus within the CIE diagram. If this requirement is met, general claims can be made. A CCT in the range of 2700-3000 K represents a so-called "warm white" hue, with an excess of yellow and red compared to the amount of blue photons. Such a value is usually associated by people as incandescent-like light and therefore highly recommended for residential lighting. If the CCT rises to values of 5500-7000 K, the amount of blue photons increases creating a slightly colder light which can be compared with sunlight at midday. Such luminaires are recommended for industrial and office lighting in order to ensure a productive and comfortable working environment. Values above 7000 K are generally associated with a "cold white" light and should therefore be avoided.
Color rendering index (CRI): The next visible metric for evaluating light sources is the CRI. It

evaluates the ability of a light source to reflect objects to the human eye accurately and was introduced by the CIE. [17] The need for an evaluating and comparing system arose in the 1960s when fluorescence lamps as the first luminaires that were not based on a black-body radiator were widely introduced. The analyzed light source and the reference light source are used to illuminate up to 14 reflective samples while their different appearance under both the reference and the test light source is used to calculate the CRI. The reference light source has to match the CCT of the test luminaire since the CRI is CCT-independent. A CRI of 100 is therefore possible for each CCT, provided the analyzed light source perfectly matches the spectral properties of a reference with the same CCT. Only the arithmetic average of the first 8 (Ra) or 9 (R9) is used for the subsequent calculation. Due to this and some further weaknesses, especially for a correct evaluation of LED-based luminaires, the CIE recently introduced the *Color quality scale* (CQS) based on the CRI invented by Davis and Ohno. The main differences and benefits of the CQS can be found in the corresponding literature [18], although it should only be noted that the CQS, in comparison to the CRI, does not penalize oversaturation and uses a root mean square of all single colors instead of the arithmetic mean.
Luminous efficacy of radiation (LER): As the first metric which can not be directly observed, the LER describes the ratio of luminous flux in lumen emitted by the light sources and the optical power of the radiation in watts. The optical power of radiation is here defined by the amount that is detected by the human eye, corresponding to the eye sensitivity curve shown in Figure 4.1. According to this relation, a maximum LER of 683 $\mathrm{lm/W}_{opt.}$ is defined for a δ-function emitter (line emitter) with its maximum at 555 nm where the human eye shows the highest perception. Based on this correlation, a reduction in LER is expected when the light sources show a high intensity in the blue or red region and the emitter in these regions show very broad spectra. Furthermore, a clear indirect correlation between LER and CRI is also derived, which means that a trade-off between efficacy and perfect color rendering has to be made.
Luminous efficacy (LE): The last relevant metric discussed in this section is the LE. In contrast to the LER, the LE is the ratio of the luminous flux in lumen emitted by the light sources and the input of electrical power in watts necessary to create this flux. Therefore, the LE can also be calculated as the product of LER and the radiant efficiency which is the ratio of human detectable photon power versus the electrical power input.
Unfortunately, the latter two values are often mixed up in scientific literature. To avoid confusion about the different values within this work, LER and LE are clearly separated by subscripts, given as $\mathrm{lm/W}_{opt.}$ and $\mathrm{lm/W}_{elect.}$, respectively.

4.2. White LEDs based on Mixed Crystals as Color Converters*

White LED light sources can be produced in two different ways. On the one hand, three (or four) semiconductor chips emitting pure blue, green, (yellow) and red can be put together. [2] The white light is generated by mixing the four emission colors in their respective ratios. By using this approach, the hue of the luminaire can easily be tuned. However, the lifetimes of the differently emitting chips strongly deviate and sophisticated electrical circuits with different driving currents for the separate electrical emitters are necessary. Moreover, the relatively low efficiency of the green ones, the so-called "green-gap", [10] makes this type of w-LEDs expensive and less stable in the long-term.

On the other hand, as already mentioned in the introduction of this chapter, w-LEDs can be produced with a blue LED as excitation source for one or more down-converting phosphors blended onto the LED. With this method, the resulting luminaire offers only a limited hue tunability during the operation while the stability of the color is not affected by differently aging LED chips. Here, the conversion layer plays a major role for the final color of the device and its long-term stability. The ideal conversion material should have high PL-QY to guarantee a sufficient efficacy of the device and a narrowly and precisely tunable PL spectrum to allow good color rendering. [13] A high temperature and long-term stability [22] as well as low ecological risks and a continuous supply of the material should furthermore also be guaranteed. While rare earth-based phosphors include risks in at least two of these categories, QDs theoretically meet all of them. It should be noted that most of the used QDs contain Cd but the amount necessary to form a suitable conversion layer is negligible. This is also expressed in the EU's attempt to expel Cd-based color converters for general and display backlighting from the Restriction of Hazardous Substances (RoHS) directive, regulating the use of toxic materials in the EU. [23] Due to these persuasive properties, the use of QDs as conversion layers sparked industrial applications. They started with the demonstration of a 40" display prototype by Samsung [24] followed by the foundation of QD Vision, Inc. [25] whose QDs are now used in the latest series of Sony products.

However, a full protection of QDs providing high photostability and processability while not deteriorating their photoluminescence at the same time is still a challenge. For instance, the rigid chemical conditions used in the polymerization of silicone or sol-gel syntheses of inorganic oxides which are commonly used materials for the encapsulation of light emitting entities

*Parts of this chapter have already been published. [19–21]

impair the PL of the embedded QDs. [26] To solve this problem, the discussed variety of QD-salt mixed crystals formation methods [19, 20, 27–32] were introduced, enabling the formation of highly stable and strongly emissive composites. The mixed crystals can be ground easily and the resulting powder can be added to the silicone polymerization solutions in requested amounts and color ratios. Consequently, no degradation of the mixed crystals and their PL was observed, as discussed in detail in Chapter 3.1.1. Composites containing mixed crystal powders appear milky due to scattering and retain the emission colors corresponding to the initial QDs as it can be seen in Figure 4.3.

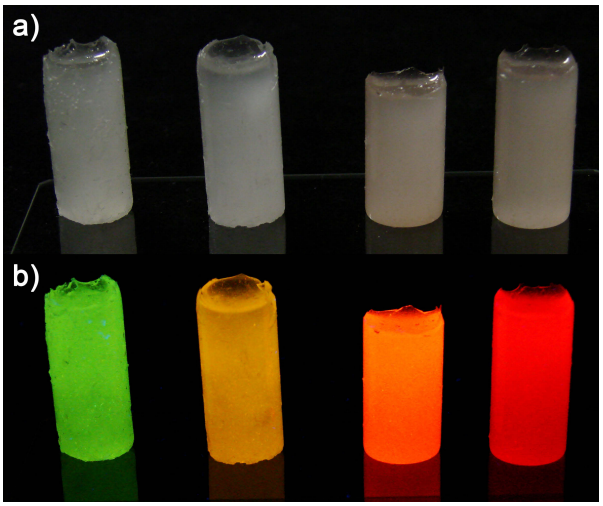

Figure 4.3.: True-color images of mixed crystal powders incorporated into silicone cylinder under a) ambient light and b) 365 nm UV excitation. The milky appearance of the silicone mixed crystal composite is related to scattering. Adopted by courtesy of Nano Lett. 2012, 12, 5348. Copyright 2012, American Chemical Society.

4.2.1. White LEDs by using "Classically" Prepared Mixed Crystals

In the first preparations, CdTe-based mixed crystals were used as color conversion layers. Composites of this kind were deposited on commercially available 1 W blue InGaN LED chips to produce a proof-of-concept white light-emitting device. Figure 4.4 a)-c) shows the basic principle of color conversion layer blended on top of the InGaN chip. The w-LEDs illuminating capacity and color coordinates are shown in Figure 4.4 d) and e) respectively. This w-LED has a CCT of 6500 K matching the CCT of midday sunlight quite well. It could therefore be used as light source for offices. Such a CCT is at the same time not appropriate for residential lighting as well as the LED's comparably low CRI of 53.4, although the device's

LER is promising with 266 $lm/W_{opt.}$. As it can be derived from the spectrum, the reason for the unfavorable performance is the lack in red and green photons emitted from the devices. Furthermore, the position of both colors is quite unsuitable for reaching high CRI and LER as well as a low CCT. While red-emitting mixed crystals are easy to access by using CdTe QDs as emissive centers, PL spectra showing their maximum intensity at a wavelength below 550 nm are hardly available.

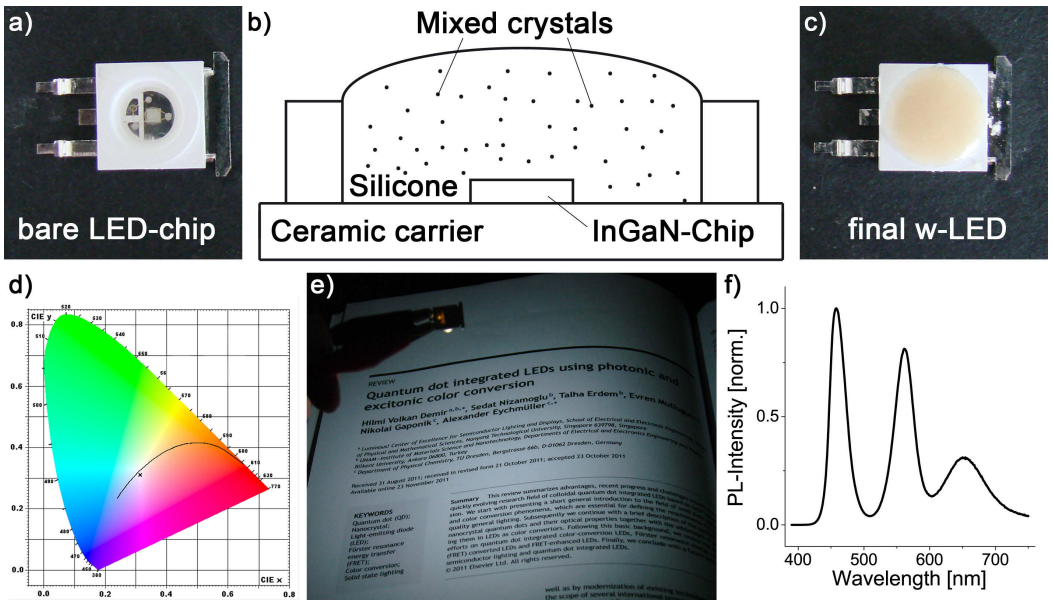

Figure 4.4.: a)True-color image to the bare blue-emitting 1 W InGaN LED chip, b) schematics of its hybridization with mixed crystals embedded in silicone and c) the resulting white LED. d) Color coordinates of the w-LED are shown as a cross in the CIE 1931 diagram. The color temperature of the device as derived from the closest point in the Planckian locus is around 6500 K. e) A title page from reference [33] illuminated by the w-LED as well as f) the corresponding PL spectrum of the shown w-LED. Adopted by courtesy of Nano Lett. 2012, 12, 5348. Copyright 2012, American Chemical Society.

Besides the lack in green-emitting mixed crystals, two more challenges occurred while using CdTe QDs as emissive centers. Firstly, the FWHM of the red-emitting mixed crystals was always between 40-45 nm reflecting a spectrum that is too broad for high-performance w-LEDs. Based on theoretical calculations in the literature [2, 34], a FWHM of 30 nm or less is crucial for the red component to achieve CRI values above 90. Secondly, large amounts of mixed crystal powder are necessary to form an emissive layer on top of the LED capable of absorbing and converting sufficient amounts of emitted blue photons. In fact, the bare blue LED shown

in Figure 4.4 a) provides a volume of approximately 100 μL above the chip, while amounts of several 100 mg of mixed crystal powder and the blending silicone would be necessary to achieve an efficient blue to white conversion.
Both QDs emitting in the range of 520-530 nm and red-emitting QDs with a FWHM are accessible when oil-based CdSe/ZnS QDs with an alloyed gradient shell are used, as shown in Chapter 2.1.2. Their properties can also be maintained easily during a ligand exchange procedure; only their limited stability within a saturated salt solution needs to be solved. Therefore, two possible crystallization approaches can be suggested. First, the use of seed-mediated LLDC or, as a second approach, the change from NaCl to disodium tetraborate decahydrate (borax) as an alternative host matrix. Detailed descriptions of these two methods can be found in Chapters 2.2.4 and 2.3.2.

4.2.2. LLDC-based Mixed Crystals for w-LED Preparation

By using seed-mediated LLDC-based mixed crystals, the beneficial properties of initially oil-based QDs could be utilized. Films of mixed QD-salts prepared by the seed-mediated LLDC method were integrated in a commercially available 1 W 460 nm blue-emitting InGaN LED in order to produce a color conversion w-LED. The emission spectrum of an exemplarily integrated electrically driven device is shown in Figure 4.5 a). Figure 4.5 b) displays the w-LED under ambient illumination and during the operation. Figure 4.5 c) and d) show the LLDC-based mixed crystals used for the w-LED preparation. Their durability and photostability can be compared to the ones of the LEDs made with classically grown mixed crystals. [19,27] Moreover, no deterioration of the emission properties is observed after an on/off test for at least 20,000 cycles. Nevertheless, the cold-white/blue shaded emission of the w-LED is clearly visible, although more than 100 mg of powder were used again. Consequently, seed-mediated LLDC-based mixed crystals are also not capable of preparing a high-performance w-LED with low CCT and high CRI.

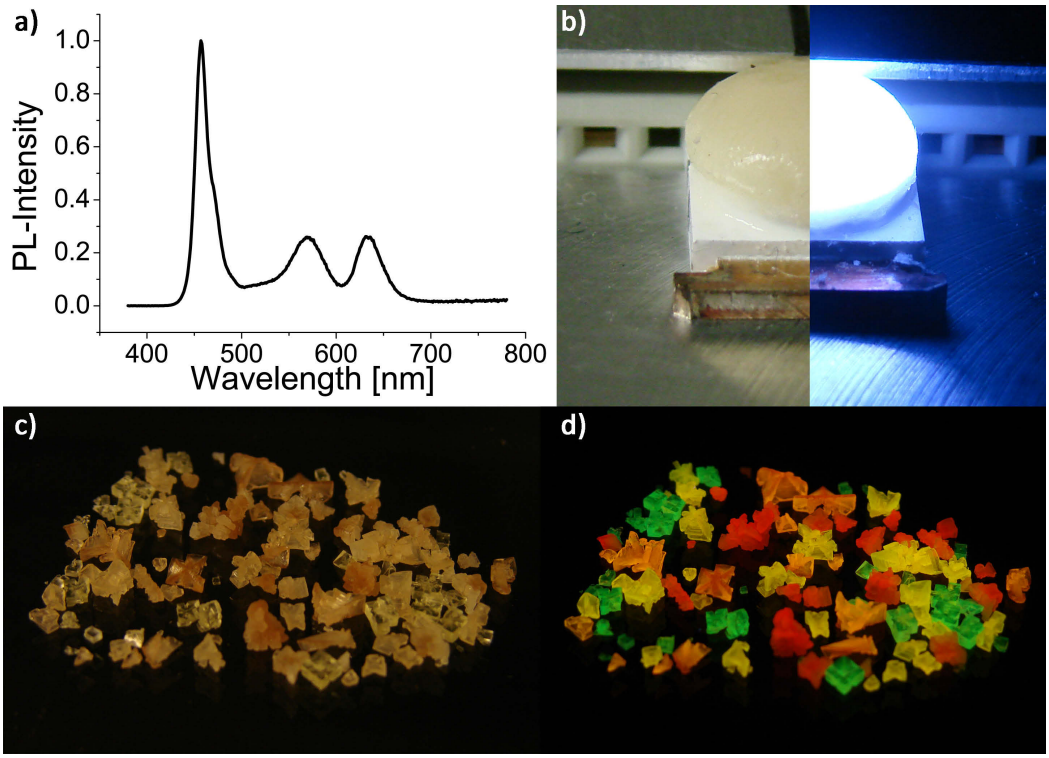

Figure 4.5.: a) Emission spectrum of a cold blue w-LED using the seed-mediated LLDC-based QD-salt mixed crystals as color converters. b) The photograph shows a true-color image of the resulting LED under ambient illumination (left part) and with the LED switched on (right part). Images of the mixed crystals under the illumination of a c) standard fluorescence lamp and d) 365 nm UV excitation are given for comparison. Reprinted by courtesy of Adv. Funct. Mater. 2015, 25, 2638. Copyright 2015, John Wiley and Sons.

4.2.3. A Model-Experimental Feedback Approach towards w-LEDs

Up to this point, only proof-of-concept w-LEDs without any photometric optimization were shown. In this section, a model-experimental feedback approach for preparing QD-salt mixed crystals was carried out. This approach is aimed to be used for producing w-LEDs with a high LER, a high CRI and a low CCT in comparison to the incandescent bulb. At first, the model [34], which is provided by the Bilkent cooperation group of Professor Hilmi Volkan Demir, was used to identify the spectral requirements for high-quality lighting employing QD PL spectra which were then implemented in the following QD synthesis. By comparing the experimental spectra at each intermediate stage with the model, the color quality and

photometric efficiency of the final w-LED were optimized. Borax-based mixed crystals with CdSe/ZnS QDs with an alloyed gradient shell as emissive centers were afterwards used as color conversion layers. As already described in Chapter 2.2.4, they have a 3.4 times higher QD loading than their NaCl-based counterparts, making them an ideal choice. Finally, it was shown that the encapsulation of the QDs in salt crystals provides an outstanding emission stability integrated with LEDs driven at high currents.

In order to maximize the photometric performance of the w-LEDs, the spectra of the LEDs were carefully designed before the experiments so that the fitting QDs can be used with the correct amounts. For this purpose, the results of the Bilkent group's previous study [34] used as starting point were highly beneficial. Within all calculations, the emission of the QDs were modelled as a Gaussian function unless the experimentally measured photoluminescence spectra were applied. In the designs, CRI and LER were maximized indicating the good rendering of the objects' real colors and the good overlapping of the light source's spectrum with the eye sensitivity curve. Furthermore, special emphasis was given generating a white light with a warm white shade acquiring a CCT below 4500 K. According to the previous results, only a tiny fraction of all possible color combinations yields LED spectra where CRI $>$ 90, LER $>$ 330 lm/W$_{opt.}$ and CCT $<$ 4500 K are obtained simultaneously. The photometric calculations were used as feedback tool for designing w-LEDs. At first, the number of color components was determined. According to Tsao [2], four color components, i.e., blue, green, yellow, and red, are required for producing a high-quality white light. Within the previous work, the required wavelengths, relative amplitudes and FWHM values of the QD emitters were determined. [34] Considering this prior work, a blue LED emitting at 460 nm, green-emitting QDs with the peak emission around 530-540 nm and red-emitting QDs with the peak emission around 620 nm were chosen here. Although the necessary condition for the yellow peak wavelength for producing high-quality lighting was found to be 570-580 nm, the yellow component was chosen to fine-tune the white LED spectrum as the experimental implementation slightly differs from the theoretical calculations. For this purpose, green and red QD mixed crystals were prepared and their photoluminescence spectra was recorded before preparing the yellow QD mixed crystals. The calculations showed that employing the blue LED together with these green and red mixed crystals cannot provide high LER and high CRI together with a warm white shade at the same time, confirming the results of reference [2]. Furthermore, to determine the conditions for high-quality white light, the required peak emission wavelength of the yellow color component were calculated by applying the PL spectra of the green and red mixed crystals along with the ones of the blue LED. Since the material composition and the synthesis methodology of the yellow QDs are similar

to those of the green QDs, the FWHM value of the yellow QDs was selected to be the same as the one of the green QDs. The calculations revealed that the peak emission wavelength around 570 nm allows to realize that CRI $>$ 90, LER ~350 lm/W$_{opt.}$ and CCT $<$ 3000 K, all at the same time. Based on this information, yellow mixed crystals emitting at 573 nm were grown. In the center of Figure 4.6, possible CRI-LER combinations of the modeled LEDs based on experimentally prepared mixed crystals are shown as black squares, while the green background is a guide for the eye showing feasible combinations.

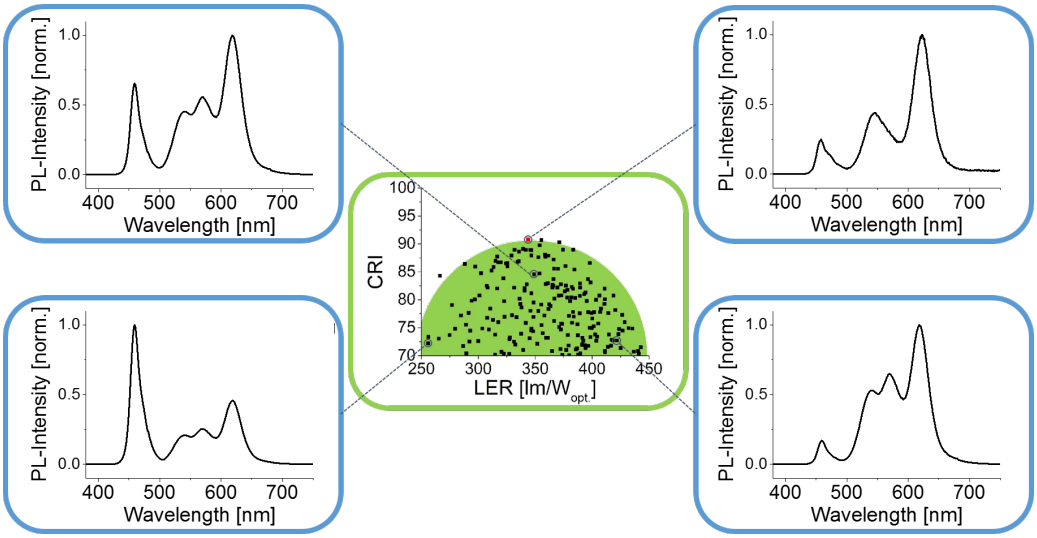

Figure 4.6.: Overview of feasible CRI-LER combinations (black squares) with the experimentally prepared mixed crystals used as color conversion materials on blue LEDs (center). The two PL spectra on the left and the bottom right one show theoretically determined combinations corresponding to the marked points on the CRI-LER plane. The top right PL spectrum and the corresponding red square show the photometric performance of the most optimized final w-LED. Adapted by courtesy of ACS Appl. Mater. Interfaces 2015, DOI: 10.1021/acsami.5b08377. Copyright 2015, American Chemical Society.

The PL spectra display exemplarily chosen possible combinations of the four colors and their corresponding photometric performance. Subsequently, the required relative amplitudes of the color components were determined by using the experimental emission spectra of the QD-salt crystals and the blue LED to be 2/9 for both the blue and the green components, 1/9 for the yellow component and 4/9 for the red color component to achieve a high-color quality and photometric performance. Based on these calculations, a white LED made of these mixed crystals was prepared experimentally achieving CRI = 91, LER = 341 lm/W$_{opt.}$ and

CCT = 2720 K simultaneously, marked as a red square in the center and the corresponding PL spectrum shown in the upper right corner of Figure 4.6.
Oil-based CdSe/ZnS QDs with an alloyed gradient shell were used due to their superior optical properties, as discussed in Chapter 2.1.2. In Figure 4.7, the PL spectra of the resulting QDs are shown. The QDs have emission maxima at 530, 570 and 617 nm, FWHMs of 40, 30 and 30 nm, and PL-QYs of 38.5%, 40.2% and 42.6% for green, yellow and red respectively. These FWHMs are in agreement with the requirements of high-quality lighting as described in reference [34]. Below the PL spectra in Figure 4.7, a photograph of the QD solutions in $CHCl_3$ under UV excitation shows their bright, pure color emission.

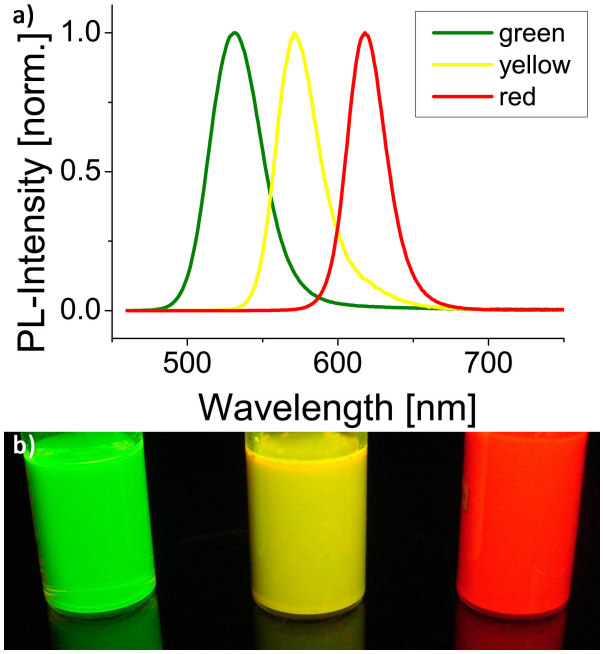

Figure 4.7.: a) PL spectra and b) true-color images under UV excitation at 365 nm of three different CdSe/ZnS QDs samples. The QDs are dispersed in $CHCl_3$ and stored under ambient conditions. Adapted by courtesy of ACS Appl. Mater. Interfaces 2015, DOI: 10.1021/acsami.5b08377. Copyright 2015, American Chemical Society.

Since Cd-based materials have an inherent toxicity, their usage for general applications is highly restricted. Nevertheless, if the benefits of using Cd-based materials strongly exceed the risks, their usage can be permitted by law, as some current attempts indicate for the use of Cd-based QDs in display color enrichment and general lighting color conversion applications within the EU. [23] Prior to the mixed crystal preparation, the QDs were subject to a ligand exchange

procedure (PT 11) replacing the long-chain aliphatic with MPA. A detailed description of PT 11 can be found in Chapter 2.2.4 and Appendix A.3.
Embedding the ligand exchanged QDs into NaCl is known to be non-trivial, since their stability in aqueous media is lower compared to the initially aqueous based CdTe QDs. [28] When NaCl is used as a host, only mixed crystals with small loading amounts of QDs can be obtained, as shown in Figure 2.24. To overcome this problem, both the different crystallization procedure LLDC [20] and another host material can be used. Since the LLDC also delivers a QD loading that is insufficient for the highest-quality color conversion (see above), borax is used as the host material. The resulting borax-based mixed crystals are displayed in Figure 4.8.

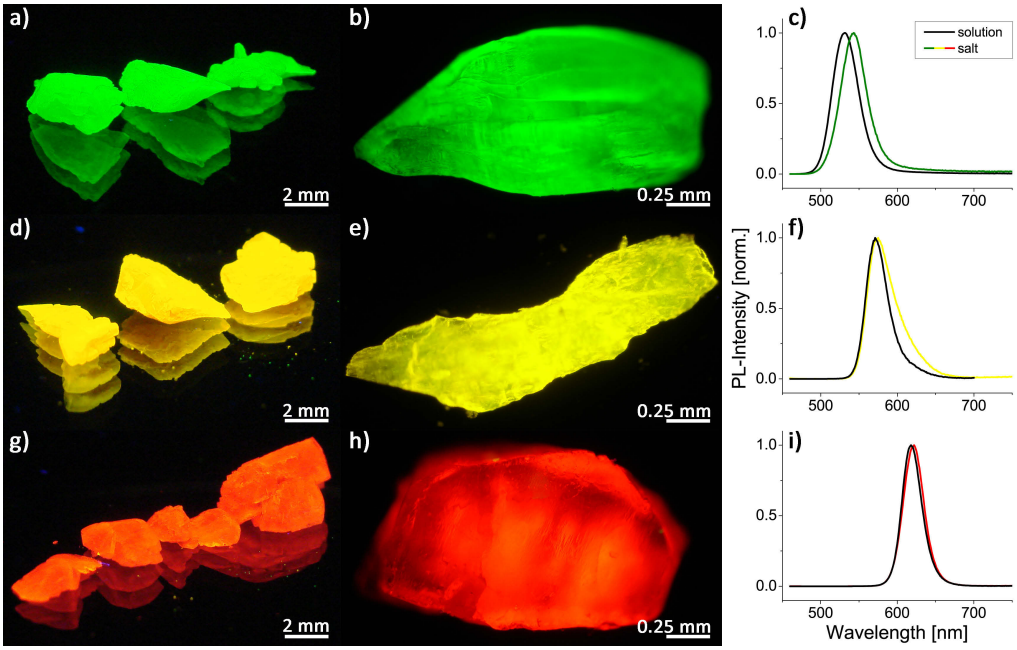

Figure 4.8.: True-color (a, d and g) and microscopic (b, e and h) images of differently emitting CdSe/ZnS QDs incorporated into borax crystals under UV excitation (365 nm). Graphs c), f) and i) show the corresponding PL spectra of the initial solutions (black lines) and mixed crystals (red lines). Adapted by courtesy of ACS Appl. Mater. Interfaces 2015, DOI: 10.1021/acsami.5b08377. Copyright 2015, American Chemical Society.

Owing to its much lower solubility in water in comparison to NaCl (0.13 mol/L compared to 6.14 mol/L respectively) [35], the ionic strength of the saturated borax solution is much lower than the one of the saturated NaCl solutions. Therefore, the stability of the ligand exchanged QDs is much higher within the borax solution, while the QD loading within the

resulting mixed crystals is higher when the same amount of QDs per mL is used. Stripping voltammetry measurements showed a 3.4 times higher amount of Cd and consequently QDs within borax in comparison to the NaCl-based mixed crystals prepared from the same batch of ligand exchanged QDs. As it can be seen from the microscopic images in Figure 4.8 b), e) and h), the QDs are reasonably uniformly distributed within the matrix. The corresponding PL spectra show that the pure color emission does not change upon incorporation, however, a small red shift of the emission maxima occurs. This shift is accompanied by the change of the surrounding dielectric media from a water to a salt matrix. [19,28] The PL spectra in Figure 4.8 f) show a reproducible slight red tailing indicating a small amount of aggregated QDs upon incorporation into borax. This slight broadening, in the case of the yellow component, does not significantly reduce the overall quality of the color converter. To ensure that the spectral properties of the mixed crystals will not change upon grinding and incorporation into silicone, thin layers of powder encapsulated into the silicone resin were prepared. As expected from the results discussed in Chapter 3.1.1, no change occurred during the silicone embedding process. These mixed crystals were also subject to PL-QY, PL-LT and TEM analyses discussed in detail in Chapter 3.1.1 and 3.2.

In order to analyze the emission intensity stability of the QD-salt mixed crystals, they were hybridized on a blue LED driven at 300 mA for 96 h. To avoid a strong heat generation, the LED was placed on an aluminum plate for passive cooling and operated with a 1 kHz on/off rate. Under these conditions, the LED temperature remained below 35 °C (see Figure 4.9 a)) while a continuous operation did cause an increase to 72 °C which would reduce the overall stability of the emissive layer. Figure 4.9 b) displays the PL spectra recorded during the analysis. The intensity of the mixed crystal emission only decreases slightly which is in good agreement with the findings on the PL stability of the mixed crystals under intense illumination, discussed in Chapter 3.3. Therefore, these mixed crystals outcompete most of other QD packaging approaches in terms of photostability, verifying their suitability in color conversion applications. It should be noted that the mixed crystals were grown under ambient conditions. A preparation under inert atmosphere could be beneficial for commercialization reasons, preventing the incorporation of dissolved O_2. This might be a crucial step for a further increase of the photostability.

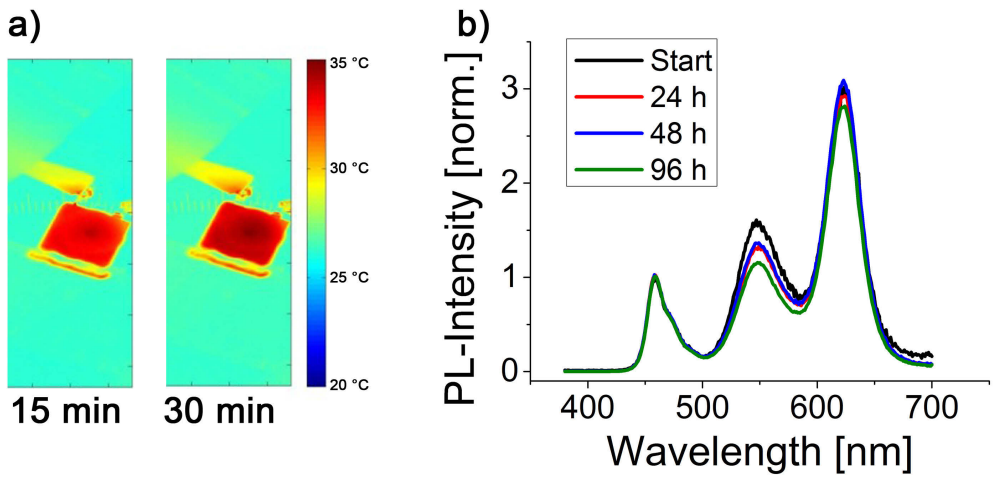

Figure 4.9.: a) IR image of a LED hybridized with mixed crystals. The image was taken after a 15 and 30 min of operation with a 1 kHz switching rate, proving that the temperate remains constant slightly above room temperature, not exceeding 35 °C. b) PL spectra of the w-LED before and during the stability tests. The w-LED was driven at 300 mA and a 1 kHz on/off rate, avoiding a significant heat generation. Adapted by courtesy of ACS Appl. Mater. Interfaces 2015, DOI: 10.1021/acsami.5b08377. Copyright 2015, American Chemical Society.

During initial preparations, a swelling of the powder-silicone mixture was observed, causing an inhomogeneous and porous conversion layer, as shown in Figure 4.10 b). These layers showed low mechanical stability (Figure 4.10 c), after manipulating the conversion layer with tweezers) and provided only weak protection of the fine powder against oxygen and water-vapor diffusion, yielding a change of the w-LEDs spectrum within a few days. Unlike the recently used matrices NaCl, KCl, etc., borax crystallizes as decahydrate. As it can be seen from the thermogravimetric analyses of the borax-based mixed crystals in Figure 4.10 d), parts of the crystal water are released at 70 °C which is the curing temperature of the silicone. Gently drying the mixed crystal powder under vacuum at 70 °C before blending it with the silicone ensures that no further crystal water is released during the curing, yielding a smooth and rigid conversion layer as shown in Figure 4.10 a). Removing parts of the crystal water during the drying step also reduces the overall mass of mixed crystal powder needed, enabling the formation of smaller conversion layers.

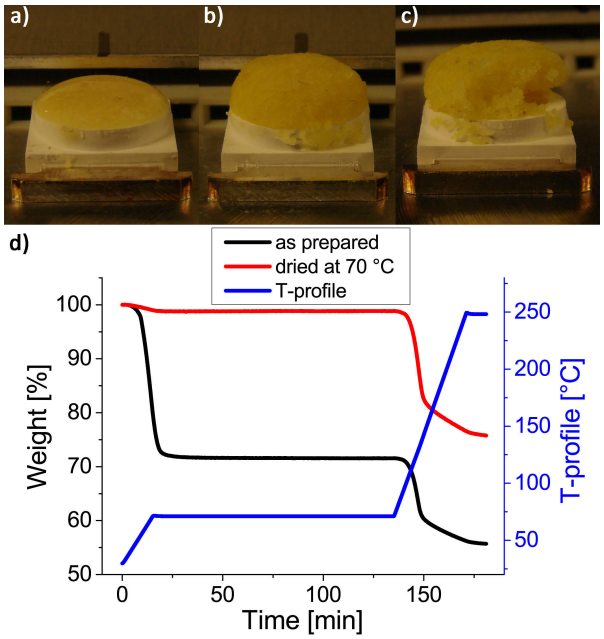

Figure 4.10.: a) True-color image of a LED prepared by using borax powder which was dried before it was blended with the silicone on top of the LED. Photographs b) and c) show LEDs produced by using non-dried mixed crystal powder. While b) shows the porous and non-homogenous silicone encapsulation, c) displays the lower mechanical stability of such layers. d) Thermogravimetric analysis of borax-based mixed crystals. The blue line displays the applied temperature program, with a two hour isothermic part at 70 °C to imitate the curing of the silicone on top of the LED. Adapted by courtesy of ACS Appl. Mater. Interfaces 2015, DOI: 10.1021/acsami.5b08377. Copyright 2015, American Chemical Society.

To produce the final w-LED, mixed crystals were ground to fine powder, while dried and defined amounts of green (20 mg), yellow (8 mg) and red (16 mg) converters were blended together with a two-component industrial standard silicone resin. These amounts represent a significant reduction of mixed crystals powder which is necessary to form high-quality w-LEDs. By adjusting the amounts of green, red and yellow powder, the hue of the final device can be tuned to a warm white. Figure 4.11 d) shows the emission spectrum of the resulting warm w-LED achieving a CCT of 2720 K, a CRI of 91 and a LER of 341 lm/$W_{opt.}$ at the same time. These values combine a warm white hue which is comparable to an incandescent bulb (CCT ~2800 K), while preserving the high efficiency of the SSL devices and giving a color rendering which meets industrial requirements. [36] Furthermore, it overcomes the CRI = 90 barrier of QD-based LEDs for the first time while reaching LER > 340 lm/$W_{opt.}$ with a warm

white shade at the same time, exceeding the current state-of-the art in literature. [37] Several studies presented promising w-LEDs with QD-based conversion layers and a CRI close to and above 90 by using either Cd-containing [37,38] or Cd-free [39–41] QDs. Nevertheless, none of them managed to reach a CRI $>$ 91 while providing a CCT $<$ 3000 K as well as a LER $>$ 340 lm/W$_{opt.}$ at the same time, thereby balancing these strongly related figures of merit.

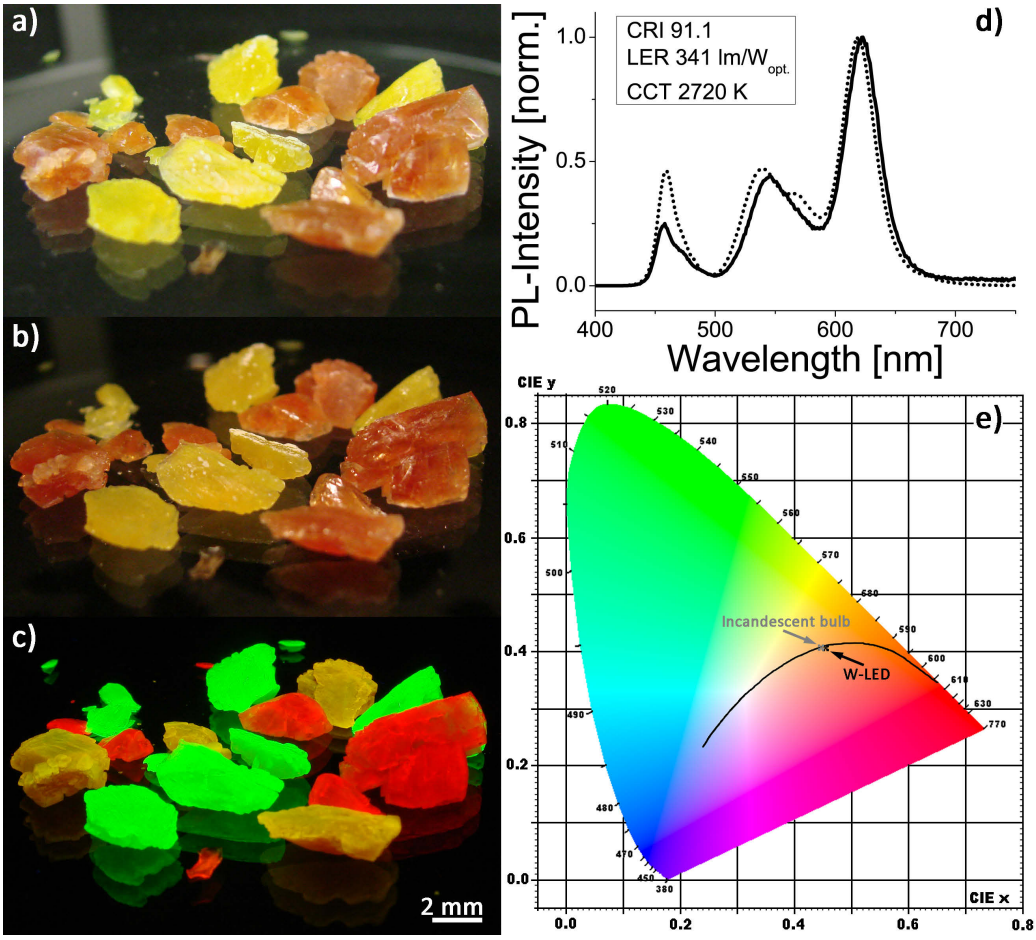

Figure 4.11.: Photographs a), b) and c) show true-color images of the mixed crystals under ambient illumination with a standard fluorescence lamp (a), with the prepared w-LED (b) and under 365 nm UV excitation. Graph d) presents the PL spectrum of the w-LED within the visible region (solid line) and the modeled spectrum used (dotted line), while e) shows a CIE 1931 diagram with the black-body radiator (black line, CRI 100) as comparison, the w-LED marked with the black cross and an incandescent bulb (grey cross). Adapted by courtesy of ACS Appl. Mater. Interfaces 2015, DOI: 10.1021/acsami.5b08377. Copyright 2015, American Chemical Society.

In Figure 4.11 e), the position of the LED spectrum within the CIE 1931 diagram (x=0.4557, y=0.4056) and a black-body radiator are marked with a cross and a black curve respectively. Figure 4.11 a) shows the QD-salt mixed crystals that were used for producing the w-LED under the illumination of a standard fluorescence lamp. In comparison, the same image was taken in the darkened room, only illuminated by the final w-LED (Figure 4.11 b)). Here, especially the red crystals have a more saturated color in comparison to Figure 4.11 a)) which is due to the LEDs' much higher amount of emitted red photons in comparison to the fluorescence lamp. Since most of today's commercially available w-LEDs also lack a sufficient amount of red within their emission spectra, the fluorescence lamp can be used for comparison. Figure 4.11 c) shows the same image taken under 365 nm UV excitation, proving the intense and pure color emission of the mixed crystals.

4.3. Summary

The applicability of mixed crystals emitting in the visible range was evaluated in this chapter. By using both the "classical" method employing CdTe in NaCl and the LLDC procedure, proof-of-concept w-LEDs were produced showing the general suitability of the mixed crystals for color conversion purposes. Afterwards, a model-experimental feedback approach was presented to prepare CdSe/ZnS QDs with an alloyed gradient shell whose emission spectra meet the requirements of high-quality white light luminaires. These QDs were successfully phase-transferred and incorporated in borax-based mixed crystals which provide a rigid and air-tight ionic matrix while ensuring a high loading density of the QDs. Throughout all steps, intermediate results were reviewed with the spectral model to ensure their applicability as color conversion materials. By hybridizing green-, yellow- and red-emitting mixed crystals onto a blue LED, a w-LED with superior optical properties was finally produced.

References

[1] VERORDNUNG (EG) Nr. 244/2009, **2009**.

[2] J. M. Phillips, M. E. Coltrin, M. H. Crawford, A. J. Fischer, M. R. Krames, R. Mueller-Mach, G. O. Mueller, Y. Ohno, L. E. S. Rohwer, J. A. Simmons, and J. Y. Tsao, *Laser & Photonics Review*, **2007**, *1*(4), 307.

[3] Navigant Consulting, *U.S. lighting market characterization; Volume I: National lighting inventory and energy consumption estimate;* Vol. I; 2002.

[4] M. I. Nathan, W. P. Dumke, G. Burns, F. H. Dill, and G. Lasher, *Applied Physics Letters*, **1962**, *1*(3), 62.

[5] N. Holonyak and S. F. Bevacqua, *Applied Physics Letters*, **1962**, *1*(4), 82.

[6] T. M. Quist, R. H. Rediker, R. J. Keyes, W. E. Krag, B. Lax, A. L. McWhorter, and H. J. Zeigler, *Applied Physics Letters*, **1962**, *1*(4), 91.

[7] R. N. Hall, G. E. Fenner, J. D. Kingsley, T. J. Soltys, and R. O. Carlson, *Physical Review Letters*, **1962**, *9*(9), 366.

[8] S. Nakamura, M. Senoh, and T. Mukai, *Applied Physics Letters*, **1993**, *62*(19), 2390.

[9] P. von Dollen, S. Pimputkar, and J. S. Speck, *Angewandte Chemie International Edition*, **2014**, *53*(51), 13978.

[10] M. R. Krames, O. B. Shchekin, R. Mueller-Mach, G. O. Mueller, L. Zhou, G. Harbers, and M. G. Craford, *Journal of Display Technology*, **2007**, *3*(2), 160.

[11] R. Mueller-Mach, G.O. Mueller, M.R. Krames, and T. Trottier, *IEEE Journal of Selected Topics in Quantum Electronics*, **2002**, *8*(2), 339.

[12] CIE; Proceedings of the Commission Internationale de l'Eclairage, **1931**.

[13] E. F. Schubert, *Light-Emitting Diodes;* Cambridge University Press, Cambridge, 2 ed., 2006.

[14] G. Hoffmann; CIE Color Space; http://www.fho-emden.de/~hoffmann/ciexyz29082000.pdf.

[15] LaCie; Farbverwaltung - Weißbuch 3; http://www.lacie.com/download/whitepaper/wp_colormanagement_3_de.pdf.

[16] M. Müller; *In Kristalle eingeschlossene Nanopartikel und ihre Anwendung als Farbkonversionsmaterialien;* Masterarbeit, TU Dresden, **2012**.

[17] CIE; Method of Measuring and Specifying Colour Rendering Properties of Light Sources.

[18] W. Davis and Y. Ohno, *Optical Engineering*, **2010**, *49*(3), 033602.

[19] T. Otto, M. Müller, P. Mundra, V. Lesnyak, H. V. Demir, N. Gaponik, and A. Eychmüller, *Nano Letters*, **2012**, *12*(10), 5348.

[20] M. Adam, Z. Wang, A. Dubavik, G. M. Stachowski, C. Meerbach, Z. Soran-Erdem, C. Rengers, H. V. Demir, N. Gaponik, and A. Eychmüller, *Advanced Functional Materials*, **2015**, *25*(18), 2638.

[21] M. Adam, T. Erdem, G. M. Stachowski, Z. Soran-Erdem, J. Lox, C. Bauer, J. Poppe, H. V. Demir, N. Gaponik, and A. Eychmüller, *ACS Applied Materials & Interfaces*, **2015**, *DOI: 10.1021/acsami.5b08377*.

[22] J. S. Bendall, M. Paderi, F. Ghigliotti, N. L. Pira, V. Lambertini, V. Lesnyak, N. Gaponik, G. Visimberga, A. Eychmüller, C. M. S. Torres, M. E. Welland, C. Gieck, and L. Marchese, *Advanced Functional Materials*, **2010**, *20*(19), 3298.

[23] Commission delegated directive amending, for the purposes of adapting to technical progress, Annex III to Directive 2011/65/EU of the European Parliament and of the Council as regards an exemption for cadmium in illumination and display lighting, **2014**.

[24] E. Jang, S. Jun, H. Jang, J. Lim, B. Kim, and Y. Kim, *Advanced Materials*, **2010**, *22*(28), 3076.

[25] QD Vision, leading company in QLED-displays. http://www.qdvision.com.

[26] Y. Yang, H. Q. Shi, W. N. Li, H. M. Xiao, Y. S. Luo, S. Y. Fu, and T. Liu, *Composites Science and Technology*, **2011**, *71*(14), 1652.

[27] S. Kalytchuk, O. Zhovtiuk, and A. L. Rogach, *Applied Physics Letters*, **2013**, *103*(10), 103105.

[28] M. Müller, M. Kaiser, G. M. Stachowski, U. Resch-Genger, N. Gaponik, and A. Eychmüller, *Chemistry of Materials*, **2014**, *26*(10), 3231.

[29] T. Erdem, Z. Soran-Erdem, P. L. Hernandez-Martinez, V. K. Sharma, H. Akcali, I. Akcali, N. Gaponik, A. Eychmüller, and H. V. Demir, *Nano Research*, **2015**, *8*(3), 860.

[30] M. Adam, R. Tietze, N. Gaponik, and A. Eychmüller, *Zeitschrift für Physikalische Chemie*, **2015**, *229*(1-2), 109.

[31] Y. Chang, X. Yao, Z. Zhang, D. Jiang, Y. Yu, L. Mi, H. Wang, G. Li, D. Yu, and Y. Jiang, *Journal of Materials Chemistry C*, **2015**, *3*, 2831.

[32] Z. Soran-Erdem, T. Erdem, P. L. Hernandez-Martinez, M. Z. Akgul, N. Gaponik, and H. V. Demir, *The Journal of Physical Chemistry Letters*, **2015**, *6*(9), 1767.

[33] H. V. Demir, S. Nizamoglu, T. Erdem, E. Mutlugun, N. Gaponik, and A. Eychmüller, *Nano Today*, **2011**, *6*(6), 632.

[34] T. Erdem, S. Nizamoglu, X. W. Sun, and H. V. Demir, *Optics Express*, **2010**, *18*(1), 340.

[35] D. R. Lide, *Handbook of Chemistry and Physics;* CRC Handbook of Chemistry and Physics. Taylor & Francis Group, 89 ed., 2008.

[36] American National Standard for electric lamps Specifications for the chromaticity of solid state lighting products, **2011**.

[37] S. Nizamoglu, T. Erdem, X. Wei Sun, and H. V. Demir, *Optics Letters*, **2011**, *36*(15), 3372.

[38] X. Wang, W. Li, and K. Sun, *Journal of Materials Chemistry*, **2011**, *21*(24), 8558.

[39] C. Sun, Y. Zhang, Y. Wang, W. Liu, S. Kalytchuk, S. V. Kershaw, T. Zhang, X. Zhang, J. Zhao, W. W. Yu, and A. L. Rogach, *Applied Physics Letters*, **2014**, *104*(26), 261106.

[40] X. Yuan, R. Ma, W. Zhang, J. Hua, X. Meng, X. Zhong, J. Zhang, J. Zhao, and H. Li, *ACS Applied Materials & Interfaces*, **2015**, *7*(16), 8659.

[41] Z. Zhang, D. Liu, D. Li, K. Huang, Y. Zhang, Z. Shi, R. Xie, M.-Y. Han, Y. Wang, and W. Yang, *Chemistry of Materials*, **2015**, *27*(4), 1405.

5. Recently Emerging Approaches to Mixed Crystal Preparation

The approaches to mixed crystallization presented in the work an firstly shown within the publication in Nano Letters [1] already attracted sufficient interest in the QD community. Several groups followed the work and contributed to the field with their ideas and new methods. This chapter overviews these recent achievements with the aim to complete a full picture of the field.

First of all, our cooperation partners at Bilkent University in Turkey developed in cooperation with our group three further mixed crystal systems which should be briefly discussed here.

As discussed in the previous chapters, the stability of the QDs is always one key parameter which is strongly affected by the high ionic strength within the saturated salt solution. One suggested solution can be the utilization of a matrix that is easily soluble in water but has no ions, e.g., sucrose. In their original study [2], they created mixed crystals with pure TGA-stabilized CdTe QDs as well as systems with CdTe QDs and Au nanoparticles (NPs). In these hybrid systems, a plasmonic enhancement of the CdTe PL-QY was observed when correct ratios of CdTe and Au were present in the mixed crystals, as it can be seen in Figure 5.1 b). The resulting mixed crystals show a relatively even distribution of the embedded NPs and an intense fluorescence (see Figure 5.1 a)). Due to non-ionic character of the media, the method is ideal for using ligand exchanged QDs with limited stability. Therefore, it was adopted for growing mixed crystals with PbS, which was discussed in Section 2.4, as well as Cu:InZnS/ZnS QDs. The embedding of Cu-doped QDs within the sucrose resulted in colored composites that only resemble the blue emission of the sucrose while no emission was detectable from the QDs. The reason therefore might be the low PL-QY of the ligand exchanged Cu:InZnS/ZnS QDs and/or an adverse interaction of the host matrix with the QDs.

Nevertheless, the use of sucrose as host matrix still needs to be optimized in further studies. First of all, the crystallization at 30 °C in an oven can take up to several weeks, although

this might be overcome by using crystallization vessels with greater diameters. Secondly, sucrose has only a reduced stability against heat and humidity limiting its fields of application. Concerning the latter point, an encapsulation into a silicone resin might reduce this weakness.

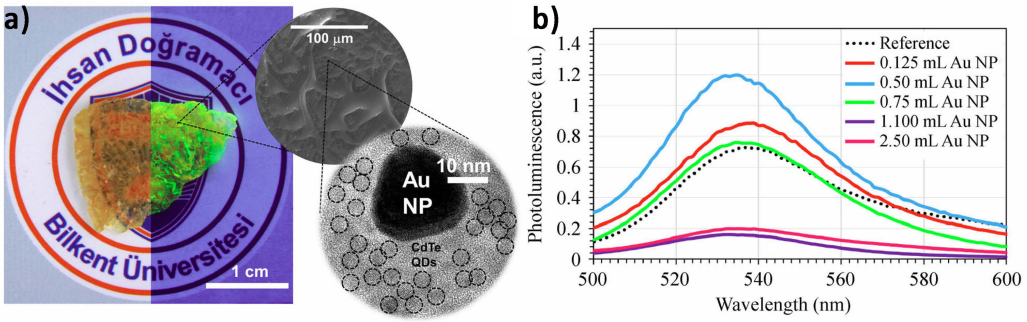

Figure 5.1.: a) True-color image of a hybrid Au NP/CdTe QD mixed sucrose crystal. The image was taken under ambient light (left part) or 365 nm UV excitation (right part). The middle inset shows the mixed crystal under a scanning electron microscope, while the right inset was taken by using transmission electron microscopy. b) PL-QY corrected PL spectra of the mixed crystals with varying amounts of Au NPs and a fixed content of CdTe QDs. Adopted by courtesy of Nano Res. 2015, 8, 860. Copyright 2015, Springer.

The following approach is sophisticated, despite the fact that the stability limitation of the host can be considered as valid. In this study [3], our colleagues at Bilkent University incorporated oil-based CdSe/ZnS QDs with an alloyed gradient shell into anthracene as host matrix. Anthracene is soluble in $CHCl_3$ eliminating the necessity for a QDs ligand exchange and is, due to its conjugated π-system, able to emit blue light if excited with UV radiation. Therefore, the QDs and the host provide a mixed emission color in the mixed crystals, as shown in Figure 5.2 a). Since the QDs on the other hand strongly absorb blue light, the host can act as donor and non-radiative transfer energy to the QDs which acts as acceptor. This process is clearly shown in Figures 5.2 b) - d) with the reduction of the anthracene's PL intensity upon QD incorporation (b) as well as an increase in the emission intensity per QD within the crystals (c). Furthermore, QDs embedded into anthracene show a PL excitation (PLE) spectrum composed of the pure QD part. It, however, also shows strong parts of the anthracene's PLE spectrum, indicating an energy transfer. This theory is supported by a decrease in the PL-LT of the donor/host and a corresponding increase of the acceptors/QDs PL-LT.

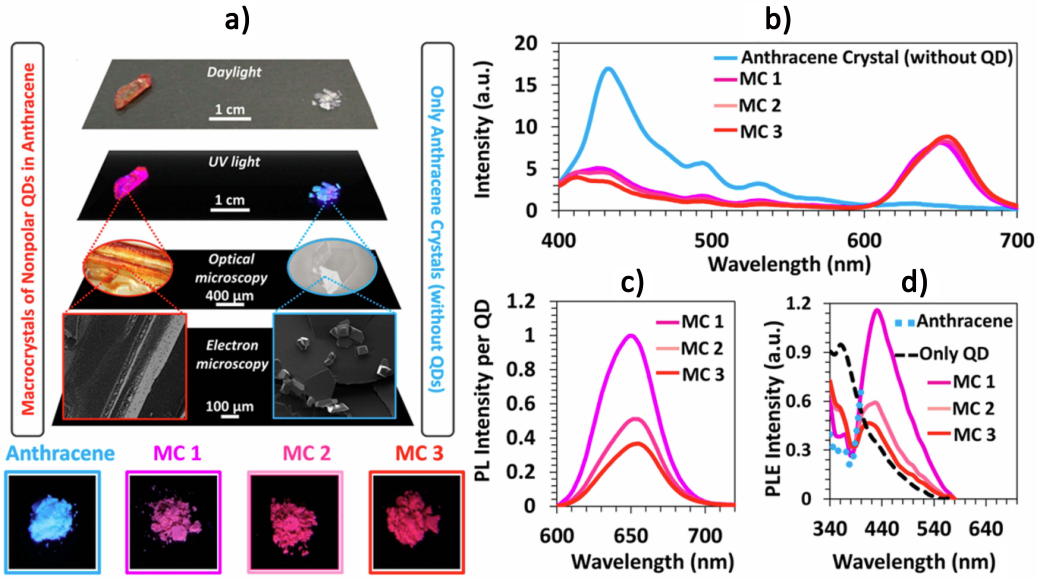

Figure 5.2.: a) Macroscopic true-color images of anthracene-based mixed crystals (left column, MC 1-3) and pure anthracene crystals (right column) under ambient light or 365 nm UV excitation. Optical and scanning electron microscopy images of the corresponding crystals as well as true-color images of the resulting powders under 365 nm UV excitation are displayed below. b) PL spectra of thin films prepared by using the powders from a) blended with silicone, λ_{ex} 375 nm. c) PL intensity normalized to the amount of QDs within the three samples. d) PLE spectra of the three mixed crystals normalized with respect to the QD amount along with the one of the only QD film, all recorded in an emission wavelength range of 600-750 nm to collect the QD emission, except the PLE of the anthracene crystal recorded between emission wavelengths of 430 and 750 nm. Reprinted by courtesy of J. Phys. Chem. Lett. 2015, 6, 1767. Copyright 2015, American Chemical Society.

To overcome the reduced stability of an organic host matrix and to avoid the necessity of a ligand exchange, the incorporation of oil-based QDs into LiCl was introduced recently. [4] LiCl is soluble in THF which also disperses the QDs relatively well and can be used as solvent for the mixed crystal parental solution, depicted in Figure 5.3. To avoid the aggregation of the QDs within THF, the evaporation of the solvent is accelerated in a vacuum chamber providing a fast procedure with resulting mixed crystals of less than 200 μm. As shown in Figure 5.3 a) - d), the mixed crystals clearly have the same strong emission as the QDs in $CHCl_3$. The graph in Figure 5.3 e) shows a small red shift of the emission maxima which can be related to the change of the surrounding media and some aggregation. This could

also explain the small broadening of the PL spectra and the slightly reduced PL-LT of the QDs within LiCl. Furthermore, the absorption spectra of the QDs in solution and within LiCl show comparable transitions, although in the case of the mixed crystals the spectrum is partly blurred supporting the theory of partial aggregation. The images f) and g) of Figure 5.3 clearly reveal that the encapsulation of these LiCl-based mixed crystals into epoxy does not alter their optical properties. Due to the direct transfer of the QDs from the solution into LiCl as host, the initial PL-QY can be retained, even during a long-term operation hybridized on a high-power blue LED driven at 100 mA. Therefore, this method provides access to highly emissive mixed crystals based on LiCl as a host and oil-based QDs without the necessity of a previous phase transfer protocol.

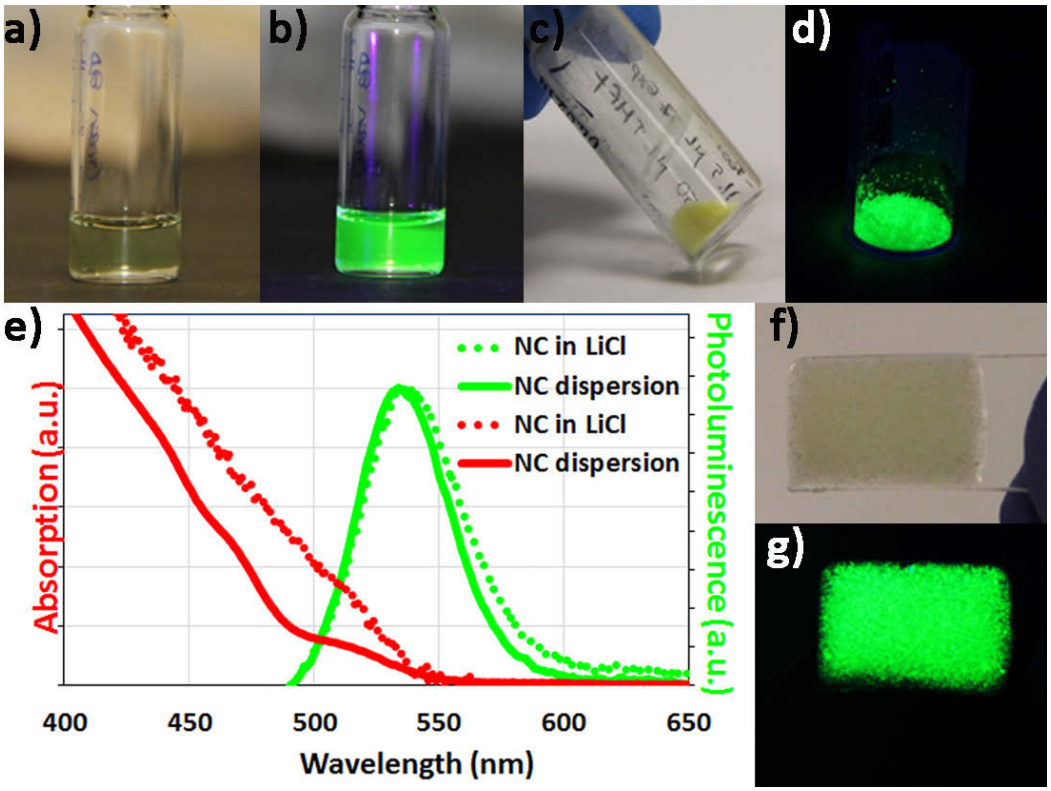

Figure 5.3.: a-d) True-color images of QD solution and corresponding LiCl-based mixed crystals under ambient lighting (a and c) and 365 nm UV excitation (b and d). e) PL spectra of the QD solution (solid green line) and the corresponding mixed crystals (dotted green line) as well as the absorption spectrum of the QD solution (red line). (f and g) True-color images of LiCl-based mixed crystal powder hybridized with epoxy under ambient light and a 365 nm UV excitation. Adopted by courtesy of Nanoscale. 2015, DOI: 10.1039/C5NR02696B. Copyright 2015, Royal Society of Chemistry.

Furthermore, Professor Rogach's group embedded CdTe in NaCl according to our first publication in 2012. They reported the formation of mixed crystal powders with enhancend PL-QY upon incorporation and emission colors covering the whole green to red spectral region. With these materials, they prepared pure-color luminaires by using a UV-LED as excitation source. [5] Applying KBr, KCl and NaCl as host matrix, Professor Li's group extended our work by using C-dots as emissive centers. [6] Aiming at an efficient and stable blue emitting system, the inorganic salt matrix proved to be distinctly more stable than silica. By using a similar approach to the LLDC, the group of Professor Jiang used a co-precipitation of CdTe QDs with NaCl in a water-EtOH mixture to prepare QD-salt mixed crystals. [7] The same group also published a protocol by using $BaSO_4$ as an alternative inorganic host material to prepare QD-salt composites for producing w-LEDs. [8] In both protocols, fine powders of mixed QD-salt crystals are generated, which proved their suitability as color conversion material although no investigations on their chemical stability was conducted. Moreover, Professor Yang's group implemented the use of cellulose as a host matrix embedding CdTe QDs to form color conversion layers on top of a blue LED. [9] The preparation of these composites proved to be highly dependent on the initial stabilizing agents as well as temperature at which to composites are formed.

5.1. Summary

The technique of embedding various QDs into ionic host matrices attracted considerable attention within the QD community around the world, sparking new areas of research. The original idea was already extended to different nanoparticles (e.g. Au NPs) and host systems (e.g. $BaSO_4$, anthracene, sucrose) by other research groups. Next to their application as color conversion materials for both, white and pure color LEDs, their optical properties were investigated in even more detail. Energy transfer between both metal and semiconducting NPs as well as the host and the embedded QDs and an acceleration of the mixed crystal formation proved to be of great interest. As no general physical limitation for further variations of host and encapsulated NPs appeared until today, a huge field of QD-host combinations can be imagined. Furthermore, emerging new applications applications for the mixed crystals will contribute towards a wide spreading of the approach.

References

[1] T. Otto, M. Müller, P. Mundra, V. Lesnyak, H. V. Demir, N. Gaponik, and A. Eychmüller, *Nano Letters*, **2012**, *12*(10), 5348.

[2] T. Erdem, Z. Soran-Erdem, P. L. Hernandez-Martinez, V. K. Sharma, H. Akcali, I. Akcali, N. Gaponik, A. Eychmüller, and H. V. Demir, *Nano Research*, **2015**, *8*(3), 860.

[3] Z. Soran-Erdem, T. Erdem, P. L. Hernandez-Martinez, M. Z. Akgul, N. Gaponik, and H. V. Demir, *The Journal of Physical Chemistry Letters*, **2015**, *6*(9), 1767.

[4] T. Erdem, Z. Soran-Erdem, V. K. Sharma, Y. Kelestemur, M. Adam, N. Gaponik, and H. V. Demir, *Nanoscale*, **2015**, *DOI: 10.1039/C5NR02696B*.

[5] S. Kalytchuk, O. Zhovtiuk, and A. L. Rogach, *Applied Physics Letters*, **2013**, *103*(10), 103105.

[6] T. H. Kim, F. Wang, P. McCormick, L. Wang, C. Brown, and Q. Li, *Journal of Luminescence*, **2014**, *154*, 1.

[7] Y. Chang, X. Yao, L. Mi, G. Li, S. Wang, H. Wang, Z. Zhang, and Y. Jiang, *Green Chemistry*, **2015**, *17*(8), 4439.

[8] Y. Chang, X. Yao, Z. Zhang, D. Jiang, Y. Yu, L. Mi, H. Wang, G. Li, D. Yu, and Y. Jiang, *Journal of Materials Chemistry C*, **2015**, *3*(12), 2831.

[9] D. Zhou, H. Zou, M. Liu, K. Zhang, Y. Sheng, J. Cui, H. Zhang, and B. Yang, *ACS Applied Materials & Interfaces*, **2015**, *7*(29), 15830.

6. Conclusion and Perspectives

Solution-synthesized colloidal semiconductor QDs have gathered considerable attention for various applications over the last decades. These materials offer unique physical and chemical properties including, but not limited to, bright and pure color luminescence as well as size-related tunable emission. Nevertheless, it is still a challenge to maintain these superior qualities in different packaging approaches for final applications. The present work helps to overcome this issue by embedding the QDs into inorganic materials, providing extremely solid and airtight matrices.

Starting with the "classical" approach, CdTe QDs as well as carbon dots were incorporated in several salts including NaCl, KBr and KCl. Applying this straightforward protocol, strongly emitting mixed crystals without altering the optical properties of the included emitters were produced, especially in the case of MPA-stabilized CdTe QDs. For TGA-stabilized CdTe QDs, some modifications of the initial crystallization protocol were implemented adjusting the amount of free stabilizer, the pH and the host matrix.

Apart from the aqueous-based QDs, oil-based synthetic protocols yield QDs with high optical qualities. In order to make them compatible with the mixed crystallization in aqueous media, their initial long-chain aliphatic ligands were replaced by short-chain bifunctional molecules making the QDs soluble in aqueous environment. The resulting colloidal solutions remained stable for up to a minimum of six months, depending on the nature of the QDs and the new ligand shell. Nevertheless, a part of the QDs PL-QY was lost in the ligand exchange which needs to be analyzed thoroughly in subsequent studies. These QDs were successfully incorporated into ionic matrices in the second step. In comparison to the initially water soluble CdTe QDs, the ligand exchanged ones proved to be less stable in high ionic strength media of the saturated NaCl solution. Therefore, disodium tetraborate (borax) was introduced as a new host material having a much lower solubility and ionic strength within its saturated solution. Borax crystallizes as a decahydrate from solution which might be a problem for some applications. Accordingly, future studies should further analyze host materials with a comparably low solubility but without having crystal water in their structure.

In order to reduce the time needed for the mixed crystal formation, the "liquid-liquid diffusion-assisted crystallization" (LLDC) was introduced. In this method, the low solubility of NaCl in MeOH was used for reducing the formation time of approximately seven days to less than twenty hours. The method can be used to incorporate both the initially aqueous soluble CdTe QDs and the phase transferred QDs without suffering from their lower stability due to the much faster mixed crystal formation. Furthermore, by extending the LLDC towards a two-step approach, oil-based QDs were embedded into NaCl by a controlled destabilization without a previous ligand exchange. This versatile protocol enabled the incorporation of QDs that were previously hardly accessible into mixed crystals, e.g., InZnP QDs. In addition, the incorporation of NIR emitting QDs was implemented by using the "classical" approach with both NaCl and sucrose as host matrix. Due to its non-ionic character, sucrose provides a high colloidal durability even for QDs with a low stability within the saturated solution. The resulting mixed crystals enabled the access of the two biological windows around 900 and 1200 nm as well as the first telecommunication window at 1300 nm. Therefore, new possible applications of mixed crystals in bioimaging and signaling processes as well as data transmission are feasible. In a subsequent study, mixed crystals reaching up to 1550 nm, which is the second telecommunication window, shall be prepared. Such materials are not yet accessible with current techniques.

In order to understand the bright emission of the mixed crystals, a systematic study allowing an interpretation of the observed changes in the luminescence behavior of QD colloids upon incorporation into the salt crystal was necessary. Consequently, CdTe QDs embedded in NaCl were chosen as the most developed system for in-depth PL-QY and PL-LT studies focusing on differently sized parent CdTe QDs as well as on CdTe QDs with low and high PL-QY in aqueous solution. Moreover, the PL behavior of CdSe/ZnS QDs with an alloyed gradient shell embedded into NaCl and borax by using the classical and LLDC approach was analyzed. The results showed a strong correlation between the PL-QY and PL-LT of the parental QDs and the refractive index of the host media regarding the development of both PL-QY and PL-LT upon the mixed crystal formation. CdTe QDs with lower PL-QY initial values and thereby more surface defects yield higher enhancement factors upon incorporation indicating a curing of these defect states, most probably by the formation of a thin $CdCl_x$ layer. This observation was supported by the result of the CdSe/ZnS QDs analyses. Upon incorporation into the mixed crystals, CdSe/ZnS QDs showed no enhancement above the refractive index induced changes. Besides, PL-QY measurements proved that a silicone encapsulation of the mixed crystals does not alter their optical properties. However, a derivatization of structure-property relationships for designing these fascinating materials requires more systematic studies. These

should involve different host materials like KCl, NaBr, and KBr as well as QDs of various and well-known surface chemistries, thereby addressing the hypothesis of curing surface defect and the influence of the refractive index of the matrix as well as the reproducibility of the mixed crystal formation. Moreover, silicones or other processable polymers with matching refractive indices for controlling the scattering characteristics of the QD-salt crystal-polymer composites should be analyzed in further studies.

Aiming at an visualization of the incorporated QDs within the ionic matrices at the crystallographic level, TEM analyses were conducted. These measurements revealed that only thin sheets of the mixed crystals could reliably be analyzed without melting the samples. Additionally, it was shown that the QDs are incorporated by an uniform distribution and not aggregated, supporting the results of the optical analyses. The TEM tomography would be a promising tool in subsequent studies to gain a three-dimensional insight into the QD-salt mixed crystals. Due to the long measuring time of ~2 h, even the thin sheets were not stable enough to remain unaltered during the procedure, requiring more sophisticated sample preparation techniques.

Regarding their long-term stability, the mixed crystals proved to be of exceptional durability in both photometric and chemical respect. The stability in conjunction with their superior optical properties encourages the use of QDs embedded in salt matrices for designing new photonic materials with tunable optical properties, e.g., for color conversion.

This, especially in the UNESCO "International Year of Light and Light-based Technologies", highly relevant topic of white light generation by using a blue LED as excitation source and down-converting phosphors was addressed in the fourth part of the current work. After the proof-of-concept w-LED by using mixed crystals with both "classical" and LLDC crystallization methods was demonstrated successfully, a model-experimental feedback approach was implemented. By defining the starting conditions and verifying every intermediate step with the underlying model, a w-LED could be prepared achieving for the first time the very challenging combination of a superior color rendering, optical efficiency as well as a warm white hue at the same time.

The approach of embedding QDs into tight ionic matrices sparked ideas within other research groups to adopt and extend the technique. Next to our partners of the Bilkent research group, who spent a lot of effort on the analyses of energy transfer processes within mixed crystals, other groups also published their ideas and results. Those included their use as color converters for pure color LEDs as well as new QD-host combinations, proving the great potential of the approach as well as the QD communities interest about it.

Future studies should include the use of anisotropic quantum structures like quantum rods,

especially in combination with an oriented incorporation of the quantum structures into the host matrices as well as a shape-directed crystallization. These mixed crystals might find highly promising applications in the field of lasing, polarized emission, display technologies and other optical areas profiting from anisotropy. Furthermore, the use of Cd-free QDs shall be analyzed in more detail with emphasis on retaining the PL-QY over all intermediate steps. To improve the optical efficiency of mixed crystals, plasmonic nanomaterials can be co-embedded as already shown with sucrose as matrix, but with the utilization of a pure inorganic host for enhanced stability. Lastly, in the field of LED application, an improvement of the PL-QY as well as the outcoupling of light from the device is required to reach not only high optical but also high electrical efficiency.

A. Appendix

A.1. Reagents

Table A.1.: Chemical substances used during the preparation of this work.

Substances	Supplier	Molar mass [g/mol]	purity or concentration
Acetone	Merck	58.08	p.a.
Al_2Te_3	Cerac	436.76	99.5%
Adenosine monophosphate	Sigma-Aldrich	391.18	99%
$Ba(NO_3)_2$	ABCR	261.35	99%
$BaBr_2 \cdot 2\ H_2O$	ABCR	333.17	99.3%
$BaCl_2$	Suprapur	208.23	99%
Benzoylperoxide	Merck	242.23	75%
Borax $Na_2B_4O_7 \cdot 10\ H_2O$	Grüssing	201.22	99%
$Cd(ClO_4)_2 \cdot 6\ H_2O$	Alfa-Aesar	419.42	99.999%
CdO	Sigma-Aldrich	128.41	99.5%
Chloroform	Sigma-Aldrich	119.37	>99%, H_2O-free
Cetyltrimethylammoniumbromid	Sigma-Aldrich	364.45	98%
$Cu(OAc)_2$	Sigma-Aldrich	181.63	99.999%
$CuSO_4$	Roth	159.61	99%
Dodecanethiol	Alfa-Aesar	202.40	98%
Ethylenediamine	Sigma-Aldrich	60.10	99.5%
Ethanol	Merck	46.94	p.a.
$GaCl_3$	Sigma-Aldrich	176.08	99.999%
Glutathione	Sigma-Aldrich	307.32	99%
H_2SO_4	Merck	98.08	0.5 M
$Hg(ClO_4)_2 \cdot 6\ H_2O$	Alfa-Aesar	507.49	99.999%
$In(OAc)_3$	Sigma-Aldrich	291.95	99.99%
$K_3[Fe(CN)_6]$	-	329.26	-
$K_4[Fe(CN)_6]$	-	368.34	-

KBr	Sigma-Aldrich	119.00	FT-IR-grade
KCl	Merck	74.55	p.a.
KOH	Grüssing	56.11	98.4%
MeOH	Sigma-Aldrich	32.04	p.a.
$MgBr_2$	Sigma-Aldrich	184.11	98%
$MnBr_2 \cdot 4\ H_2O$	Sigma-Aldrich	296.81	98%
$MnCl_2$	Sigma-Aldrich	125.84	98%
$MnSO_4 \cdot H_2O$	Merck	169.02	p.a.
3-Mercaptopropionic acid	Merck	106.14	98%
11-Mercaptoundecanoic acid	Sigma-Aldrich	218.36	95%
NaCl	VWR	58.44	p.a.
NaOH	Merck	40.00	0.1-1 M
Octadecene	Sigma-Aldrich	254.50	90%
Oleic acid	Alfa-Aesar	282.46	90%
Oleylamine	Acros	267.49	99%
Palmitic acid	Sigma-Aldrich	256.42	98%
i-Propanol	VWR	60.10	p.a.
QSil 218 Silicone	ACC-Silicones	-	-
Selenium	Sigma-Aldrich	78.97	99.999%
Sodium *bis*(2-ethylhexyl)-sulfosuccinate	Sigma-Aldrich	444.56	97%
Sucrose	Sigma-Aldrich	342.30	99%
Sulfur	Sigma-Aldrich	32.06	99.98%
Thioglycolic acid	Merck	92.11	99%
Tetramethylammoniumhydroxid	Sigma-Aldrich	91.15	95%
Toluene	Merck	92.14	p.a.
Trioctylphosphine	ABCR	370.64	97%
Tris(trimethylsilyl)phosphine	Grüssing	250.54	98%
$Zn(OAc)_2$	Sigma-Aldrich	183.48	99.99%
$Zn(OAc)_2 \cdot 2\ H_2O$	Sigma-Aldrich	219.50	99.999%
$ZnSO_4$	Grüssing	287.54	99.5%

A.2. Synthesis of Quantum Dots

CdTe nanocrystals were synthesized following the protocol of ref. [1] by dissolving 2.305 g (5.5 mmol) of $Cd(ClO_4)_2 \cdot 6\ H_2O$ in 250 mL of water and adding 7.15 mmol of the thiol stabilizing agent dropwise under stirring, followed by an adjustment to pH 12, using a 1 M solution of NaOH. The solution was placed in a three necked flask and deaerated with Ar for 30 min. H_2Te gas was generated by reacting 0.4 g (0.916 mmol) of Al_2Te_3 lumps with 10 mL of a 0.5 M H_2SO_4 solution and passed through the solution with a slow argon flow under vigorous stirring. The growth of the QDs to the desired size proceeded under open air

conditions upon refluxing at 100 °C with a condenser attached. Nanocrystals obtained by this well established approach possess PL-QYs in the range of 10-60%. [2] The sizes of the CdTe QDs were derived from the 1s-1s transition maximum, following Rogach et al. [3]
$Cd_{1-x}Hg_xTe$ QDs were synthesized according to the protocol given in reference [4]. The approach is generally the same as for CdTe QDs. Only a small molar fraction (e.g. 3-10 mol.%) of the initial $Cd(ClO_4)_2 \cdot 6\ H_2O$ is replaced by, according to Hg, an equal molar amount of $Hg(ClO_4)_2 \cdot 6\ H_2O$, while all other reaction parameters and steps are kept the same. QDs prepared by this manner possess PL-QYs up to 60%, according to reference [4].
CdSe/ZnS QDs with an alloyed gradient shell were synthesized according to reference [5], using slight modifications of the synthetic protocol. All amounts used for the synthesis can be found in Table A.2.

Table A.2.: Amount of precursors for the synthesis of three different CdSe/ZnS quantum dots (QDs) with an alloyed gradient shell. The synthesis are modified procedures of reference [5].

Color	CdO	$Zn(OAc)_2$	Oleic acid	ODE	Se	S	TOP
green	0.3 mmol 38.5 mg	4.0 mmol 733.9 mg	5.5 mL	20.0 mL	0.25 mmol 19.7 mg	3.50 mmol 112.0 mg	3.0 mL
yellow	1.8 mmol 231.1 mg	2.6 mmol 477.0 mg	5.5 mL	20.0 mL	1.00 mmol 84.2 mg	2.45 mmol 78.7 mg	3.2 mL
red	1.0 mmol 127.5 mg	2.0 mmol 367.0 mg	5.0 mL	23.2 mL	0.20 mmol 15.8 mg	2.00 mmol 64.1 mg	Se: 0.2 mL, 1.6 mL ODE, S: 1 mL

For green (530 nm) and yellow (570 nm) emitting QDs, a defined amount of CdO, $Zn(OAc)_2$, OA and ODE were placed in a 50 mL three-necked flask. The mixture was degassed for 1 h and backfilled with inert gas at 100 °C. After heating to 310 °C, defined amounts of S and Se dissolved together in TOP were rapidly injected into the flask accompanied with a temperature reduction to 300 °C. After 10 min, the QD solution was cooled to room temperature, quenched with 20 mL of $CHCl_3$, and followed by two washing steps with an excess of acetone.
For red (617 nm) emitting QDs, CdO, $Zn(OAc)_2$, OA and ODE were placed in a 50 mL three-necked flask and degassed for 1 h at 100 °C. After backfilling with inert gas and heating to 300 °C, Se dissolved in TOP and ODE was injected rapidly into the flask, followed by a dropwise addition of 0.3 ml DDT after 30 s. 20 minutes later, S dissolved in TOP was added dropwise to the reaction solution, while holding the mixture at 300 °C for further 10 min. The QD solution was cooled to room temperature, quenched with 20 mL of $CHCl_3$ and washed two times with acetone and *i*-propanol. Finally, the QDs were redispersed in 4 mL $CHCl_3$ to gain a concentrated solution for the ligand exchange and characterization.
The InZnP cores were synthesized according to reference [6] by mixing 35.4 mg (0.12 mmol)

$In(OAc)_3$, 13.8 mg (0.06 mmol) $Zn(OAc)_2 \cdot 2\ H_2O$, 94.2 mg (0.36 mmol) palmitic acid, and 8 mL ODE in a 25 mL three-necked flask. The suspension was degassed twice, heated to 110 °C, and degassed again for 30 min. After backfilling with Ar and heating to 300 °C, 17.4 μL (0.06 mmol) $(TMS)_3P$ in 1 mL ODE were rapidly injected into the flask and held at 230 °C for 2 h. For the GaP shell, a solution of 5 mg (0.03 mmol) $GaCl_3$ and 31.5 μL (0.1 mmol) oleic acid in 2 mL ODE was added dropwise to the InZnP core solution at 200 °C. For the ZnS shell formation, 55 mg (0.3 mmol) $Zn(OAc)_2$ were added to the reaction flask at room temperature and the suspension was heated to 230 °C for 4 h. Finally, 117 μL (0.5 mmol) DDT were slowly injected into the flask and the mixture was kept at 230 °C for further 2 h. The obtained multi-shell QDs were purified three times by precipitation with acetone/methanol (MeOH) and redispersed in toluene, exhibiting a PL-QY of ca. 70%.
The Cu-doped InZnS/ZnS QDs were synthesized according to reference [7]. In a typical synthesis, 0.051 g (1.6 mmol) S were placed in a 50 mL three-necked flask, degassed threefold and backfilled with Ar. Subsequently, the desired amounts of 0.4 M $In(OAc)_3$ in OAm, 0.4 M $Zn(OAc)_2$ in OAm/ODE 3:7 v/v ratio and 0.05 M $Cu(OAc)_2$ in OAm were injected into the flask. The system is degassed again following the addition of 4 mL DDT and heated under a continuous Ar flow to 220 °C using a 15 K/min heating rate. After 10 min at 220 °C, the system is quenched to 100 °C to stop the core growth and 1 mL 0.4 M $Zn(OAc)_2$ in OAm/ODE 3:7 v/v ratio is added. To initiate the subsequent shell growth, the solution is heated to 240 °C and kept at this temperature for 20 min. The resulting QD solution is cooled to room temperature and 10 mL of toluene are added to the crude solution. The QDs were purified two times by precipitation with MeOH, dried and redispersed in 4 mL of toluene, exhibiting PL-QYs of 10-20%.

A.3. Ligand Exchange Procedures

PT 1: This protocol is adopted from reference [8]. Water soluble CdSe/ZnS QDs with an alloyed gradient shell were obtained by mixing 10 mg of QDs dispersed in 10 mL of $CHCl_3$ with 2 mL of pure MPA. The mixture was stirred at 60 °C for 2-3 h, cooled to room temperature and centrifuged at 5500 rpm. After washing them twice with $CHCl_3$, the QDs were redispersed in water with a basic pH and stored under ambient conditions.
PT 2: This protocol is based on reference [9] and was designed for CdS capped CdSe QDs. Here, the QDs were diluted in 10 mL hexane and 10 mL of MeOH containing 0.1 g KOH and 0.12 mL MPA were added. The mixture was vigorously shaken, centrifuged and the QDs were redispersed in water with a pH of 10.
PT 3: This procedure is adopted from reference [10] and can be used for CdSe/CdS/ZnS core/shell/shell QDs. Here, 20 mL of 1 μM QD solution is stirred for 30 min with 3 mL of EtOH containing 1 g of AMP at a pH of 10. Subsequently, water is added to the mixture till the phases separate and the aqueous phase is washed twice by precipitation with acetone.

PT 4: In this protocol, 30 mg/ml AOT was added to a 235 μM solution of CdSe QDs in hexane. 0.5 ml of this solution are then mixed with 10 mL of an aqueous 0.05 M NaCl solution at pH 6 to form an oil-in-water emulsion. Subsequently, the mixture is stirred and heated to 85 °C to boil off the hexane, leaving a turbid solution. A precipitation at 8300 g for 1 h was used to clean the turbidity and the resulting clear solution was used for further investigations. This protocol is based on reference [11].
PT 5: Based on reference [12], CdSe/ZnS QDs were phase transferred using the following steps: 2 mL of a QD solution in $CHCl_3$ with an optical density of ca. 2 were added to 2 mL of an aqueous MPA solution with roughly 150 mol.% of MPA corresponding to the total number of Cd and/or Zn atoms on the QDs surface. The resulting mixture was stirred for two hours, centrifuged and the precipitated QDs were redispersed in water with a pH of 10.8.
PT 6: In this protocol based on reference [13], 1 mL of CdSe/ZnS QDs with an OD of 1 were mixed with 1 mL of a 1:1 v:v ratio of MPA:MeOH and vigorously stirred. After 30 s, 1 mL of water and 0.1 mL of 1 M KOH solution are added to the QDs and stirred for 20 min. Afterwards, the phases are separated and the aqueous phase is used without further purification.
PT 7: Using the approach of reference [14], 5 mL of an 0.1 mM solution of CdSe/ZnS QDs in $CHCl_3$ were stirred for 30 min together with 0.5 mL of a 1:10 v:v mixture of MPA and MeOH at pH 12. Subsequently, 5 mL of water were added and the mixture was further stirred for 20 min. The phases were then separated and the aqueous phase could be used without further purifications or after a precipitation using acetone.
PT 8: Based on reference [15], CdSe/ZnS QDs dissolved in $CHCl_3$ were mixed with pure TGA, to gain a 1 M TGA solution. After stirring for 2 h, an equal volume of aqueous phosphate buffered saline solution at pH 7.4 is added. The resulting system is shaken vigorously, the phases were separated and the aqueous layer was washed four times by precipitation using acetone.
PT 9-11: Here, long chain aliphatic acids on the QDs surface were exchanged with short chain bi-functional thiols using a modified protocol of reference [16]. 30 μL of concentrated CdSe/ZnS QDs solution were diluted with 500 μL $CHCl_3$ and mixed with a 0.2 M aqueous mercaptocarboxolic acid (TGA, MUA or MPA) solution at pH of 10. After shaking vigorously for 4 h, phases were separated and the aqueous phase was used without further purification.
PT 12: This approach, based on reference [17], uses a two-step ligand exchange procedure instead of the other, one-step methods. In the first step, 0.5 mL diluted QD solution (either CdSe/ZnS or CdSe/CdS) in $CHCl_3$ are mixed with an equal amount of EDA and shaken for 30 min. Subsequently, 1 mL of a 0.2 M alkaline aqueous solution (pH 11-12) of the new stabilizing agent (e.g. TGA, MPA, MUA or MSA) is added. The resulting mixture is vigorously shaken for further 1-2 h. Afterwards, the phases are separated and the QDs are precipitated by *i*-propanol and centrifuged at 5500 g for 60 min, dried and redispersed in pure water.
PT 13: In this procedure, a 3 mM solution of PbS QDs in $CHCl_3$ stabilized by OA is mixed with a 0.15 M solution of GSH in water (pH 5) of equal volume. The resulting two phase system is shaken for 10 min at room temperature and the phases were separated afterwards.

Water soluble PbS QDs obtained by this method based on reference [18] can be used directly or after filtering through a 22 μm pore size filter.

A.4. Preparation of Mixed Crystals

The preparation of the mixed crystals using the classical procedure was performed by mixing 25 mL of a saturated salt/sucrose solution with 5 mL of a QD solution in a 30 mL beaker. Protected from dust, the solutions were stored under ambient conditions or at 30 °C in an oven. The crystallization was complete when the parental solution turned colorless. The crystals formed were removed from the parental solution, rinsed with cold water and dried. Although the influence of the colloidal species on the growth and structure of ionic crystals is expected, not any remarkable effects were observed in the experiments. Except from this, only the change from cubic to an octahedral shape in the case of NaCl as host matrix could be observed. This can be explained with the coordinating properties of the QDs stabilizing agent, as discussed in Chapter 2.2.1. Most probably, the low loading values of the QDs into the crystals (below 1%) are responsible for the absence of influences on the crystallographic structure.
LLDC-based mixed crystals were prepared using a different approach. The fast preparation of the mixed crystals with an aqueous suspension of CdTe QDs was performed by firstly placing 5 mL of MeOH in a glass vial. Subsequently, a mixture of 0.5 g NaCl and 1.7 mL CdTe QDs was slowly injected to the bottom of the vial, forming an aqueous layer below the MeOH with a stable interface between the two liquids. Due to the spontaneous diffusion of MeOH into the NaCl solution, the solubility of the salt is gradually decreased which leads to the formation of mixed crystals within 15-20 h. For the phase transferred CdSe/ZnS and InZnP/GaP/ZnS QDs, a similar approach is used. Preparing mixed crystals directly from organic solvent-based QDs uses a modified, two-step LLDC-approach. Here, first 3 mL of saturated NaCl in MeOH are injected into 2 mL of a diluted QD solution (50 μL QDs and 1950 μL $CHCl_3$). Within this mixture, NaCl crystal seeds are formed within seconds, causing a slight turbidity of the solution. The solution is then centrifuged for 3 min at 3260 g to separate the supernatant solution from the seeds, which are washed three times with MeOH and redispersed in 5 mL of pure MeOH afterwards. To form the proper mixed crystals, 1.7 mL of water dissolving 0.5 g NaCl is injected under the seed-MeOH layer and stored for 20 h.
Furthermore, one single batch of MPA-stabilized CdTe QDs was mixed with saturated solutions of the following, multiionic salts shown in Table A.3. These salts were chosen according to their non-acidic character, to avoid potential pH induced destabilization of the QDs. Directly following the addition of the QDs towards the salt solutions, the formation of more or less pronounced turbidity was observed, a clear indication for rapid destabilization of the QDs. A problem related to the CdTe batch itself can be excluded, since the control experiment with NaCl as host matrix delivered a highly stable parental solution and strongly emitting mixed

crystals. For bivalent cations, a formation of complexes analogous to tetrazole stabilized QDs can be assumed. This would also explain the gel-like character of the resulting precipitate after 24h of storage, indicating the formation of a not completely aggregated network and the remained fluorescence of it. On the other hand, this explanation cannot be used for the monovalent potassium ions in case of the two prussiates of potash. Here, a chemical interaction (e.g. oxidation) between the salt ions and the QDs is more likely, also since the fluorescence of the precipitate was completely quenched.

Table A.3.: Salts used within the multivalent mixed crystallization approach

Salt	Formula
Barium bromide	$BaBr_2$
Barium chloride	$BaCl_2$
Barium nitrate	$Ba(NO_3)_2$
Copper sulfate	$CuSO_4$
Magnesium bromide	$MgBr_2$
Manganese bromide	$MnBr_2$
Manganese chloride	$MnCl_2$
Manganese sulfate	$MnSO_4$
Potassium ferrocyanide	$K_4[Fe(CN)_6]$
Potassium ferricyanide	$K_3[Fe(CN)_6]$
Zinc acetate	$Zn(CH_3COO)_2$
Zinc sulfate	$ZnSO_4$

A.5. LED Preparation

To prepare color conversion LEDs, mixed crystals were milled to a fine powder and varying amounts of the differently emitting powders were blended with a two component silicone resin (ACC Silicones) on top of a blue emitting commercial InGaN LED. The mixture was hardened for 2 h at 70 °C, forming a homogeneous phosphor layer. In case of borax-based mixed crystals, the powder was dried under vacuum at 70 °C over night to remove main parts of the crystal water before preparing the conversion layer.

A.6. Stability Tests

Emission stability tests: All of the samples were placed in the focus of a 1000 W xenon lamp equipped with a water filter to cut of the NIR part of the spectrum. The samples were carefully prepared to achieve comparable optical densities. The cuvettes containing the

samples were placed in a holder with a fixed temperature of 25 °C, reducing the temperature influence on the stability investigations.
The mixed crystals were used without further treatment and placed as solid samples within a cuvette. For mechanically mixed references, the QDs have been concentrated in a rotary evaporator ~10 times and were precipitated with *i*-propanol. Precipitates were separated, dried under inert atmosphere and carefully mechanically mixed with either NaCl, PMMA or glass powder.
The polymer-QD-composites were prepared according to reference [19]. The QDs were concentrated with a rotary evaporator ~10 times. 2 mL of the resulting concentrated solution was mixed with 1 mL freshly distilled styrene and 20 mg of Octadecyl-p-vinylbenzyldimethyl-ammonium chloride (OVDAC) were added. The mixture was intensively stirred for 30 min until all the QDs were functionalized with OVDAC and transferred into the styrene. The styrene was separated from the water phase and either diluted with 1 mL of styrene or methylmethacrylate. The monomer solutions were polymerized at 70 °C in an oven for 24 h using 0.2 wt.-% azobisisobutyronitrile (AIBN) as initiator.
Chemical stability test: The prepared mixed crystals, either with aqueous or organic-based QDs, were placed in a 0.5 M solution of benzoyl peroxide, a strong oxidizing agent, in toluene for 24 h to confirm that the QDs are incorporated into the salt matrix. The test was performed with the pure QDs (for the $CHCl_3$ soluble QDs) and, with mixed crystals prepared by both, the classical method as well as the LLDC-approach.
LED stability test: The stability of the mixed crystal emission was tested by integrating green, yellow, and red mixed crystals on a blue LED. The LED was driven at 300 mA for 4 days. The emission intensity of the LED was recorded using a FluoroMax-4 spectrofluorometer (Horiba Jobin Yvon). The temperature of the LED chips was measured using an FLIR A655sc infrared camera. The LEDs were operated by application of a square wave modulation (1 kHz, 50% duty cycle, 300 mA peak-to-peak current).

A.7. Instrumentation

For all optical characterizations, cuvettes made from SUPRASIL® quartz were used.
UV-Vis absorption spectra were recorded at room temperature using a Cary 50 spectrophotometer (Varian). The spectra were measured together with a baseline of the corresponding, spectroscopic grade pure solvent.
PL-measurements, including relative PL-QY determinations, were conducted on a FluoroMax-4 spectrofluorometer (Horiba Jobin Yvon). PL-QYs of the QDs were measured by a comparison with Rhodamine 6G and Rhodamine 101 (both Radiant Dyes Laser) in ethanol, assuming their PL-QY as 91% and 91.5% respectively. [20]
Absolute PL-QY measurements were conducted both in Dresden and at the BAM (Bundesanstalt für Materialprüfung und -forschung) in Berlin.

In Dresden, a FluoroLog-3 spectrofluorometer (Horiba Jobin Yvon) equipped with a Quanta-Φ integrating sphere was used for absolute PL-QY determinations. QDs in solution were investigated in 10 * 4 mm quartz cuvettes in order to minimize reabsorption. Powders of milled QD-salt crystals were distributed uniformly within Spectralon®-holders, covered with a quartz-glass slip and mounted at the bottom of the integrating sphere. A solvent-filled cuvette or a Spectralon®-holder with the corresponding pure salt were used as blanks.
In Berlin, a home-built, calibrated system was used. Further details on the setup, calibration, and measurement protocols can be found in reference [20]. Sample excitation was fixed at 480 nm using a xenon lamp coupled into a single monochromator. Sample and blank were center mounted in a 6 in. spectraflect-coated integrating sphere (Labsphere GmbH). The emitted and scattered light was collected with a quartz fiber coupled to the integrating sphere, attached to an imaging spectrograph (Shamrock303i, Andor Inc.) and detected with a Peltier-cooled thinned back side illuminated deep depletion charge coupled device (CCD array). The spectral responsivity of the detection channel was determined with a calibrated tungsten lamp (integrating sphere-type spectral radiance transfer standard from Gigahertz of known spectral radiance), thus providing traceability to the spectral radiance scale. [20–22] QDs in solution were investigated in 10 * 4 mm quartz cuvettes in order to minimize reabsorption. Powders of milled QD-salt crystals were distributed uniformly in a 200 μm thick round cuvette (diameter 15 mm) or embedded into a silicon pellet (see Figure 3.3). The powder samples were tilted with respect to the entrance port of the sphere in order to collect most of the scattered excitation light to ensure minimal measurement uncertainties. Either a solvent-filled cuvette, a round cuvette filled with the pure salt used as a QD matrix or a silicone pellet doped with QD-free pure salt were used as blanks for the determination of the number of absorbed photons from the transmitted and reflected incident spectral radiant flux and the blank correction of the emission spectra. [21, 23]
PL-LT measurements were conducted in Dresden on a FluoroLog-3 spectrofluorometer (Horiba Jobin Yvon) equipped with a pulsed LED diode and a TCSPC module at room temperature. In Berlin, an Edinburgh Instrument lifetime spectrometer (FLS 920) equipped with a supercontinuum laser (SC400-PP, Fianium) as a pulsed excitation light source (pulse frequencies of 0.5 or 1 MHz and a pulse width of 150 ps), a double monochromator, a MCP-PMT (R3809U-50, Hamamatsu), and a time-correlated single- photon-counting (TCSPC) module (TCC 900) were used for signal detection.
In both setups, the instrument response function was measured with a non-luminescent scatterer at the excitation wavelength. The luminescence decays of the QDs in solution, in the crystal matrices, and in the silicon pellets were measured with identical instrument settings to obtain comparable values, e.g., identical excitation wavelengths, detection at the emission maximum, identical detection/excitation bandpasses, and repetition rates. For data evaluation, the PL-LTs of these multiexponential decays were set equal to the time when the intensity corresponds to 10,000/e of the initial intensity.
Fluorescence microscopic investigations of the mixed crystals were performed on a Zeiss Axiostar plus fluorescence microscope on glass slides.
Thin sheets for the TEM measurements were prepared following the method of Glauert using a

Leica ultramicrotome. Two different epoxy hosts were used during the preparation of the thin sheets. As the first host, an epoxy resin Araldite 6005 Kit (Electron Microscopy Sciences) was warmed and the components were mixed according to reference [24], filled into the mold, and the mixed crystals were placed within the resin. After curing at 60 °C, the epoxy-mixed crystal composite was trimmed and sectioned into 200 nm thin sheets, using an ultramicrotome and an ethanol bath. Secondly, mixed crystals were embedded into histological resin (Kulzer) which is prepared by mixing resin and cross-linker with the ratio of 15:1 v:v. In order to initiate the cross-linking process, samples were exposed to UV light at 254 nm for 15 min and then stored at room temperature for complete solidification. After one week, sheets of 200 nm thickness were obtained using a Leica ultramicrotome. The sheets were placed on 200 mesh carbon-coated copper grids for the subsequent TEM investigations. TEM measurements were performed using a FEI Tecnai G2 F30.
Thermogravimetric analysis were performed on a TGA/DSC1 STARE System (Mettler Toledo) using alumina crucibles and pressured air as purging gas.
Anodic stripping voltammetric (ASV) analyses were performed on a PGSTAT 128N electrochemical workstation (Metrohm). The measurements were conducted in usual three electrode configuration using a glassy carbon as working-, a saturated calomel electrode (SCE) as reference- and a Pt-flag as counter-electrode. A detailed description of the measurement procedure is described in the literature. [25, 26] The analyte concentration was determined by applying the standard addition method using a Cd standard solution.
LED stability tests were conducted by application of a square wave modulation (1 kHz or 1/3 Hz, 50% duty cycle, 300 mA peak-to-peak current).

A.8. Sample Overview on PL-QY Measurements

Table A.4.: Synthetic information about the samples investigated during the comparative PL-QY investigations. Adopted by courtesy of Chem. Mater. 2014, 26, 3231. Copyright 2014, American Chemical Society.

Size	PL-QY in H_2O/ $CHCl_3$	PL-QY in NaCl	PL-QY in salt-silicone	PL-QY in borax	Enhance-ment factors	Material	Stabilizer	Synthetic route	PL-LT in H_2O/ $CHCl_3$	PL-LT in NaCl	PL-LT in salt-silicone
nm	%	%	%	%					ns	ns	ns
2.10	10.70		29.59		2.77	CdTe	MPA	aqueous	11.0		28.3
2.54	17.30	24.20			1.40	CdTe	MPA	aqueous	20.8	15.6	
2.62	20.30		26.54		1.31	CdTe	MPA	aqueous	18.6		13.2
2.77	25.23	29.70			1.18	CdTe	MPA	aqueous	17.8	16.6	
3.03	31.00	35.00	35.55	33.53	1.15	CdTe	MPA	aqueous	31.3	23.4	22.5
2.98	13.47		33.91		2.52	CdTe	MPA	aqueous	25.4		23.9
2.98	13.47		31.91		2.37	CdTe	MPA	aqueous	25.4		
2.54	27.70	23.20			0.84	CdTe	MPA	aqueous	20.3	25.1	
2.31	30.40		47.49	34.30	1.56	CdTe	TGA	aqueous	16.0		18.6
2.31	30.40		34.04		1.12	CdTe	TGA	aqueous	16.0		
2.68	48.40	79.60	60.88		1.26	CdTe	TGA	aqueous	14.9	21.5	
2.71	57.70		61.67		1.07	CdTe	TGA	aqueous	16.6		15.7
mix.	26.10		38.44		1.47	CdTe	MPA/TGA	aqueous			
mix.	27.48		60.61		2.21	CdTe	MPA/TGA	aqueous	21.5		17.6
n.d.	17.91/ 53.13	23.35			1.30	CdSe/ZnS	MPA/OA	hot injec-tion	19.5/ 13.3	25.0	
n.d.	37.60/ 72.93	38.60			1.03	CdSe/ZnS	MPA/OA	hot injec-tion	17.1/ 21.7	11.5	

Table A.5.: Spectroscopic data of the CdTe samples shown in Figure 3.7. The samples were ordered by their emission maximum shift. The first samples show a PL-QY increase, that fall below the maximum enhancement predicted by the virtual cavity model, as discussed in reference [27]. All samples starting from the seventh line exceed the predicted PL-QY enhancement. It can be seen clearly, that those samples show a larger shift towards lower energies in PL maximum except for the last sample with the largest shift. This particular sample was, in comparison to all others, washed from the excess of stabilizer prior to incorporation into the salt matrix. This procedure can facilitate the formation of small aggregates resulting in larger PL red-shifts. Adopted by courtesy of Chem. Mater. 2014, 26, 3231. Copyright 2014, American Chemical Society.

PL-max in solution	PL-QY in solution	PL-max in salt	PL-QY in salt	PL-QY enhancement	Enhancement explained by models	Shift of PL-max related to nm	Shift of PL-max related to eV
nm	%	nm	%	%	%	%	%
627	25.2	624	29.7	17.72	36.80	-0.48	0.48
614	17.3	612	24.2	39.88	42.40	-0.33	0.33
612	27.7	616	23.2	-16.25	35.50	0.65	-0.65
648	31	655	35.5	14.52	32.90	1.08	-1.07
611	20	621	27	35.00	40.20	1.64	-1.61
546	30	555	34	13.33	33.50	1.65	-1.62
578	48	589	61	27.08	22.90	1.90	-1.87
550	11	561	28	154.55	46.90	2.00	-1.96
645	13	659	34	161.54	45.30	2.17	-2.12
550	11	562	30	172.73	46.90	2.18	-2.14
546	30.3	558	79.6	162.71	33.50	2.20	-2.15
546	30	559	48	60.00	33.50	2.38	-2.33
550	11	565	23	109.09	46.90	2.73	-2.65
645	13	663	32	146.15	45.30	2.79	-2.71
584	58	615	62	6.90	17.70	5.31	-5.04

List of Figures

List of Tables

References

[1] A. Shavel, N. Gaponik, and A. Eychmüller, *The Journal of Physical Chemistry B*, **2006**, *110*(39), 19280.

[2] M. Grabolle, M. Spieles, V. Lesnyak, N. Gaponik, A. Eychmüller, and U. Resch-Genger, *Analytical Chemistry*, **2009**, *81*(15), 6285.

[3] A.L. Rogach, T. Franzl, T.A. Klar, J. Feldmann, N. Gaponik, V. Lesnyak, A. Shavel, A. Eychmüller, Y.P. Rakovich, and J.F. Donegan, *The Journal of Physical Chemistry C*, **2007**, *111*(40), 14628.

[4] V. Lesnyak, A. Lutich, N. Gaponik, M. Grabolle, A. Plotnikov, U. Resch-Genger, and A. Eychmüller, *Journal of Materials Chemistry*, **2009**, *19*(48), 9147.

[5] W. K. Bae, J. Kwak, J. Lim, D. Lee, M. K. Nam, K. Char, C. Lee, and S. Lee, *Nano Letters*, **2010**, *10*(7), 2368.

[6] S. Kim, T. Kim, M. Kang, S. K. Kwak, T. W. Yoo, L. S. Park, I. Yang, S. Hwang, J. E. Lee, S. K. Kim, and S.-W. Kim, *Journal of the American Chemical Society*, **2012**, *134*(8), 3804.

[7] W. Zhang, Q. Lou, W. Ji, J. Zhao, and X. Zhong, *Chemistry of Materials*, **2014**, *26*(2), 1204.

[8] W. K. Bae, K. Char, H. Hur, and S. Lee, *Chemistry of Materials*, **2008**, *20*(2), 531.

[9] T. Otto, P. Mundra, M. Schelter, E. Frolova, D. Dorfs, N. Gaponik, and A. Eychmüller, *Chemphyschem: a European Journal of Chemical Physics and Physical Chemistry*, **2012**, *13*(8), 2128.

[10] L. Liu and X. Zhong, *Chemical Communications*, **2012**, *48*(46), 5718.

[11] H. G. Bagaria, G. C. Kini, and M. S. Wong, *The Journal of Physical Chemistry C*, **2010**, *114*(47), 19901.

[12] R. Xie, U. Kolb, J. Li, T. Basché, and A. Mews, *Journal of the American Chemical Society*, **2005**, *127*(20), 7480.

[13] A. Aharoni, T. Mokari, I. Popov, and U. Banin, *Journal of the American Chemical Society*, **2006**, *128*(1), 257.

[14] W. Zhang, G. Chen, J. Wang, B.-C. Ye, and X. Zhong, *Inorganic Chemistry*, **2009**, *48*(20), 9723.

[15] W. C. Chan and S. Nie, *Science*, **1998**, *281*(5385), 2016.

[16] S. Tamang, G. Beaune, I. Texier, and P. Reiss, *ACS Nano*, **2011**, *5*(12), 9392.

[17] M. Q. Dai and L. Y. L. Yung, *Chemistry of Materials*, **2013**, *25*(11), 2193.

[18] A. N. Jumabekov, F. Deschler, D. Bohm, L. M. Peter, J. Feldmann, and T. Bein, *The Journal of Physical Chemistry C*, **2014**, *110*(10), 5142.

[19] H. Zhang, Z. Cui, Y. Wang, K. Zhang, X. Ji, C. Lü, B. Yang, and M. Gao, *Advanced Materials*, **2003**, *15*(10), 777.

[20] C. Würth, M. Grabolle, J. Pauli, M. Spieles, and U. Resch-Genger, *Nature Protocols*, **2013**, *8*(8), 1535.

[21] C. Würth, J. Pauli, C. Lochmann, M. Spieles, and U. Resch-Genger, *Analytical Chemistry*, **2012**, *84*(3), 1345.

[22] U. Resch-Genger, W. Bremser, D. Pfeifer, M. Spieles, A. Hoffmann, P. C. DeRose, J. C. Zwinkels, F. Gauthier, B. Ebert, R. D. Taubert, C. Monte, J. Voigt, J. Hollandt, and R. Macdonald, *Analytical Chemistry*, **2012**, *84*(9), 3889.

[23] C. Würth, M. Grabolle, J. Pauli, M. Spieles, and U. Resch-Genger, *Analytical Chemistry*, **2011**, *83*(9), 3431.

[24] A. M. Glauert, *Microscopy and Analysis*, **1991**, *25*, 15.

[25] J. Wang, *Electroanalysis*, **2005**, *17*(15-16), 1341.

[26] C. Prior and G. S. Walker, *Electroanalysis*, **2006**, *18*(8), 823.

[27] M. Müller, M. Kaiser, G. M. Stachowski, U. Resch-Genger, N. Gaponik, and A. Eychmüller, *Chemistry of Materials*, **2014**, *26*(10), 3231.

Danksagung

Zuerst möchte ich Prof. Dr. Alexander Eychmüller für die Möglichkeit danken, dieses vielversprechende Thema am Lehrstuhl für Physikalische Chemie zu bearbeiten, sowie Prof. Dr. Stefan Kaskel in seiner Funktion als zweiter Gutachter der Arbeit. Mein direkter Ansprechpartner, nicht nur während der Promotion, sondern während der gesamten letzten 6 Jahre in allen Problemstellungen war Prof. Dr. Nikolai Gaponik. Ohne ihn, seine Erfahrung und Hinweise, sowie seine stets offene Tür wäre diese Arbeit nicht vollstellbar gewesen. Dafür möchte ich ihm von ganzen Herzen danken. Weiterhin haben mir beide Betreuer bei der Ausführung der Untersuchungen fast vollständig freie Hand gelassen und mich jederzeit ermutigt, die gefundenen Ergebnisse zu vertiefen und zu präsentieren. Dies soll hier ebenso wie die zahlreichen Möglichkeiten von Konferenzteilnahmen und Forschungsaufenthalten im In- und Ausland nicht ohne Dank bleiben.
Einer der Hauptanlaufpunkte für die genannten Forschungsaufenthalte war die Gruppe um Prof. Dr. Hilmi Volkan Demir an der Bilkent University nahe Ankara. Ihm und ganz besonders Talha Erdem und Zeliha Soran-Erdem, sowie dem Rest des Arbeitskreises, möchte ich für die immer wieder herzliche Atmosphäre und die große Menge an Zeit, die sie für unsere gemeinsame Arbeit verwendeten, danken. Zudem soll ihre ungebrochene Bereitschaft, mich und auch die anderen Gruppenmitglieder aus Dresden mit der türkischen (Ess)-Kultur vertraut zu machen, hervorgehoben werden. Dafür und auch für all die anderen lustigen, ereignisreichen und spannenden Momente: Teşekkürler.
Weiterhin möchte ich der Gruppe von Dr. Ute Resch-Genger an der BAM in Berlin danken, die in Person von Martin Kaiser, Ralf Schneider und Florian Weigert einen Teil der diskutierten Photolumineszenz-Quantenausbeute und -Lebenszeit-Messungen durchgeführt und gemeinsam mit mir ausgewertet haben.
Zudem möchte ich Prof. Andrey Rogach, Dr. Sergii Kalytchuk und dem Rest des Arbeitskreise für die großartige Zeit danken, die ich in ihrem Arbeitskreis an der City University of Hong Kong verbringen durfte, in dessen Rahmen wir die Eigenschaften von IR emittierenden Mis-

chkristallen untersucht und, an den freien Tagen, die Besonderheiten dieser beeindruckenden Stadt erkundet haben.
Ein großer Dank soll auch an meine beiden Bachelorstudenten (und natürlich Forschungspraktikanten), Josephine Lox und Remo Tietze gehen, welche einen wichtigen Beitrag geleistet haben. Zum einen haben ihre Ergebnisse die vorliegende Arbeit vervollständigt, doch noch interessanter und reizvoller war es für mich, ihre Entwicklung zu verfolgen sowie ein wichtiger Teil ihrer Ausbildung zu werden und damit durch und mit ihnen Teamführung zu erlernen. Es hat wahnsinnigen Spaß mit euch beiden gemacht!
Im Weiteren will und darf ich ein großes Dankeschön an Prof. Dr. Zhiyu Wang und Gordon Stachowski aussprechen, ohne deren synthetisches Geschick und damit einhergehende Probenbereitstellung es nicht möglich gewesen wäre, die vorliegende Arbeit in dieser Qualität zu verfassen. In diesem Zusammenhang der Probenbereitstellung möchte ich ebenfalls noch Dr. Stefanie Gabriel, Dr. Christian Waurisch, Dr. Klaus Boldt, Dr. Vladimir Lesnyak, sowie Laura Kühn, Christian Meerbach und Christoph Bauer danken, welche mir in verschiedene Proben für meine Experimente zur Verfügung stellten. Außerdem möchte ich all jenen Danken, die mir beim Korrekturlesen der Arbeit zu Hilfe gekommen sind und ordentlich ihre eigenen, knappen Zeit investiert haben. Zudem sollen hier Wenke Markgraf und Thomas Jacob nicht unerwähnt bleiben, welche bei mir ein einwöchiges Praktikum und im Fall von Thomas anschließend noch eine mehrmonatige WHK-Stelle ausgeübt haben und mit ihrem Einsatz und ihren Ergebnissen zum Gelingen dieser Arbeit beigetragen haben.
Bis zu diesem Punkt hat es sich vorrangig um fachliche Aspekte gehandelt, doch die meisten Leser dieser Arbeit werden wissen und verstehen, dass eine Promotion nicht geleistet werden kann, wenn nicht auch das soziale Umfeld passt. Den Einstieg dazu möchte ich mit meinen beiden "Mitbewohnern" des Büros 317 im Erich-Müller-Bau, Christin Rengers und André Wolf setzen, welche oft genug für ein wenig Zerstreuung, einen Lacher, den (bei mir) seltenen Fall der akuten Schokoladennotversorgung und, das wichtigste zuletzt, einen steten und nie endenden Strom von Caramel-Krokant Cappuccino garantierten. Nähere Informationen zum Ausmaß des Letztgenannten findet der geneigte Leser im zweiten Band der sehr lesenswerten "Research on Physical Chemistry & Electrochemistry" Reihe. Doch nicht nur diese beiden, auch der gesamte restliche Arbeitskreis der physikalischen Chemie schafft ein so angenehmes Arbeitsklima, dass selbst kurzfristige Tiefs ohne Schwierigkeiten überwunden werden und aus vielen Kollegen gute Freunde geworden sind.
Abschließend möchte ich mich bei all jenen Bedanken, die außerhalb des Erich-Müller-Baus in den letzten Jahren für mich da waren. Als erstes möchte ich mich bei Marion, seit einigen

Jahren Mittelpunkt meines Lebens und seit mittlerweile gut einem Jahr meine Frau, für alles was wir zusammen erlebt haben bedanken. All die schönen Momente aufzuzählen würde schlicht den Rahmen sprengen, doch ich bin sicher, es wird noch viel, viel mehr in Zukunft dazukommen. Dann möchte ich meinem Vater Uwe für seine unerschütterliche Geduld mit mir, seine oftmals weisen Ratschläge und seine immerwährende Sorge, nur das Beste sei gut genug für mich, von ganzem Herzen danken. Zudem geht ein ganz großes Dankeschön an alle meine weiteren Freunde, Familienangehörigen und Bekannten. Den Abschluss in diesem Reigen sollen Alexander Kohl, Benjamin Vater, Henning Schneider und Jeannine Tändler bilden, die, auch wenn die regionalen Entfernungen zwischen uns nicht kleiner werden, doch immer mit einem offenen Ohr, einer helfenden Hand und einem guten Ratschlag zur Stelle sind!

Versicherung

Hiermit versichere ich, dass ich die vorliegende Arbeit ohne unzulässige Hilfe Dritter und ohne Benutzung anderer als der angegebenen Hilfsmittel angefertigt habe; die aus fremden Quellen direkt oder indirekt übernommenen Gedanken sind als solche kenntlich gemacht. Die Arbeit wurde bisher weder im Inland noch im Ausland in gleicher oder ähnlicher Form einer anderen Prüfungsbehörde vorgelegt.

Dresden, den 12.10.2015

Marcus Adam

Die Dissertation wurde an der Technischen Universität Dresden am Lehrstuhl für Physikalische Chemie unter der wissenschaftlichen Betreuung von Prof. A. Eychmüller angefertigt. Zudem versichere Ich, dass bisher keine erfolglosen früheren Promotionsverfahren stattgefunden haben.
Ich erkenne die Promotionsordnung der Technischen Universität Dresden der Fakultät Mathematik und Naturwissenschaften vom 23.02.2011 in geänderter Fassung vom 15.06.2011 und 18.06.2014 an.

Dresden, den 12.10.2015

Marcus Adam